
Universidad de Navarra

Facultad de Ciencias

# Numerical study of defibrillation mechanisms using a one-dimensional model of cardiac tissue

Ana Šimić

Universidad de Navarra

School of Science

# Numerical study of defibrillation mechanisms using a one-dimensional model of cardiac tissue

Submitted by **Ana Šimić** in partial fulfillment of the requirements for the Doctoral Degree of the University of Navarra

This dissertation has been written under my supervision in the Doctoral Program in Complex Systems, and I approve its submission to the Defense Committee.

Signed on November 7, 2014

Dr. Jean Bragard

Declaración:

Por la presente yo, **Dª. Ana Šimić**, declaro que esta tesis es fruto de mi propio trabajo y que en mi conocimiento, no contiene ni material previamente publicado o escrito por otra persona, ni material que sustancialmente haya formado parte de los requerimientos para obtener cualquier otro título en cualquier centro de educación superior, excepto en los lugares del texto en los que se ha hecho referencia explícita a la fuente de la información.

(I hereby declare that this submission is my own work and that, to the best of my knowledge and belief, it contains no material previously published or written by another person nor material which to a substantial extent has been accepted for the award of any other degree of the university or other institute of higher learning, except where due acknowledgment has been made in the text.)

De igual manera, autorizo al Departamento de Física y Matemática Aplicada de la Universidad de Navarra, la distribución de esta tesis y, si procede, de la "fe de erratas" correspondiente por cualquier medio, sin perjuicio de los derechos de propiedad intelectual que me corresponden.

Signed on November 7, 2014

Ana Šimić

A mi familia

# Acknowledgements

In this small paragraph I would like to give thanks to all the people and institutions that in some way or another were part of this work.

First and foremost I would like to give thanks to my family, who was there always with me from the start. I would like to give a special thanks to my husband, Maximiliano A. Giuliani.

To my supervisor, Jean R. Bragard, for his help and patience, especially during the last stages of the thesis. To the professors of department of Physics and Applied Mathematics of the University of Navarra, especially to Ángel Garcimartín, Maria Jesús Chasco and Raúl Cruz Hidalgo.

To many fellow students and friends I had pleasure to meet during my stay in Pamplona, Daniela Urribarri, Celia Lozano Grijalba, Neus Carmona Cervelló, Hugo Bello, Martin Pastor, Andrea Pino Del Carpio, Karol V. Asencio Acevedo, Raheema M. Aslam, Jose Guadarrama Cetina, Jose Damas, Miguel López Caballero, Manuel Francisco Acevedo, Moorthi Pichumani, Álvaro Janda, Ana Laura De La Garza, Ivana Grbeša, Miljana Valdec.

To the University of Navarra and Asociación de Amigos for the PhD scholarship that made this thesis possible.

To the Ministry of Education and Sciences of Spain for financial support through project FIS2011-28820-C02-02 and co-ordinated projects FIS2005-06912 and FIS2008-06335.

To the contribution from the European Science Foundation (ESF).

# Contents

# Preface

According to some estimates [1], sudden cardiac death accounts for almost a quarter of all deaths. The main cause of sudden cardiac death is ventricular fibrillation. The electrical activity of a fibrillating heart is in a highly disorganized state maintained via one or more meandering spiral waves [2]. The coordinated mechanical contraction is thus disrupted and the heart is not able to eject blood properly. If not treated within minutes, ventricular fibrillation is lethal.
The only existing treatment for ventricular fibrillation is defibrillation. This means the application of external stimulus via two electrodes placed either externally over the chest or implanted subcutaneously in the case of the internal cardioverter-defibrillator (ICD). The delivered energy is around 150J in the case of transthoracic defibrillation [3] and in the range of 30 to 40J in the case of the ICD [4, Chapter 6].
Due to the large amount of energy involved, it is not surprising that diverse side-effects to defibrillation have been reported, related to pain [5], cardiac hemodynamics malfunctions [6], increased pacing thresholds [7], loss of excitability [8], post-defibrillation arrhythmias [9] etc. ICD devices have an additional problem of size, as storage of the required energy for defibrillation is related to the size of the device. These adverse problems and the very nature of ventricular fibrillation that requires immediate attention have fueled the search for a solution. There has been two main ways of confronting the cardiac arrhythmias. One was a search for a silver bullet, i.e. a pharmacological treatment of the cardiac arrhythmias. The second is the optimization of defibrillation in order to reduce the delivered energy. Both approaches have been hampered with the lack of understanding of the basic mechanisms involved in both fibrillation and defibrillation. The incomplete understanding of processes involved in arrhythmia initiation and maintenance was particularly reflected in several anti-arrhythmic drug trials, CAST [10], CAST-II [11] and SWORD [12] in which mortality increased for post-myocardial infarction patients receiving anti-arrhythmic drug compared to mortality in the placebo group. Clinical use of defibrillators started in the mid 1950 [13] and has come a long way from the 120 kg Kouwenhoven defibrillator [14] to portable automated external defibrillators and implantable devices (roughly the size of a pocket watch). However, despite the long history, the development of the electric therapy has not always gone hand by hand with the current research. Optical mapping studies developed in the early 1990s [15] allowed for the recording of electrical activity during and after the defibrillation shock, which due to the large number of electrical artifacts was not possible with other available experimental methods. A number of important insights into the mechanisms of shock-tissue interaction was made [16–20]. However, optical mapping only provides information for the surface layer of the tissue, while electrical dynamics within bulk tissue remains unknown. The second major breakthrough was brought by the bidomain model and the increasing computational power. Equations

of the bidomain model govern the propagation of the electrical signal in the cardiac tissue taking into account the anisotropy of intracellular and extracellular spaces. Paired with the model representing the currents at the cellular level, it can grow to be very computationally expensive. Three-dimensional simulation of cardiac dynamics typically has $10^5$-$10^7$ degrees of freedom [4, Chapter 2.2]. For example, simulating 200 ms of cardiac electrical activity in a mesh with 862 525 points representing 3D rabbit ventricular model, takes 6.4 h on 64 processors [21].

Despite the significant advances in the understanding of cardiac arrhythmias, the design of the defibrillator devices is based on experimental animal studies and ideas stemming from the similar field of tissue excitation led by Hoorweg, Weiss, Lapicque and Blair in the early 1900s. Most commercial defibrillators employ a capacitor discharge to produce a defibrillation waveform, thus producing a exponentially decaying waveform that in addition is truncated to achieve a higher efficiency. This gives three parameters available to optimize the waveform: initial voltage, decay constant and duration. Apart from the shape of the waveform, in the late 1980s it was established empirically that reversing a polarity of the waveform can increase the efficiency of the defibrillation [22–24]. A monophasic protocols denotes a defibrillation in which polarity of the electrodes is maintained during the shock as opposed to the biphasic protocol in which polarity of the electrodes is reversed during the shock. To this day, there is no full understanding why biphasic shocks are better than monophasic shocks. There has been a numerous theoretical and experimental efforts to find optimum values for initial and final voltage of the shock, decay constant, shock duration and polarity reversal timing [25, 26].

In this work the study of defibrillation mechanisms is approached by using a relatively simple one-dimensional model, but incorporating important ingredients known to influence the defibrillation outcome. Low dimensionality of the model is to serve two purposes. The computational cost can be kept low and thus provide a fast method to assess the efficiency of the shock, provided the model can reproduce experimentally known data. This is particularly important if we have in mind the stochastic nature of defibrillation and large number of parameters that can be used to optimize energy delivered by the defibrillating shock. Let us note at this point that one-dimensional geometry is often employed as a simplification of the reentrant dynamics of the electric wave and was used to study interaction with the external shock. In that sense the model used in this thesis extends on the previous work started by the seminal work by Glass and Josephson [27] in which one dimensional geometry was used to study annihilation and resetting of reentrant wave. Secondly, by keeping the model (relatively) simple, one hopes to gain a clear insight into the mechanisms throughout the range of low to high defibrillation energies. In **chapter 1** we will review important concepts in the field of cardiac bioelectricity in order to provide a general framework for the rest of the thesis. We will introduce equations governing the propagation of the electrical signal in the heart tissue and review the relevant properties of the cell membrane currents. Main concepts of ventricular fibrillation initiation and maintenance, existing defibrillation theories and main design principles for defibrillation waveforms are also reviewed. In **chapter 2** we will present in detail the one-dimensional model used to study defibrillation mechanisms. In particular, in this chapter we will also present four different defibrillation mechanisms that lead to successful outcome. One identifies four different types: direct block, delayed block, annihilation and direct activation. Which defibrillation mechanism prevails depends on the energy level, the current dynamic state of the system and the shock protocol. In **chapter 3** we will use the one dimensional model to study three different protocols commonly used in

defibrillation practice: monophasic, biphasic symmetric and biphasic asymmetric. Results of the numerical simulations reveal that monophasic shocks defibrillate with higher rate of success than the two biphasic shock protocols at lower energies. On the contrary for higher shock energies, the biphasic shock are significantly more efficient than monophasic shocks. This latter result confirms the medical common wisdom about defibrillators. The protocols will be tested for two different dynamical states prior to the shock and again confirming that more organized arrhythmias are easier to defibrillate. The detailed comparative study of the three protocols will be presented for medium shock duration of 8ms. Behavior for shorter and longer shock durations are also examined and presented in the form of strength-duration curves. In **chapter 4** we will propose a new shock protocol that is based on a four electrode system instead of the of standard procedure based with only two electrodes. Results will reveal a huge reduction in defibrillation threshold for asymmetric biphasic protocol and significant reduction for the other two tested protocols as compared to standard two-electrode defibrillation. Mechanism of successful defibrillation are analyzed and revealed that the advantage of asymmetric biphasic shocks for the case of four electrodes protocol lies behind the interplay of the duration of the cathodal and anodal phase.

# Chapter 1

# Introduction

## 1.1. The heart

The heart is a muscle organ located near the center of the chest cavity whose purpose is to exchange blood between the circulatory system and the lungs where the waste is removed and the blood is oxygenated. The structure of the heart is made of four pumping chambers, each performing a distinct task. Two upper chambers, left (LA) and right atria (RA), are responsible for collecting the blood and two lower chambers, left (LV) and right ventricle (RV), are responsible for pumping the blood. The blood flow between the chambers on each side of the heart is regulated by heart valves. The bicuspid or mitral valve regulates the blood flow between left atria and ventricle and tricuspid valve between the right chambers of the heart. The proper functioning of a healthy heart is a complex and detailed process in which all four chambers and valves need to contract synchronously. Mechanical contraction is controlled by the underlying electrical conduction system of the heart. Once the LA is filled by oxygenated blood from the lungs and RA with the blood from the venous system, a wave of depolarization is triggered by the pacemaker cells in the sinoatrial node. A wave of electrical excitation spreads across the atria causing them to pump blood to the ventricles. Propagation velocity through the atrial muscle is approximately 0.5 m/s [28]. The excitation crosses to ventricles through the atrioventricular (AV) junction, the only conducting path between the atria and ventricles. The velocity of the depolarization propagation is slowed down to 0.05 m/s [28] allowing the atria to completely contract before the ventricles begin to contract. Cells in the AV node also exhibit self-excitability as the cells in the SA node and can fire an action potential in the absence of the action potential coming from the SA node. The wave enters the ventricles at the bundle of His where it spreads to left and right bundle branches along the inter-ventricular septum. The conduction velocity through the bundle of His reaches 2m/s [28]. The bundle branches then divide into an extensive system of Purkinje fibers that conduct the impulses at high velocity (about 4 m/s) throughout the ventricles [28]. This results in rapid depolarization of ventricular myocytes throughout both ventricles. The ventricles contract and eject blood. The right ventricle pumps the blood into the pulmonary artery via the pulmonary valve from where the blood flows to the lungs. Left ventricle pumps the blood into the aorta via the aortic valve from where the blood further flows through the arterial system.

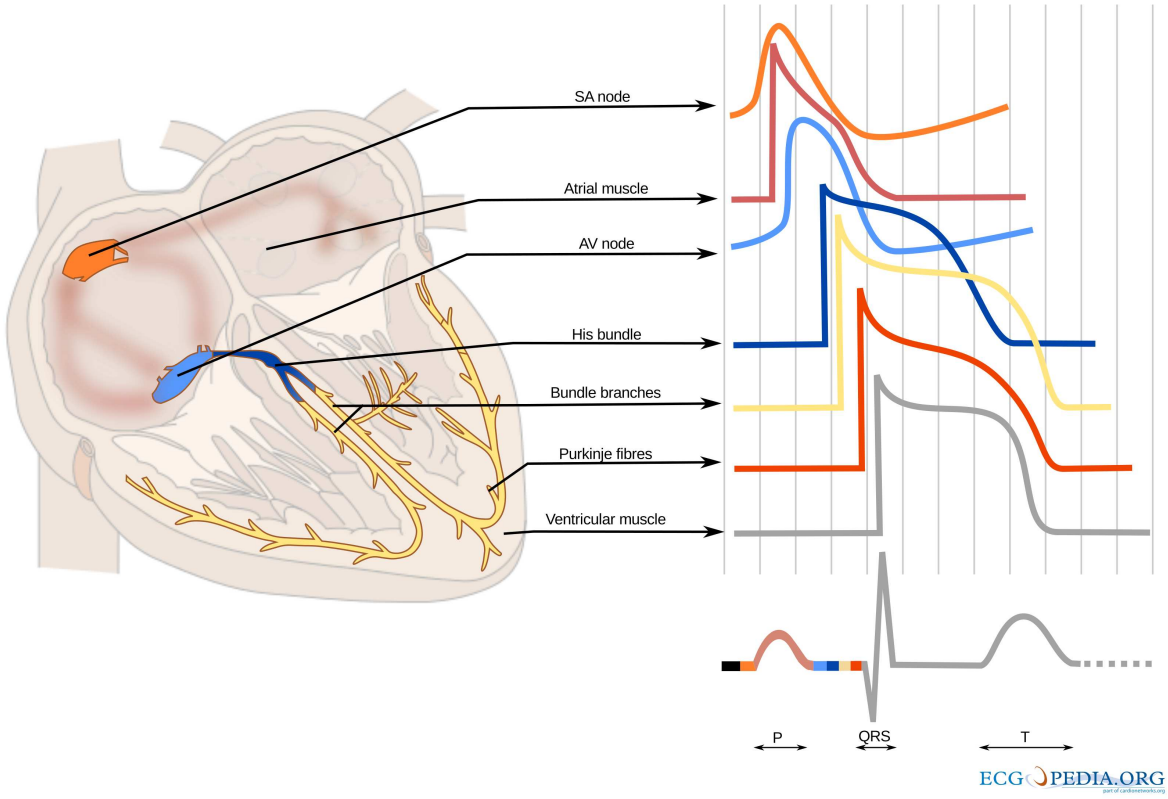


Figure 1.1: Cross section of the heart structure. Arrows indicate functionally different parts of the electrical conduction system and associated action potentials. A wave of depolarization is triggered by the self-excitable cells in the SA node. The wave spreads into the ventricles by crossing the AV node. Depolarization then spreads onto the bundle of His, bundle branches and finally to Purkinje fibers. Image taken from en.ecgpedia.org, shared under Creative Commons Attribution Non-Commercial Share Alike.

### 1.1.1. Heart cell properties

Single myocyte is approximately cylindrical in shape with typical dimensions in the human ventricular tissue of 80 to 100 $\mu m$ in length and 10 to 20 $\mu m$ in diameter. Sarcolemma, the cardiac cell membrane, is composed mainly of the phospholipid bilayer that provides the barrier between the intra- and extracellular compartments. The exchange of ions through the membrane is only possible through pores formed by proteins. Functionally, the transport of ions across the pores can be divided into ion channels, pumps and exchangers. The currents through the ions channels are the main determinants of the shape of the cardiac action potential. There are two fundamental properties of the ion channels : selectivity and gating. Each ion channel is selectively permeable to one or more ion species. Gating of the channel refers to the opening or closing of ion channels as a response to voltage change, shear stress, intracellular messengers or neurotransmitters. It is known that channel can be found in one of the three conformational states: open, closed and inactive [29]. While open, selected ions can freely pass across the channel. Open state is followed by a conformational change to inactive state, in which the channels are nonconducting and are

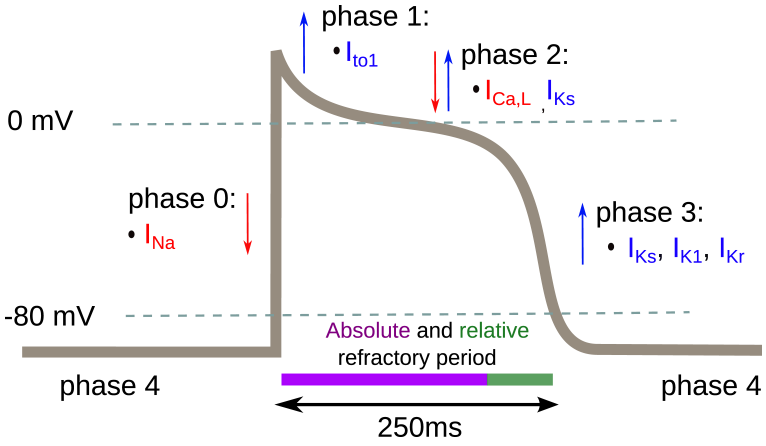


Figure 1.2: Ventricular action potential. Four different phases of action potential are indicated. Depicted are also the most significant ion-channel currents. The upstroke that defines the phase 0 is caused by the strong influx of the sodium current ($I_{Na}$). Phase 1 or early repolarization is characterized by sodium channel inactivation and outflux of potassium current ($I_{to1}$). Phase 2 denotes the plateau characteristic of cardiac action potential. It is maintained by L-type calcium current ($I_{Ca,L}$) and potassium current through slow delayed rectifier channels ($I_{Ks}$). Phase 3 denotes the repolarization brought by potassium current through slow delayed rectifier ($I_{Ks}$), rapid delay rectifier ($I_{Kr}$) and inwardly rectifying current ($I_{K1}$). Phase 4 denotes the rest state.

undergoing a recovery process. Inactivation is followed by closed state in which channels are also nonconducting, but with the ability to open. This channel dynamics lies behind the cardiac refractory properties. Important properties of the ventricular action potential are depicted in Fig. 1.2. It consists of five distinct phases [30]. Phase 0 starts with stimulus arriving from an adjacent cell that depolarizes the transmembrane potential to a threshold for sodium channels activation ($\sim$ -65mV). Large influx of sodium ions ensues which further depolarizes the membrane. Phase 1 or early repolarization is mostly due to the inactivation of sodium channels. In addition, several outward currents are also activated, the most important of which is the transient outward current ($I_{to}$). Phase 2 or the plateau is characteristic of the cardiac action potential, although it is not present in the pacemaker cells. Main currents present are the L-type calcium inward current and the potassium current through the slow delayed rectifier channels ($I_{Ks}$). Phase 3 denotes repolarization by the outflux of the potassium ions. $I_{Ks}$ channels are still open and the negative change in the transmembrane potential opens more potassium channels, most significant of which are the rapid delayed rectifier ($I_{Kr}$) and the inwardly rectifying current ($I_{K1}$). This repolarization brings the transmembrane potential back to the resting state or phase 4.

### 1.1.2. Modeling electrophysiology of the cell

Cell membrane can be modeled by an equivalent electrical circuit with a capacitive component and one or more resistive components in parallel.

$$I_m = C_m \frac{\partial V_m}{\partial t} + I_{ion} \tag{1.1}$$

where $V_m = \phi_i - \phi_e$ denotes the transmembrane potential, $C_m$ membrane capacitance and $I_{ion}$ the sum of all the resistive components. Each resistive components is different for different ion species and can be dependent on time or voltage. There are two approaches to modeling $I_{ion}$ current: phenomenological and biophysical models. The former are created by fitting macroscopic properties of the action potential, for example AP and velocity restitution properties to the parameters of the model. The advantage of these models lies in the low computational cost and to an easier comprehension of the model due to small number of variables. Biophysical model describe the dynamics of each identified current based on experimental data. The complexity and computational cost has grown considerably since the beginning of cardiac cell modeling in the early 1960s. The first model was proposed by Noble [31] for a Purkinje cell and it included three currents : sodium, potassium and background current with a total of four variables. The model was based on the formalism developed by Hodgkin and Huxley [32] intended to describe electrical potential of the squid giant axon. Their model has remained the most used representation of the channel dynamics. An alternative approach is to model the gating dynamics with Markov chains [33]. Hodgkin-Huxley model contained three currents : sodium, potassium and a leakage current and three gating variables. More recent versions of the ventricular cell model, like Luo-Rudy dynamic contains eleven currents, four fluxes and eleven gating variables. Each current in the Hodgkin-Huxley formalism is described with conductance(s) multiplied with the difference between the transmembrane potential and the reversal ion for that current Eq.(1.2).

$$I_x = g_{x_1} g_{x_2} \cdots g_{x_n} (V_m - E_x) \tag{1.2}$$

They proposed that the conductance dynamics of a particular channel is regulated with activation and inactivation (opening and closing) of an ion channel. The general form for a conductance of channel $x_i$ is given by

$$g_{x_i} = \bar{g}_{x_i} \cdot y \tag{1.3}$$

where $\bar{g}_{x_i}$ is the maximal conductance of that channel and $y$ is the gating variable whose dynamics is described with Eq.(1.4).

$$\frac{dy}{dt} = \frac{y_\infty - y}{\tau_y} \tag{1.4}$$

$y_\infty$ represents the steady state behavior of the variable $y$ and the $\tau_y$ the time constant associated with the activation/inactivation process.

### 1.1.3. Heart tissue

The cardiac tissue is composed of interconnected cardiac cells or myocytes organized in the extracellular matrix. Myocytes are connected by the interwoven membrane called the intercalated disc that contains both contractile proteins and gap junctions. Gap junctions are the main determinants of the intracellular resistivity as they allow the passage of the small molecules and ions. One gap junction is composed of two hemichannels, one coming from each cell and is usually located at the longer end of the cell. The number of gap junctions and their position on the cell can vary. Most gap junctions are located at the longer end of a irregularly rod shaped cell. Connected cells further organize into sheets that are in average 4 cells thick [34]. Three dimensional orientation of muscle layers and the coupling between adjacent layers varies across

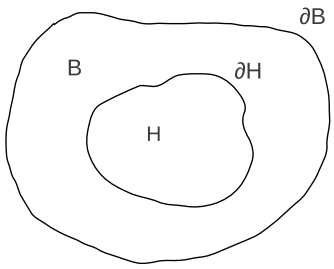


Figure 1.3: Schematic representation of the bidomain model. The region H denotes the myocardial tissue. At every point in space both extracellular and intracellular potentials are defined with their respective conductivities. Outside the myocardial region, an extramyocardial region can be defined (B). The boundary between the two region is denoted by $\partial H$

the ventricular wall. Extracellular space is composed of blood vessels (60%), ground substance (23%), connective tissue cells (7%), collagen (4%) and empty space (6%) [4].

### 1.1.4. Modelling the heart tissue

#### Bidomain model

Two most widely used representation of cardiac electrophysiology are the bidomain and monodomain models. Bidomain formulation comes with higher computational cost and a more realistic representation or cardiac electrophysiology compared with the monodomain model. Bidomain representation of electrical propagation in the heart tissue models the heart tissue as a continuum, where the relevant properties are averaged over many cells. The model was first proposed by Schmitt in 1969 [35] and formulated by Tung [36] in 1978. The bidomain model defines intracellular, extracellular and if needed, the extramyocardial region (Fig.1.3). The intra- and extracellular space occupy the same physical space, while extramyocardial region is adjacent to the space defined by intra- and extracellular domain. The intra- and extracellular space are separated by the cell membrane. The basis of the bidomain model is the Ohm's law.

$$\mathbf{J}_e = -\sigma_e \nabla \phi_e \tag{1.5}$$

$$\mathbf{J}_i = -\sigma_i \nabla \phi_i \tag{1.6}$$

where $\mathbf{J_e}$, $\sigma_e$ and $\phi_e$ are the extracellular and $\mathbf{J_i}$, $\sigma_i$ and $\phi_i$ the intracellular current density, conductivity tensor and electrical potential, respectively. The current can pass from one region to another only through the cell membrane. Thus, in the absence of external or internal stimulus, the change in current density in extra- or intra cellular region must be equal to the current flow across the membrane.

$$-\nabla \mathbf{J_i} = \nabla \mathbf{J_e} = \beta I_m \tag{1.7}$$

where $I_m$ represents the transmembrane current density per unit area and $\beta$ surface to volume ratio of the membrane. On the basis of these two equations, the bidomain model can be written as a coupled system of reaction-diffusion equations.

$$\nabla(\sigma_i \nabla \phi_i) = \beta I_m \tag{1.8}$$

$$\nabla(\sigma_e \nabla \phi_e) = -\beta I_m \tag{1.9}$$

In case of the simulation studies of defibrillation, the principal advantage of the bidomain model is the possibility of integration of the external stimulus. This can be done in two ways. One option is to add a member representing external source to Eq.(1.9)

$$\nabla(\sigma_e \nabla \phi_e) = -\beta I_m - I_{se} \tag{1.10}$$

This inclusion of external stimulus could represent the stimulation via wire or catheter electrodes. Another option is the change of boundary condition in the place where electrodes are to be placed. The change is done to the $\phi_e$ potential at the border between the extracellular and the external region.

Bidomain equations together with the expression for the transmembrane current Eq.(1.1) are often written in a different form, more suitable for numerical solvers:

$$\nabla \cdot ((\sigma_i + \sigma_e)\nabla \phi_e) = -\nabla \cdot (\sigma_i \nabla V_m) - I_{si} - I_{se} \tag{1.11}$$

$$\nabla \cdot (\sigma_i \nabla V_m) + \nabla \cdot (\sigma_i \nabla \phi_e) = \beta(C_m \frac{\partial V_m}{\partial t} + I_{ion}) - I_{si} \tag{1.12}$$

Maintaining $\phi_e$ and $V_m$ as independent variables is also advantageous for comparison with experimental data. $\phi_e$ can be measured via electrical probes and $V_m$ via optical mapping techniques. Eq.(1.11) and (1.12) can be reduced to the monodomain model by assuming equal anisotropy ratio $\sigma_i = k\sigma_e$.

$$\nabla(\sigma \nabla V_m) = \beta(C_m \frac{\partial V_m}{\partial t} + I_{ion}) \tag{1.13}$$

where $\sigma$ now is :

$$\sigma = \sigma_i(\sigma_i + \sigma_e)^{-1}\sigma_e \tag{1.14}$$

## 1.2. Cardiac arrhythmias

Cardiac arrhythmia denotes any disruption in the normal heart rate. A very common classification divides arrhythmias according to the heart rate into two types: bradycardia and tachycardia. The former represents arrhythmias with the heart rate slower then 60 beats per minute and the latter represents arrhythmias in which the heart beats faster than normal, the limit being set to 100 beats per minute. Both bradycardia and tachycardia can occur in ventricles and atria. However, when trying to classify the arrhythmias according to the underlying mechanism of either initiation or maintenance, there is no such clear limit as in the above case. It is possible to divide them according to the mode of persistence to reentrant and non-reentrant arrhythmias [37]. Non-reentrant arrhythmias encompasses the arrhythmias caused by single repetitive event, such are alternans, parasystole arrhythmia or AV block. Reentrant arrhythmias refer to arrhythmias maintained via one or more circulating waves of excitation. The work exposed in this thesis is based on the existence of a reentrant source of arrhythmic behavior. Therefore is convenient to further review only the latter mechanism.
Reentrant arrhythmias can be divided into anatomical and functional. The idea that selfmaintained wave of excitation can underlay certain arrhythmias was first conceived in the early 1900

separately, but almost simultaneously by English physiologist George Ralph Mines and American physiologist Walter Garrey. Experiments performed by Mines on ventricular and atrial tissue of various animals were inspired by findings of a zoologist Alfred Mayer who performed experiments on subumbrella tissue of a jellyfish [38]. Mayer cut the tissue into rings and observed that if appropriately stimulated, a single wave of contraction could propagate indefinitely in clockwise or anticlockwise direction along the ring. Mines was first to suggest that this phenomena could be linked to cardiac arrhythmias and performed similar experiments using the rings of cardiac tissue [4, 39]. Mines observed that in order for the anatomical reentry to happen the following conditions need to be met : existence of the intact anatomical circuit, unidirectional block and the wavelength of the impulse needs to be shorter than the length of the ring. Fig. 1.4 explains the basic mechanism of anatomical reentry. Fig. 1.4a shows a normal propagation, where the impulse arrives from above and passes freely through both channels. Fig. 1.4b shows the example where one channel has a region of slow conduction and long refractory phase. If a premature beat has been triggered, it may stumble upon the refractory zone in the right branch. The propagation is stopped, but the tissue continues to the state of relaxation. The wave emerging from the left side, with no conduction block, continues, excites the left side and reaches excitable tissue in the left branch. The excitation can then continue to circulate around the anatomical pathway. This description fits the mechanisms of several important arrhythmias, among which are supraventricular tachycardias observed in patients with Wolff-Parkinson-White syndrome and bundle branch reentrant ventricular tachycardia. Garrey suggested that such reentry can exist without any anatomical obstacle based on his experiments on turtle heart. Direct experimental confirmation came in the work of Allessie et al. [40] who demonstrated that tachycardia in small pieces of turtle heart can be maintained by circus movement without any anatomical obstacle. Reentrant mechanism of some arrhythmias was also confirmed with potentiometric dyes [41–43] in the early 1990s and since then became a well studied phenomenon in experiments.

*Concepts of reentrant arrhythmias.* There are two concepts present in the literature regarding the maintenance of reentry in cardiac tissue: the leading circle concept and the spiral wave theory. The ”leading circle concept of reentry” was developed by Allessie [44] . Circular movement follows the smallest possible path around an unexcitable tissue. The center of the circular path is continuously excited by smaller wavelets emanating from the leading circle. The frequency of the centripetal wavelets is thought to be higher than the frequency of the leading circle and therefore render the core unexcitable for the leading circle. The resulting wavelength is close to the length of the circle. It is unclear whether leading circle concept underlines arrhythmias. Research that stemmed from excitable media showed that circular reentry can exist even with a large excitable gap. These findings led to a new concept of functional reentry named spiral waves. Although very similar to the concept of the leading circle, there are few important differences. A key concept that marks the difference is the curvature of the spiral front. Each cell on the convex part of the spiral wave front needs to stimulate more than one cell, as opposed to the concave part of the front where each cell needs to stimulate less than one cell. As a result, convex part will propagate with lower velocity then the concave part. At the tip of the spiral wave, the curvature is high enough so it cannot propagate into the core around which it revolves. This marks another difference with respect to the leading circle concept, namely, core of the reentry is excitable, but not excited. The accumulated experimental, theoretical and numerical evidence supports the spiral wave theory of reentry. In addition, spiral wave, viewed as a solution to a system of equations describing the

excitable system, also has a three-dimensional analogue called the scroll wave. Heart myocytes, in the end form a three-dimensional structure.
Important arrhythmias believed to be maintained by reentrant activity include ventricular tachycardia (VT), ventricular fibrillation (VF), atrial tachycardia, atrial flutter and atrial fibrillation [37]. As mentioned, tachycardia is characterized by high but regular heart beat, ranging from 100-200 beats/min. Flutter is associated with even higher rates than 250 beats/min, but still regular. Fibrillation is characterized by complete loss of coordination and thus proper contraction is lost. Fibrillation is more dangerous when occurring in ventricles, rather than atria. If ventricles cannot pump blood correctly, blood pressure drops to zero and if not treated within minutes, death ensues. For this reason, there has been lot of research devoted to the study of initiation, maintenance and termination of VF.

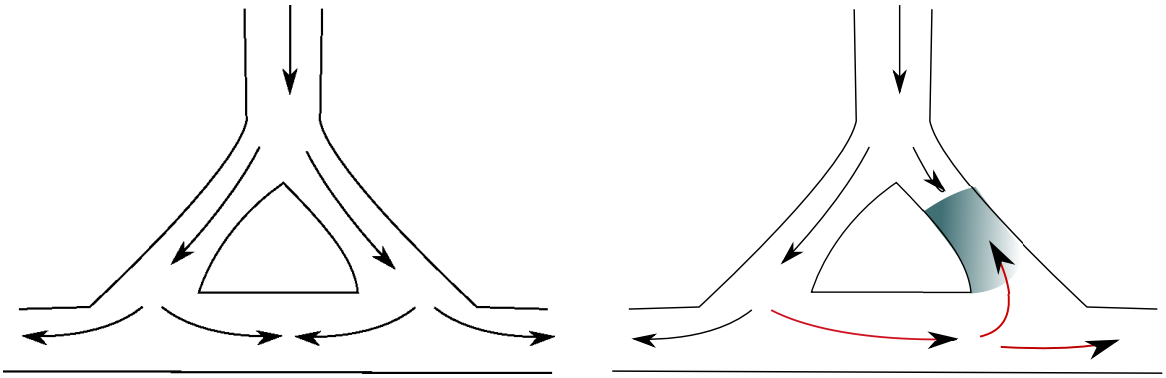

(a) (b)

Figure 1.4: Mechanisms of anatomical reentry. (a) Normal propagation, impulse arrives from above and freely passes through both channels. (b) One channel has a region of slow conduction and long refractory phase. If a premature beat has been triggered, it may stumble upon the refractory zone in the right branch where the wave is stopped but the tissue continues to relax toward the rest state. The wave emerging from the side with no conduction block, continues, and if it reaches the initially refractory channel in the rest state, anatomical reentry is formed.

### 1.2.1. Ventricular fibrillation

*Initiation of ventricular fibrillation.* It is thought that ventricular fibrillation is a result of the deterioration of the ventricular tachycardia. While VT is described with single reentrant wave, VF is viewed as result of aperiodic and random reentrant waves. There are two hypothesis explaining the VT/VF transition. First hypothesis, formed by Moe [45, 46], explains the VF initiation as a result of heterogeneity in action potential duration and refractoriness. Moe performed simulations on two-dimensional cellular automata with randomly distributed refractory periods. After a train of sufficiently short external stimuli, cells with refractory period longer then the stimulation period, are not recovered on time and fail to respond. This results in the fragmentation of the waves and the onset of VF. In addition, VF is associated with diseases that affect the structural or electrophysiological changes of the heart tissue like coronary artery disease or cardiomyopathies. These diseases cause changes in refractoriness. Second hypothesis regarding VT/VF transition,

called also the restitution hypothesis, relates the alternans with steep action potential duration (APD) restitution. APD and conduction velocity (CV) restitution curves relates APD or the CV to the previous diastolic interval. Electrical alternans denote alternate-beat variation in the direction, amplitude, and duration of any component of the ECG waveform. Restitution hypothesis initially claimed that a APD restitution curve with a slope greater then one leads to the creation of alternans [47, 48]. More recent studies revealed that the slope greater than one might not be a sufficient condition for the spiral breakup to occur. A more accurate description should include other factors such as electrotonic coupling, CV restitution, cardiac memory, range of diastolic intervals for which the slope is greater than one, etc.[49–55].

*Maintenance of ventricular fibrillation.* There are two main hypothesis regarding the maintenance of VF in the heart tissue, both supported by experimental and numerical findings. Multiple wavelet hypothesis describes the state of fibrillation as maintained by wandering and short-lived reentry patterns. These wavelets can either be extinguished by colliding with another wavelet or non-conducting barrier or fractionate into daughter wavelets. This hypothesis was formed by Moe in the aforementioned paper [46]. Significant amount of experiments is performed supporting multiple wavelet hypothesis [56–59]. For example, more recent work by Choi et al. [57] analyzing frequency distribution in a fibrillating tissue, found it consisted of dynamically changing frequency blobs with a short life span. Second hypothesis is called mother rotor hypothesis and was first proposed by Lewis [60] in 1925 and later by Gurevich [61]. According to this hypothesis, fibrillation is maintained by a single stable rotor which can also give rise to smaller wavelets on the periphery of the main spiral. The smaller wavelets are caused by refractory tissue, i.e. excitation emanating from the fast central rotor is unable to excite equally all areas, so it breaks on the refractory tissue, causes the conduction blocks which leads to the formation of the smaller rotors on the periphery of the mother rotor [62]. This description has also found the confirmation in the experimental findings [63–65].

These two descriptions are to an extent similar as they involve the reentrant pathway(s) as an underlaying source for the fibrillation. One difference could be emphasized: if the single rotor drives the VF, then the VF could be stopped by stopping the main source, while this could not be possible if the multitude of reentrant sources drives the VF. Compatible with the mother rotor hypothesis, Haïssaguerre performed successfully radiofrequency ablation in 27 patients with idiopathic VF [66]. Another possible possible explanation was offered by Wu [67]. The study used Langendorff-perfused rabbit hearts to test the hypothesis that the two types of VF can occur in the same heart under different conditions. Authors describe two types of VF: (1) type I is associated with steep APD restitution, flat CV restitution ; (2) Type II is associated with flat APD restitution and a broad CV restitution as a result of low excitability. Type II is characterized by large and repeatable pattern of epicardial activation with occasional wavebreaks thus resembling to the mother rotor description of the VF. Type I is characterized by randomly changing patterns of activation consistent with the previously published results supporting wandering wavelet hypothesis of fibrillation [57, 57, 58].

## 1.3. Defibrillation

The application of external electrical stimulus to cardiac tissue for therapeutic purposes has proven to be indispensable for treating certain heart pathologies. We might say that the use of clinical tools like defibrillation or pacing has preceded the understanding of the basic mechanisms of the underlaying processes. However, all the methods used have serious shortcomings and the desire to improve the efficiency and safety of these commonly used clinical approaches has motivated active research in the past and present century. Here we will review briefly the advances in the field of the design of defibrillation protocol and existing defibrillation theories. Defibrillation is a procedure where controlled electrical energy is applied to the myocardium in order to terminate an unstable or pulseless rhythm [68]. To this days, defibrillation is the only available treatment for ventricular fibrillation. Defibrillators can be implanted (ICD), external or wearable. State of the art external defibrillators typically deliver 150 J [69] of energy and implanted 30-40 J [70]. Design of defibrillation devices is based mainly on empirical experience or extremely simplified models of RC circuit representing cardiac cell membrane. Theories and hypothesis of the defibrillation mechanisms have established that in order for the stimulus to be efficient it must fulfill the following conditions [4, Ch. 4.4] :

- Terminate all or most wavefronts that sustain VT/VF
- Not reinduce VT/VF
- Suppress sources of VT/VF if they are focal in nature;
- Not suppress post-shock recovery of the normal sinus rhythm

#### A historical note

Early origins of the defibrillation can be attributed to the research of Prevost and Batelli. In experiments performed in 1899 using capacitor discharge waveform on animal, authors observed that weak current induced "ventricular tremulation" and stronger current reversed the affect, enabling heart to perform regular contractions again [71]. This life-saving result was shelved until the early 1920 when Consolidated Electric Company of New York City funded research to deal with the alarming number of fatal electric accidents among its workers [72]. This enabled Hooker, Kouwenhoven and Langworthy to study direct effects of electricity on the heart. Initially unaware of the Prevost and Batelli discovery, the authors confirmed their results on a series of experiments performed on open chest dog heart using AC current shock [73, 74]. In 1946 surgeon Claude Beck (Case Western Reserve University in Cleveland, Ohio) performed first successful defibrillation on a human [13]. A 14 year old boy was undergoing a open chest surgery for severe congenital funnel chest. During the closure, the pulse stopped and blood pressure went to zero. After a 30 minutes manual heart massage, AC internal defibrillator designed by Beck, arrived. The first shock resulted unsuccessful, but after a second try a feeble pulse was observed. Three hours after, the boy was awake and lucid. He suffered no neurological damage. This significant result was publicly advertised and further research was undergoing. Next big leap was the closed chest defibrillation and it was undertaken almost simultaneously by Kouwenhaven and Zoll in the mid 1950s. Interesting to note, it was general opinion at the time that closed chest defibrillation

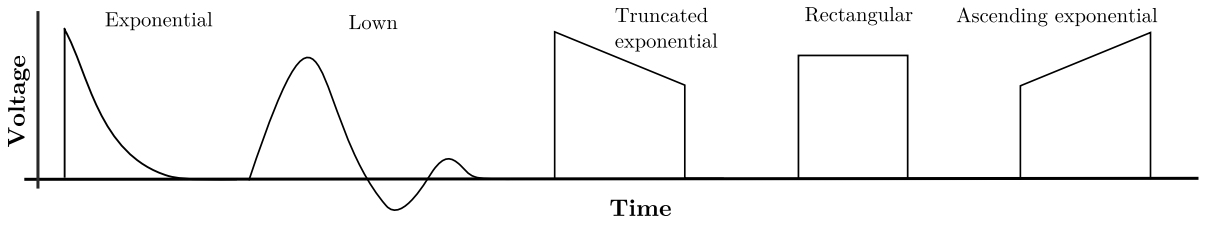


Figure 1.5: Schematic review of the defibrillation waveforms. Capacitor-discharge waveforms were used in experiments of Prevost and Batelli that resulted in the first published description of defibrillation. Lown waveform or damped sinusoidal was achieved by capacitor discharge through an inductance. Alongside truncated capacitor discharge waveform, it was a standard waveform for defibrillation until late 1980s. Today, most common waveform is the truncated capacitor discharge waveform used in a biphasic protocol. Rectangular waveforms are mainly used in theoretical or numerical calculations. Ascending exponential waveform is currently present only in the research papers. Though experimental and theoretical evidence suggest that this form is superior to both descending and rectangular waveform, technical difficulties for now prevent the use in clinical settings.

is not possible since necessary current to accomplish defibrillation would cause damage to the patient [4, Ch.1.2]. Both Zoll and Kouwenhaven defibrillators used AC current and contained transformer used to step up the line current from 110V up to 1000V. The use of transformer made the defibrillator weigh more then 100 kg which limited the portability and use to the hospital setting. Portability problem was solved by Bernard Lown in 1960s who developed a defibrillator that used DC [75]. This allowed for battery operation and eliminated the need for heavy transformer allowing for a design of a portable device. Soon the idea of implanted defibrillator began to develop [76, 77], again despite the overall resistance in the medical community. In 1980 team led by Mirowski [78] succeeded in first human implant with a device of a size roughly a deck of cards and weighing 250g [4, Ch.1.2]. Further accomplishments were achieved by optimizing the defibrillation wavefront. This was an important problem for internal defibrillators, since higher energy defibrillation requires a larger defibrillator. It would be unfair not to mention the developments made in the former USSR started by Lina Shtern, a former student of Prevost and Batelli. Shtern's student, Gurevich, together with his colleague Yuniev, during 1938-1939 period developed a method for transthoracic defibrillation on animals using capacitor discharge pulses [4, Ch.1.2]. Gurevich was the first to recognize advantage of DC over AC waveforms. He was also the first to apply a biphasic waveform, which by 1950s he adapted to humans.

### 1.3.1. Defibrillation waveforms

Important classification of the defibrillation waveforms is the division to monophasic, biphasic or other multiphasic protocols. A monophasic protocol maintains the polarity of the electrodes during the shock application, while in biphasic protocol polarity of the electrodes is reversed during the shock. With triphasic protocol the polarity is switched two times etc.
Each protocol in addition can be have a different waveform. A variety of monophasic waveforms

is shown in Fig. 1.5. Until early 1990s external defibrillators came with either monophasic damped sinusoidal waveform also called Lown waveform or truncated exponential waveform also called trapezoidal waveform . The latter were truncated because it was shown that the long tail of the exponentially decaying waveform can refibrillate the heart [79]. It is interesting to note that Lown waveform has a small negative component, so technically is not monophasic. Today, truncated exponential is the most employed waveshape in the modern defibrillators. The exclusion of inductor, needed for damped waveshape, reduces the overall size, a very important parameter in design of implanted devices. Truncated exponential waveforms can be described with three parameters : initial voltage $V_i$, final voltage $V_f$ and duration or tilt. Tilt is defined with expression :

$$Tilt = 1 - \frac{V_f}{V_i} \tag{1.15}$$

Therefore, a waveform can be truncated either by duration or tilt. In practice, it is also possible to tune the defibrillator parameters to produce the approximately rectangular waveform which is commonly used in theoretical approaches. Presently, under investigation is another type of waveform, truncated ascending waveform shown in Fig.1.5. First theoretical results were presented by Fishler [80] who used a simple RC representation of the myocardium to show that ascending defibrillation waveform are superior to both descending and rectangular waveforms. To some extent, this result has been confirmed experimentally. Namely, experiments comparing ascending ramp waveform with traditional waveforms [81–84] found supremacy over both rectangular, truncated exponential descending waveform or descending ramp. Shorofsky, for example, studied biphasic waveforms in which a first phase is a ramp ascending waveform [83] . When compared to an optimized biphasic waveform, authors reported a decrease in delivered energy at defibrillation threshold (DFT) of 18% and reduction of peak voltage at DFT of 24%. However, this is only one of many other combinations of ascending waveform that are not investigated. What is the optimized ascending waveform or what is the optimized combination of ascending and possibly other waveform is not known.

Research performed in the late 1980s showed that biphasic waveforms can be superior to the monophasic ones [23, 24, 85–89]. Initially used only with ICD devices, biphasic waveforms became standard with external application also. Optimum monophasic and biphasic shocks deliver 200J and 150J of energy, respectively [89]. However, not every biphasic waveform is superior to monophasic of the same duration. The duration of the second phase has proven to be crucial. For the biphasic shock to be superior to monophasic, duration of the second phase needs to be shorter then the duration of the first phase [87]. It is not completely understood why biphasic are more efficient than monophasic waveforms.

### Defibrillation efficacy

Defibrillation threshold (DFT) is defined as minimum energy or voltage required to successfully terminate ventricular fibrillation [90]. However, due to complex heart structure and chaotic nature of fibrillation, defibrillation is best described as a probabilistic phenomenon. Defibrillator with equal output applied consecutively to the same patient or to two different patients might not

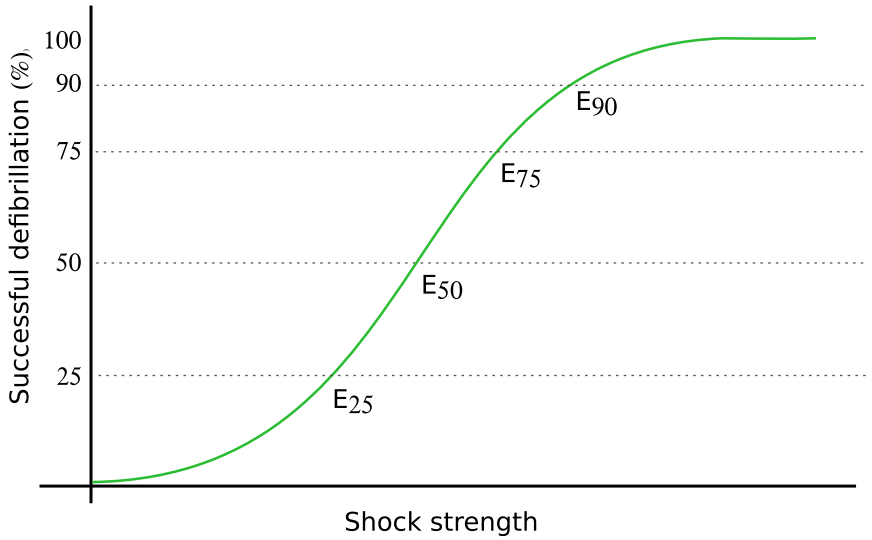


Figure 1.6: Defibrillation threshold is a term used often to denote the minimum shock strength necessary to achieve successful defibrillation. As first noted by Schuder et al. [91], defibrillation threshold is not a single defined value, as might be implied by the word threshold. Instead, successful defibrillation as a function of the applied shock strength can be described with a sigmoid-shape curve [91]. One can then define defibrillation thresholds associated with different percentages of success. For example $E_{50}$ denotes the shock strength necessary to achieve percentage of successful defibrillation of 50%.

result in the same outcome. Therefore, defibrillation threshold is not a threshold in the usual sense of the word with a defined cutoff for successful defibrillation, but a probability function of the defibrillator input. It was first noted by Schuder [91] that there exists a sigmoid-shape curve that represents percent-successful defibrillation versus shock strength for a particular shock duration. This curve is usually called dose-response curve in analogy to dose-response curve for drugs. Therefore, we could speak of defibrillation threshold associated with different success rate, i.e. 90% success rate or 50% success rate. An example of defibrillation dose-response curve is shown in Fig. 1.6. Defibrillation success as a function of shock strength is described in terms of percentage of success. One can define defibrillation thresholds corresponding to different percentages of success. For example $E_{25}$ is the shock strength necessary to achieve successful defibrillation in 25% of the cases. Clinical evaluation of dose-response curve has obvious difficulties since it requires multiple episodes of fibrillation/defibrillation trials. In clinical setting, usually DFT is tested using small number of trials, starting from the highest to lowest energy to defibrillate successfully (or vice versa). Several experimental studies have compared clinical defibrillation threshold and defibrillation threshold given by dose-response construction [92–94]. Overal conclusion is that experimental or clinical threshold corresponds to 50-60% percent success ($E_{50}$-$E_{60}$).

### Modelling defibrillation waveform

To this day it was not possible to design optimal defibrillation waveform based on first principles. Up to now, only model successfully clinically applied [4, Ch. 6.1] is based on viewing the

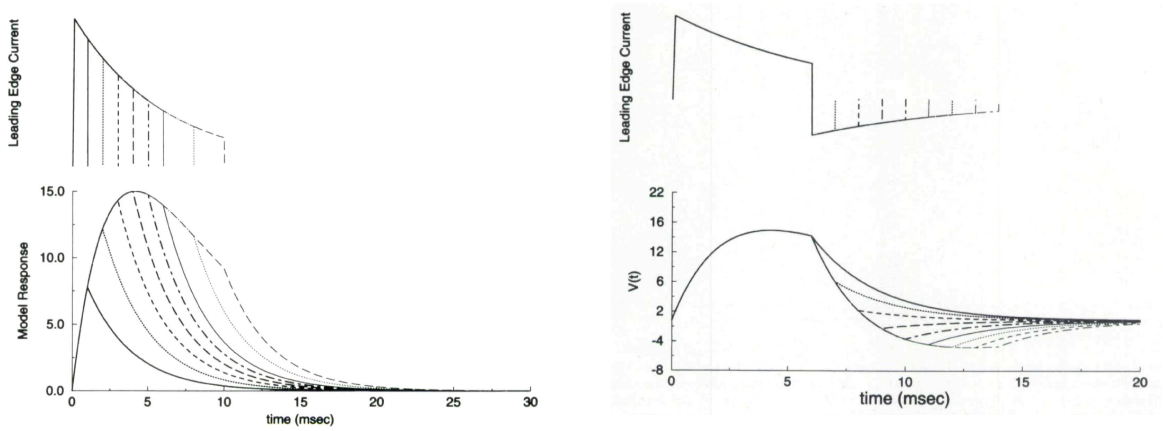


(a) (b)

Figure 1.7: Walcott et al. [95] used the RC model to predict the optimal truncated exponential decay waveform. (a) Upper panel shows the waveform shape that is truncated at different times : 1,2,3,4,5,6,7,8,10 ms. Lower panel shows the model response, V(t). V(t) increases, until reaching a peak after which it begins to decrease. It is hypothesized that the optimal monophasic waveform needs to be truncated at the time V(t) reaches a maximum. (b) It is hypothesized that the optimal duration of the first phase biphasic is optimal monophasic waveform. Phase 1 is truncated at 6ms. The role of the second phase is to return the response back to the initial baseline. The model response does not change polarity until phase 2 duration is longer than 2ms.

cell membrane a simple RC circuit proposed by Blair in 1932 [97, 98]. Membrane is modeled to have capacitance $C_m$, passive resistance $R$ and thus a membrane constant $\tau_m = RC$. Most commonly used value for membrane time constant is 3.5ms [4, Ch. 6.1]. Experimental studies on animal and human report values in the range of 2-5ms [87, 99, 100]. The voltage across RC circuit is calculated during the defibrillation shock of certain duration. The relative efficacy of the RC model response is then determined according to two assumptions : (1) for monophasic and first phase of the biphasic shock, the shock must maximize the voltage change in the cell membrane at the end of the shock for given stored energy; (2) Optimized second phase of the biphasic shock returns the voltage back to the zero potential, removing the charge deposited by the first phase [101], the process also called the charge burping. Despite the simplicity, the main predictions of the waveforms based on this model [101–103] have been confirmed experimentally [95, 104, 105, 105–107]. To complete this section, we cite the work done by Walcott et al [95] in which optimum defibrillation waveform is determined based on the aforementioned Blair model. The authors extended the Blair model by using exponentially decaying waveform rather than the rectangular waveform used originally. Fig. 1.7 shows basic principles of the Walcott model. Upper panels show the waveforms applied across the RC circuit and the lower panels show the response of the RC system. It is hypothesized that the optimal monophasic shock is truncatated at the time that corresponds to the maximum value of the model response. Regarding the biphasic shocks, the model predicts the optimal truncation of the second phase that corresponds to the time that the model response is brought back to zero.

Another approach to duration-wise optimization of defibrillation waveform is based on strength-

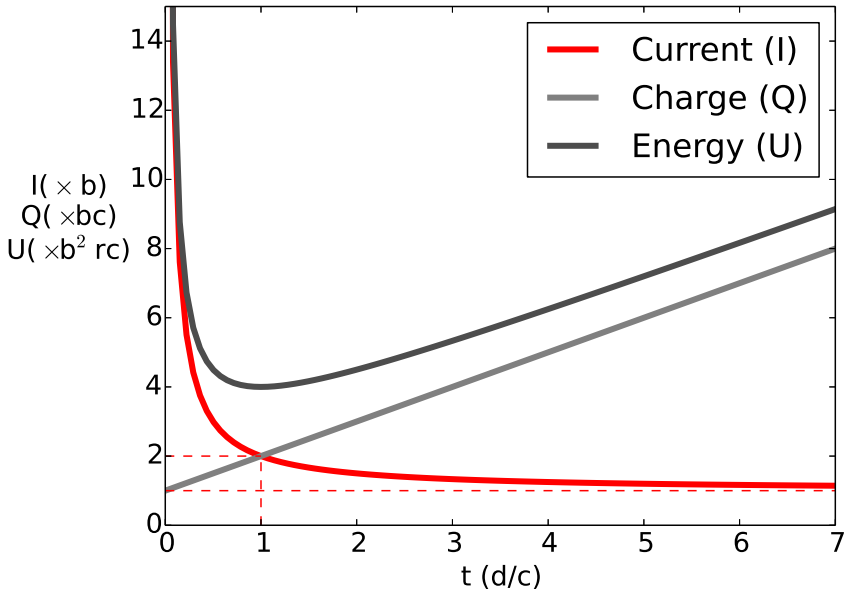


Figure 1.8: Adapted from [96]. Graph shows current, charge and energy necessary to elicit a stimulus in a resting tissue as formulated by Weiss and Lapicque (Eq.(1.16)). Current is applied with a rectangular current pulse. All three strength-duration curves are normalized. The two broken line serve to show chronaxie (c) and rheobase (b). Horizontal broken red line denotes the rheobase, the current of the infinitely long pulse. Chronaxie is defined as time corresponding to current equal to that of twice the rheobase.

duration relationship stemming from the stimulation theories developed in the beginning of the 20th century. The hypothesis behind this connection of tissue stimulation and defibrillation is that the heart responds to stimulation pulses and defibrillation pulses in a quantitativly similar fashion [95]. Fundamental law of stimulation was developed by Hoorweg, Weiss and Lapicque. The latter described the relationship between a stimulus duration $d$ and current $I$ necessary to elicit a response with a hyperbolic expression :

$$I = b(1 + \frac{c}{d}) \tag{1.16}$$

where $b$ denotes the rheobase current and $c$ the chronaxie time. Rheobase is the current corresponding to infinitely long pulse and chronaxie is defined as pulse duration corresponding to twice the rheobase current. Fig. 1.8 shows a normalized strength-duration curve for current, charge and energy that follow from the Weiss-Lapicque model (Eq. (1.16)), as first shown in [96]. The results shown in Fig. 1.8 correspond to a square wave pulse. For square wave pulses, minimum energy occurs for pulse duration equal to chronaxie [96]. Starting from Weiss-Lapicque equation, Kroll [102] found that optimum pulse duration for capacitive-discharge waveform is : $d = 0.58c + 0.58\tau_S$, where $\tau_S = RC$, R is the pathway resistance and C is the device capacitance. Blair model gives a similar form of strength-duration relationship

$$I = b\frac{1}{1 - e^{-d/\tau_m}} \tag{1.17}$$

where d is pulse duration, $\tau_m$ membrane time constant and b the rheobase current. Theoretically, membrane time constant is related to the chronaxie time [108] : $c = 0.69\tau_m$. The existence of

the rheobase current implies that there is a current below which there cannot be a successful defibrillation. At the same time, most cited parameter used to optimize the wavefront or describe the defibrillator is the energy. It is obvious that this is not the optimal choice since energy does not describe the ability to defibrillate the heart. A shock may have energy high enough to defibrillate, but if the current is below rheobase current, defibrillation will not be successful.

### 1.3.2. Electrical stimulation of cardiac tissue

Experiments performed on cardiac tissue have shown that external shock can cause changes in transmembrane potential in the bulk tissue, many centimeters away from the stimulating electrodes. These changes will lead to new propagating potentials, conduction blocks or prolongation of action potentials and ultimately to failure or success of the shock. Several mathematical formulations have been proposed to explain the mechanisms by which shock elicits changes throughout the cardiac tissue. The cable model has explained the bulk excitations with the so called sawtooth pattern and bidomain model with the virtual electrodes.

#### Insights from the cable model: the sawtooth pattern

The cable model is the one-dimensional predecessor of the bidomain model. Extra- and intracellular spaces are formulated as one-dimensional low-resistance medium separated with a highly resistive membrane. When a defibrillation shock is applied, the cable model predicts that the tissue near the anode will be hyperpolarized and tissue near the cathode will be depolarized. The magnitude of both changes will decrease exponentially from the electrode site. The membrane length constant was found to be in the range 0.5-1 mm [109, 110]. Thus the bulk tissue would be left unaffected by the shock. In the study done by Plonsey [111] the intracellular space of the cable model is divided by a series of high-resistance barriers envisioned to model the gap junctions. The response of the system to the external stimulus resulted in change of transmembrane potential on every gap junction resistance site. Upon reaching the resistive barrier, the current is forced to leave the intracellular space and enter again on the other side of the barrier. For the cell nearest to the anode, the membrane will be depolarized and hyperpolarized on the end closer to the cathode. With this pattern repeated in every gap junction site the overall appearance of the one-dimensional response was the sawtooth pattern, hence the name of the model. However, the major difficulty with the predictions of the sawtooth model is the experimental verification. In order to separate the influences of different types of tissue inhomogeneities Fast [112] used cultured monolayers of neonatal cells and optical mapping techniques to measure the results. The results showed complete absence of the abrupt change of $\delta V_m$ on the cell borders. However, when similar experiments were repeated with tissue including intercellular clefts, results were consistent with the predictions of the sawtooth model. Cells depolarized on the anodal side of the cleft and hyperpolarized on the cathodal site of the cleft. These findings were confirmed in the study done by Zhou et al. [113] in which double barrel microelectrode was used to measure $\delta V_m$ along guinea pig papillary muscle. The exception to these experimental limitations of the sawtooth model are the experiments done with single cells [114].

**Bidomain model: the virtual electrodes**

Virtual electrodes denote the regions of positive and negative polarization of the tissue that are produced during the stimulation of the tissue, but away from the stimulus site. Virtual cathode refers to the sites of positive polarization change and virtual anode to the sites of negative polarization change. This phenomenon, although not termed like that, was first identified experimentally. Hoshi and Matsuda, in 1962, studying the excitability of Purkinje fibers, suggested that anodal stimulus could cause cathodal effects in the vicinity of the electrode and vice versa for the cathodal stimulus. Also, in 1970, Wiederholt et al., studying the electrical stimulation of the nerve observed that sufficiently long stimulus can give rise to propagation of the wave at some distance from the electrode. These experimental results were in obvious disagreement with the predictions of the cable theory, but the multidimensional bidomain model proved to be able to accomodate these phenomena. Experimental evidence suggest [115] that conductivity of the heart tissue is anisotropic for both extra- and intracellular tissue. The conductance is higher in the direction of the fiber than in the direction perpendicular to the fiber. ($\sigma_{il}$=0.17 S/m,$\sigma_{it}$=0.019 S/m, $\sigma_{el}$=0.62 S/m,$\sigma_{et}$=0.24 S/m). The anisotropy ratio of the intracellular ($\sigma_{il}/\sigma_{it}$) and extracellular ($\sigma_{el}/\sigma_{et}$) space differ and this fact proved to be the cause of the above phenomena. The paper by Sepulveda et al. [116] described numerical experiment using bidomain model with passive properties of the two dimensional tissue in which unipolar stimulus is applied to tissue with equal and unequal anisotropy ratios. The results revealed that spatial distribution of currents and potentials is significantly different for the two cases of anisotropy ratios. For the case of equal anisotropy ratio, transmembrane potential decayed monotonically with increasing distance from the electrode. The tissue with unequal anisotropy ratio resulted with adjacent areas of both hyperpolarized and depolarized tissue, despite the fact the stimulus was unipolar. The area under the cathodal stimulus was depolarized, as expected. Approximately 1-2mm from the stimulus site two virtual anodes were located symmetrically around the stimulus site. This characteristic position of negatively and positively polarized regions resulted in the name "dog-bone" pattern. Several years later, optical mapping studies performed by three groups [18, 117, 118] confirmed these theoretical predictions.

### 1.3.3. Defibrillation theories

**Critical mass hypothesis**

The critical mass hypothesis assumes that the basic mechanism behind the defibrillation is that the shock induces depolarization of refractory and rested tissue. Activating fronts collide with the unexcitable tissue and cease to exist. According to this hypothesis, in order for the heart to be defibrillated, not all the myocardium needs to be stimulated, only a critical mass. This notion was first observed by Garrey [119] in 1914 and later expanded in experiments performed by Zipes [120] and Witkowski [121]. Garrey observed that around 75% of the fibrillating mass needs to be removed before fibrillation ceases. Zipes studied induction of fibrillation in canine hearts. He used epicardial electrodes to record electrical activity. A hyperkalemic infusion was infused to selected parts of the coronary artery. The role of the hyperkalemic solution was to depolarize the tissue and subsequently render it unexcitable. It was found that as the percentage

of depolarized tissue increased, the probability of defibrillation also rose. The authors also noted that fibrillation would continue in the remaining parts of the myocardium, not affected by the hyperkalemic solution, but cease briefly. The conclusion "Therefore, the remaining number of excitable cells represented a critical mass insufficient to maintain fibrillation" [120]. Witkowski undertook another comprehensive experimental study to test this hypothesis. The experiment was designed to record voltage gradient generated by the shock at 120 locations on left and right ventricles. The authors find that for "subthreshold defibrillation shocks, multiple areas were found fibrillating and VF resumes initiated from multiple sites. As one approaches defibrillation threshold, greater volumes of fibrillating tissue are terminated with resultant smaller areas left fibrillating, and the locations of these residual areas lie in the regions in which the voltage gradient produced by the shock is the lowest".

### Upper limit of vulnerability hypothesis

The upper limit of vulnerability hypothesis states that the defibrillation shock needs to be strong enough to stop all existing fronts, but also small enough not to induce new ones. Fabiato and colleagues [122] were the first to observe a correlation between defibrillation threshold and what is now called upper limit of vulnerability (ULV). Fibrillation was induced in canine hearts by delivering external stimulus during the T-wave of cardiac cycle. As the shock energy was increased, it was harder to induce the VF up to a limit above which it was not possible at all to induce VF. Thus, induction of fibrillation by premature stimulus not only has lower limit, but also has a upper limit, later called upper limit of vulnerability. In addition, they found that strength of upper limit was similar to defibrillation threshold. The latter was also confirmed in other experiments. This finding was further broadened by experiments of Chen and colleagues [22, 123–126]. Using electrical mapping technique experiments revealed that failed defibrillation shocks are followed by cessation of electrical activity (for 64±22ms) after which ventricular fibrillation ensues again [123]. The successful defibrillation is followed by longer window of quiescent electrical activity (339±292). This was in direct contradiction with critical mass hypothesis. The ULV hypothesis proposed that in order for the defibrillation to be successful, it must halt all the existing fibrillating fronts, but also it must not induce new ones. Given the correlation between defibrillation threshold (DFT) and ULV, it was reasoned that the same mechanism inducing VF can underlay defibrillation process. If the VF is sustained by reentry, then some portions of the myocardium are in the vulnerable phase. Therefore, it is possible that the external shock induces new fibrillating fronts. According to the ULV hypothesis, potential gradient caused by the shock needs to be greater then the ULV throughout the fibrillating tissue. The question brought up was how does the external stimulus induce new fibrillating fronts not present prior to shock. The answer was offered by progressive depolarization hypothesis.

### Progressive depolarization hypothesis

The progressive depolarization hypothesis, also known as refractory period extension hypothesis, was proposed by Dillon and Kwaku [127] and is based on the their optical mapping studies. It incorporates elements of both critical mass and ULV hypothesis in an effort to unify the differences of the two proposed hypotheses. Dillon and Kwaku observed that, defibrillation shock, if sufficiently strong, will elicit a propagating front. At the same time, shock will prolong repolariza-

tion and refractory period of the myocardium. The strength of the shock will determine the area of the shock-depolarized myocardium. In summary : (1) Progressively stronger shock depolarize (2) Progressively more refractory myocardium to (3) Progressively prevent postshock waveforms and (4) prolong and synchronize postshock repolarization, in a (5) Progressively larger volume of the ventricles, to (6) Progressively decrease the probability of fibrillation after the shock."

**Virtual electrode theory of defibrillation**

Previous theories of defibrillation have accounted for the stimulatory effect (tissue depolarization) of the defibrillation. As a consequence of that, action potential will be prolonged if the tissue is found in refractory state or a new AP will ensue if the tissue was excitable. Virtual electrode theory of defibrillation takes into account an additional effect of the shock: hyerpolarization of the tissue by the shock. Hyperpolarization can shorten the action potential duration, a process that is called de-excitation. If de-excitation is followed by another excitation, the event is called re-excitation. Virtual electrode theory of defibrillation takes into account that a shock can induce a reentrant arrhythmia and assumes that "defibrillation shock will fail because they either leave the fibrillating myocardium unaffected or because they produce a new reentrant arrhythmia". The key factor in the arrhythmia induction is the hyperpolarization induced de-excited tissue that can serve as a substrate for new reentrant wave. A monophasic shock will result in hyperpolarized and depolarized regions adjacent to one another. Depolarized region will interact electrotonically with the hyperpolarized region to create a new wave of reentry in a process called break excitation [19, 128]. Thus every virtual anode created during the shock can serve as an excitable gap for a reentry pattern. If the post-shock excitable gap is not eradicated on time, defibrillation fails. Higher shock strength will create a higher gradient between negative and positive polarizations which will lead to smaller latency of break excitations [129]. Higher shock will also cause higher propagation velocity of the break excitations [130]. Thus, a break excitation with a higher shock strength will move through excitable gap faster and reach depolarized tissue by the (virtual) cathode faster. If the shock is high enough, the returning depolarization wave will encounter the refractory tissue which will impede further propagation. The shock of smaller strength will lead to smaller velocity of the break excitation and the returning wavefront will encounter the tissue in the rest state thus allowing for the reentrant pattern to ensue.

# Chapter 2

# One-dimensional ring as a model to study defibrillation

In this thesis our main concerns are the underlaying mechanisms behind the defibrillation process. Prior to the application of the external stimulus, the cardiac tissue is in a completely disordered state, considered to exhibit spatio-temporal chaos. The application of high external shock to this highly disorganized system, i.e. defibrillation, is done in order to reset the dynamics, i.e. to allow to the sinoatrial cells to set the regular pace again. What are the processes that are taking place between the initial chaotic dynamics and the posterior resting state are not completely known. The parameter space of the whole-heart simulation is huge and three-dimensional simulations computationally expensive. Therefore, it seems reasonable to start with a (relatively) simpler model. Reentrant wave in one dimension is often employed as a simplified model of reentrant waves in higher dimensions. As such, this simplification of tachyarrhythmic behavior was also used to study interaction of reentrant dynamics with external stimuli. Starting with the work by Glass and Josephson [27], in which one dimensional geometry was used to study annihilation and resetting of reentrant wave, it was further broadened by inclusion of heterogeneities and multiple stimuli [131–136].

The numerical experiments described in this thesis use a one-dimensional geometry to test for different shock protocols and elucidate the underlaying dynamics. The circulating wave that is present prior to the application of the external shock mimics the reentrant properties of the tachyarrhythmias and the fibrillation. Fig. 2.1 depicts the scheme of the numerical experiments performed here. Ring-like structure denotes the circulating wave on a ring. The darker shading corresponds to the depolarized front and lighter colors correspond to the back and to the parts of the ring in the resting state. Two oppositely placed arrows denote electrode locations where the stimulus is applied. The two electrodes are opposite in polarity so that the total external current is equal to zero. The shock is applied and the events that ensue lead either to the successful or unsuccessful result. The shock is evaluated unsuccessful if, after a certain lapse time, a circulating wave front is still observed. If the dynamics has ceased and the ring is in the resting state, the shock is considered as successful.

In this chapter we will introduce the details of the one-dimensional system representing the arrhythmic dynamics and the numerical experiment design to study defibrillation protocols.

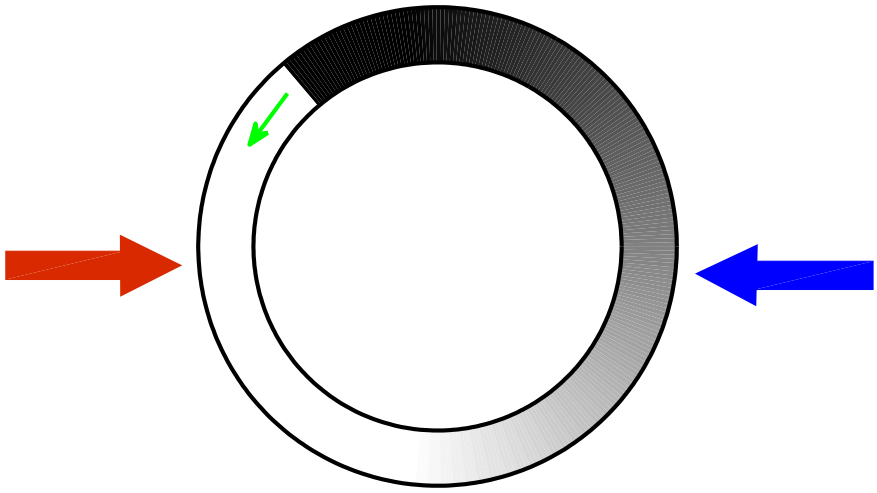

Figure 2.1: Scheme of a typical numerical experiment performed in this thesis. A shock is applied to a wave circulating in counter-clockwise direction. One-dimensional geometry with periodic boundary conditions mimics the reentrant properties of tachycardia and fibrillation. The shock is evaluated successful if all the activity has ceased and unsuccessful if a reentrant wave is still found after a certain lapse of time.

## 2.1. Cellular model

Active properties of the cell membrane are described using the Beeler-Reuter model [137] with two modifications to account for the phenomena occurring during defibrillation, namely electroporation and anode break phenomena. Fig. 2.2 shows a schematic view of the currents and corresponding gates (in brackets) included in the simulations. The currents depicted with black arrow correspond to the Beeler-Reuter model [137], the red arrows denote the additional currents to account for electroporation and anode break phenomena and the gate colored in green represents a change done to achieve a chaotic dynamical state [138] on the one-dimensional ring. The sum of all ionic contributions as used in simulations is given by Eq.(2.1). The first four members are part of Beeler-Reuter model, $I_{fu}$ denotes the current associated with the anode break phenomenon and $I_{ep}$ the electroporation current.

$$I_{ion} = I_{Na} + I_s + I_{x_1} + I_{K_1} + I_{fu} + I_{ep} \tag{2.1}$$

### 2.1.1. Beeler-Reuter model

The Beeler-Reuter model, formulated in 1977, was the first model that described dynamical behavior of ventricular cells. The model has served for a large number of important discoveries [128, 139, 140]. It is still widely used today, mainly due to significantly lower computational cost with respect to newer and more detailed models for cardiac cells. The original Beeler-Reuter model describes four currents: fast inward current carried by sodium ions $I_{Na}$, slow inward carried mainly by calcium ions $I_s$, time-independent outward potassium current $I_{K_1}$ and a time-dependent

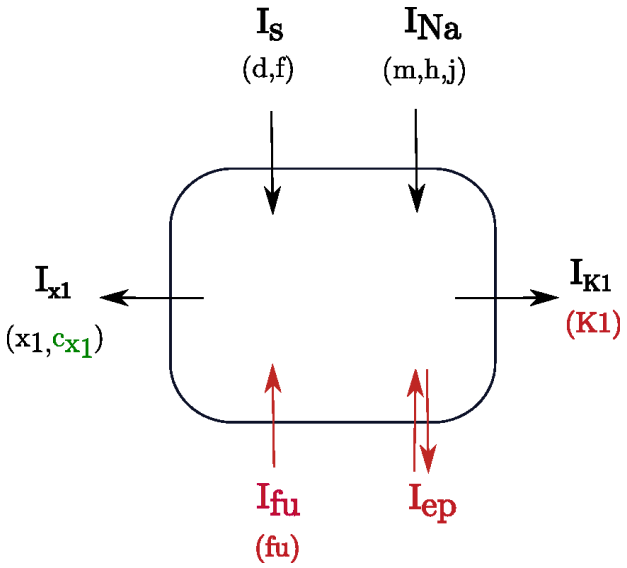


Figure 2.2: A schematic diagram showing the currents and associated gates. Black color depicts the original Beeler-Reuter model, green the modification done in order to render the dynamics chaotic and red the modifications to account for defibrillation induced phenomena: electroporation ($I_{ep}$) and anode break phenomena ($I_{fu}$).

outward potassium current $I_{x_1}$ (see Eq.(2.2)). In addition, the model also incorporates a basic description of intracellular calcium concentration dynamics Eq.(2.3). The gating dynamics is described with the Hodgkin-Huxley formalism Eq.(2.4). Besides the transmembrane potential $V_m$, the Beeler-Reuter model uses seven state variables : $[Ca^{2+}]_i$, the intracellular calcium concentration, $d$ the calcium activation gate, $f$ the calcium inactivation gate, $m$ the sodium activation gate, $h$ sodium inactivation gate, $j$ sodium inactivation gate, $x_1$ potassium activation gate.

$$I_{BR} = I_{Na} + I_s + I_{x_1} + I_{K_1} \tag{2.2}$$

$$\frac{d[Ca]_i}{dt} = -10^{-7} I_s + 0.07(10^{-7} - [Ca]_i) \tag{2.3}$$

$$\frac{dy}{dt} = \frac{(y_\infty - y)}{\tau_y} \tag{2.4}$$

The parameters of the Beeler-Reuter model were fitted to experimental data obtained in the normal physiological range. When an external stimulus is applied to the cardiac tissue, the transmembrane potential reaches values much higher or lower with respect to the ones observed in normal conditions. What are the effects of elevated values of $V_m$ and how numerous adverse effects associated with defibrillation are produced is not yet fully understood. However, some phenomena are described in the literature and both numerical and experimental studies have demonstrated that they indeed do play a role in defibrillation process. For that reason, we have modified the original Beeler-Reuter model.

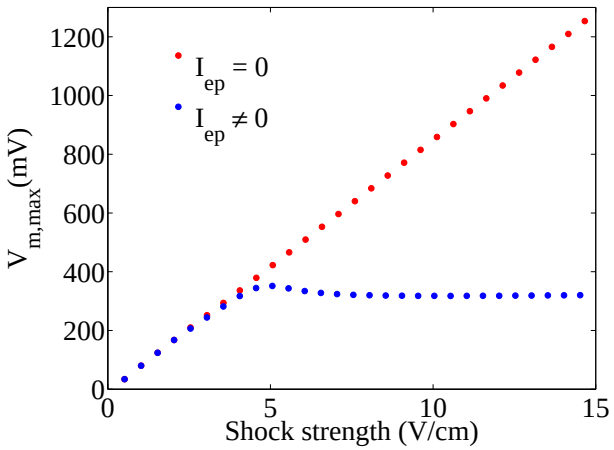


Figure 2.3: Comparison of simulation result with and without electroporation current in the one-dimensional model used in this thesis. Here, the electroporation current $I_{ep}$ is modified following the work by DeBruin and Krassowska [141].

### 2.1.2. Electroporation

Electroporation is an abrupt increase in the conductivity of the cell membrane due to the presence of a large external electrical field. For the case of lipid bilayer membrane the increase in membrane conductance is from five to six orders of magnitude [4]. This increase in the membrane conductivity is achieved by the formation of unselective, water filled pores in the cell membrane. The process can end with the pores resealing in which case the membrane is enabled to form the pores in subsequent similar conditions, or it can end in mechanical rupture of the cell membrane. The presence of electroporation for myocardial cells was found experimentally on single cell [142, 143] and tissue level [144–146]. The size of the created pore is of the order of the nanometer and the time scale associated with the creation and growth of a single pore is of the order of microseconds. Thus experimental study of the electroporation process was hindered by the spatial and time scales of the pore creation. Electroporation is usually considered as an undesirable effect of the defibrillation stimulus. However there are experimental and numerical studies showing both profibrillatory and tissue damage effects of the electroporation [147] as well as the anti-arrhythmic effects [146].

Experiments have shown that the saturation of the transmembrane potential with increasing strength of the external electric field. Specifically, experiments performed by Zhou et al. on guinea pig papillary muscle showed the saturation of the $V_m$ for field strengths greater than 7V/cm [148]. This behavior was not reproduced with known physiological models of the membrane kinetics. DeBruin and Krassowska suggested that this behavior might be attributed to the electroporation and developed a formalism in which an electroporation current ($I_{ep}$) depends on the opening and resealing of pores and has a nonlinear dependence on $V_m$. Electroporation conductance is an instantaneous function of $V_m$ based on the Planck-Nernst equation for movement the of ions through the membrane. It is described with a first-order differential equation for pore creation kinetics. The electroporation current $I_{ep}$ as modeled by DeBruin and Krassowska [141] was incorporated to the present cellular model. Fig. 2.3 shows a comparison of the maximum $V_m$ value on a one-dimensional ring with and without the incorporation of electroporation current.

From Fig. 2.3 it appears clearly that without the inclusion of electroporation, the maximum $V_m$ grows linearly with increasing stimulus, while with the inclusion of the electroporation current, the maximum $V_m$ saturates.

$$I_{ep} = g_p(V_m)NV_m \tag{2.5}$$

$$\frac{dN}{dt} = \alpha e^{\beta(V_m)^2}(1 - \frac{N}{N_0}e^{-q\beta(V_m)^2}) \tag{2.6}$$

where $g_p$ is the conductance of a single pore and $N$ is the number of pores per unit membrane area, $N_0$ is the number of pores per unit area for $V_m = 0$, and $\alpha$, $\beta$ and $q$ are physical parameters. The values of these parameters are $\alpha = 200.00\text{cm}^{-2}\text{ms}^{-1}$, $\beta = 6.25 \cdot 10^{-5}\text{mV}^{-2}$, $q = 2.46$ and $N_0 = 1.5 \cdot 10^5\text{cm}^{-2}$.

### 2.1.3. Anode break phenomena

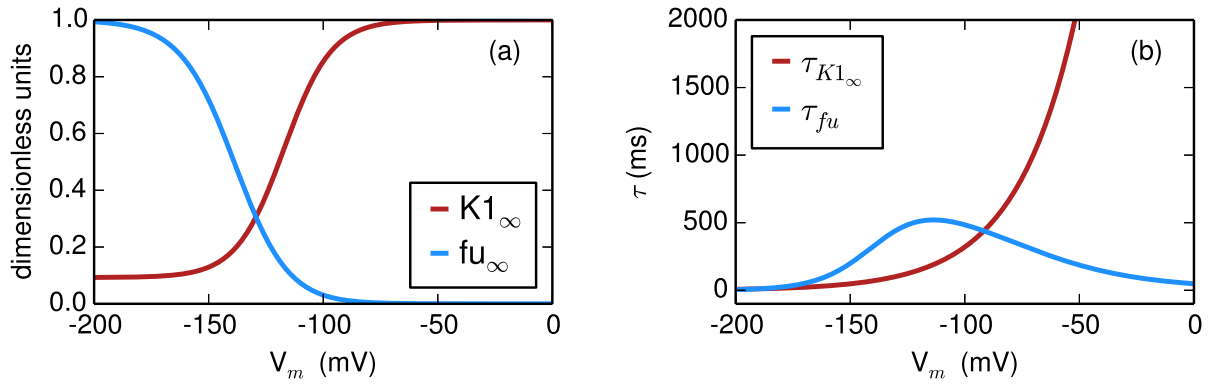


Figure 2.4: $I_{fu}$ current is modeled with one gate variable following the Hodgkin-Huxley dynamics. An additional gate is also added to the $I_{K1}$ current. a) Asymptotic values and b) Time constants of the added gates for the $I_{fu}$ current.

Experiments on mammalian ventricular tissue have shown that both cathodal and anodal stimulus can excite the tissue during (make excitation) or upon (break excitation) the termination of the external stimulus [149–151]. Cathodal stimulation is readily explained as the tissue beneath the electrode is directly depolarized. Anodal stimulations presented a curious paradox since the tissue beneath the electrode is hyperpolarized during the stimulus application. To this day there are two possible and mutually compatible explanations, one based on electrotonic effects and the other on the active membrane properties. The first explanation was developed with the use of simulations with bidomain model on two-dimensional cardiac tissue [116, 128]. It was shown that in the case of the tissue with unequal anisotropy ratio, virtual cathodes and anodes can be produced in the vicinity of the stimulus site. It was seen, that upon the termination of the anodal stimulus, excitation formed in virtual cathodes would diffuse into the area hyperpolarized by the anode, where the sodium channels were excitable and spread thereon. However, this hypothesis could not explain anode break phenomena on the single cell level, which was reported in experiments performed Ranjan et al. [151] on canine, rat and guinea pig ventricular myocytes.

In the paper by Ranjan et al., the authors propose the mechanism for the anode break phenomena that involves the appropriately timed dynamics of two membrane current. First, time independent potassium current $I_{K1}$ is blocked as the transmembrane potential becomes more hyperpolarized. As reported in [152], the blocking is both time and voltage dependent, being faster as the voltage becomes more negative. As the values of $V_m$ become more positive, but still hyperpolarized, channels of the $I_{K1}$ current are unblocked, and, again, the unblocking dynamics is both time and voltage dependent [151].

The second current involved in the anode break phenomena is found experimentally in mammalian ventricular myocytes to be activated for hyperpolarized values of transmembrane potential [151, 153, 154]. In papers describing the current it was called tentatively "the funny current" or "if-like" current due to its similarity with the original "funny current" described as a part of the DiFrancesco-Noble model for the pacemaker activity. This current was also found to be activated in the hyperpolarization range of the SA cells (-40 to 45 mV), inward in direction and composed mainly of sodium and potassium ions. Hence, it was considered that this current drives the transmembrane potential to the sodium threshold and enables the automaticity of the SA cells. The work done by Yu et al., using the whole-cell patch experiments on canine ventricular myocytes revealed that this analogue current in ventricular myocytes was activated in the range -120 mV to -170mV, and that it was also composed mainly of sodium and potassium ions and inward in direction. Similar finding were confirmed in [151] on canine, rat and guinea pig ventricular myocytes. Ranjan et al proposed the following hypothesis. During the anodal stimulus, the $V_m$ values are hyperpolarized and, depending on the stimulus strength and duration can activate the "funny current" ($I_{fu}$). This current, inward in direction, can help in bringing the $V_m$ values to the threshold for the sodium channels. The potassium $I_{K1}$ outward current, until the unblocking has terminated, will be reduced and thus potentiates the effect of any inward current. This hypothesis was validated with the model for the membrane kinetics incorporating the blocking and unblocking dynamics of the $I_{K1}$ current and $I_{fu}$ current. These current, fitted to the experimental finding, were added to the Luo-Rudy I model [155]. The simulation results confirmed the importance of the $I_{K1}$ unblocking in eliciting action potential in a single cell.

In the simulation study by Roth et al. [156], both active and passive influences were compared in cathodal make, cathodal break, anodal make and anodal break. The study used bidomain model for passive properties of two-dimensional media and Luo-Rudy I model with the modifications proposed by Ranjan et al. The conclusion was that the cathodal make and break and anodal make excitations are insensitive to $I_{fu}$ current. However, in the case of anode break excitation, both mechanisms contributed, but $I_{fu}$ contribution was dominant. In addition, for both cathodal and anodal excitations, $I_{fu}$ current improved the agreement between measured and calculated strength-duration curves.

Taking into account experimental and numerical results presented by Yu, Ranjan and Roth, we will assume that such active mechanisms of the membrane play a role in the anode break phenomena. During defibrillation, potential values are driven outside of the normal physiological range. Thus, anode break phenomena, as it can elicit an action potential, will presumably play a role in the defibrillation outcome. For that reason, we will add the model proposed by Ranjan et al. to the modified Beeler-Reuter model. Ranjan's "funny current" is modeled with the following equation:

$$I_{fu} = fu \cdot (V_m - E_{fu}) \cdot 0.1 \tag{2.7}$$

where $E_{fu}$ is the reversal potential for the $I_{fu}$ current (-29mV). The dynamics of the gate $fu$ is governed by the equation 1.4. The associated steady state value $fu_\infty$ and the time constant $\tau_{fu}$ of the $fu$ gate are given with the following equations (Eq. 2.8–2.11)

$$fu_\infty = \frac{\alpha_{fu}}{\alpha_{fu} + \beta_{fu}} \qquad (2.8) \qquad \tau_{fu} = \frac{1}{\alpha_{fu} + \beta_{fu}} \qquad (2.9)$$

$$\alpha_{fu} = 0.01824 \cdot \exp\left(-\frac{V_m + 170}{12.36}\right) \mathrm{ms}^{-1} \qquad (2.10)$$

$$\beta_{fu} = \frac{-0.074655}{1 + \exp\left(\frac{V_m - 29.056}{27.7}\right)} + 0.075955\,\mathrm{ms}^{-1} \qquad (2.11)$$

The steady state variable $fu_\infty$ and the time constant $\tau_{fu}$ are shown in Fig. 2.4 along with the steady state variable and the time constant associated with the potassium current $I_{K1}$.
The gating variable added to the potassium current $I_{K1}$ is also modeled with the Hodgkin-Huxlex formalims (Eq. 1.4). The steady state variable $K1_\infty$ and the time constant $\tau_{K1_\infty}$ are given by:

$$K1_\infty = 1 + \frac{-0.9075}{1 + \exp(\frac{V_m + 117.1}{10.37})} \qquad (2.12)$$

$$\tau_{K1_\infty} = 7.0602 \exp(\frac{V_m + 200.0}{26.22}) \qquad (2.13)$$

To conclude this section, we show in Fig. 2.5 the results of the stimulus application to the one-dimensional geometry. Stimulus current includes current given by the Beeler-Reuter model described in Sec. 2.1.1 and the current as modeled by Ranjan et al. [151] described in this section. Cathodal stimulus is applied at $3\pi/2$ and anodal stimulus at $\pi/2$. Extracellular stimulus is applied during 8ms. Fig. 2.5a shows the space-time plot of the $V_m$ values, while Fig. 2.5b shows values of $V_m$ at stimulus positions. One can see the onset of the excitation during the stimulus application at the position of the cathodal stimulus ($3\pi/2$). At the position of the anodal stimulus ($\pi/2$), where the tissue was hyperpolarized during the stimulus, one can also observe the onset of the two oppositely moving wavefronts, but this occurs after the stimulus has ceased.

## 2.2. Tissue model

Electrical properties of the cardiac tissue are described with the bidomain model (see section 1.1.4). Here we summarize the full equations as used in the simulations :

$$\frac{\partial V_m}{\partial t} = \frac{-I_m}{C_m} + \nabla(\mathbf{D_i}\nabla V_m) + \nabla(\mathbf{D_i}\nabla\Phi_e) \qquad (2.14)$$

$$\nabla[(\mathbf{D_i} + \mathbf{D_e})\nabla\Phi_e] = -\nabla(\mathbf{D_i}\nabla V_m) - \frac{I_e}{\chi C_m} \qquad (2.15)$$

where $V_m = \Phi_i - \Phi_e$ is the transmembrane potential, $\Phi_e$ the extracellular potential, $\Phi_i$ the intracellular potential, $C_m$ the membrane capacitance, $\chi$ the surface to volume ratio and $D_i$ and $D_e$ the intracellular and extracellular diffusion coefficients. $I_m$ is the total membrane current and $I_e$ the externally applied current. The possibility of including the $I_e$ term is a principal advantage of the bidomain model. The $I_e$ current can be a function of space and time, thus allowing for simulating shocks of different durations and locations in space. However, even though bidomain

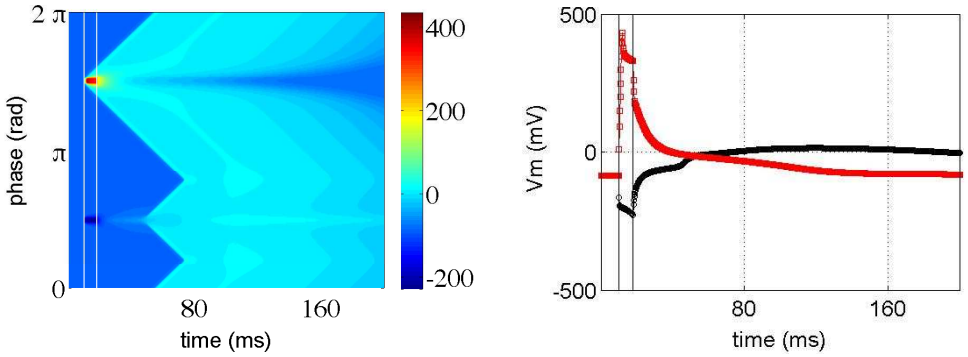


(a) (b)

Figure 2.5: (a) Space-time plot of the $V_m$ values on the one dimensional ring. Stimulus current is injected for a time duration of 8ms (within the vertical white lines). Cathodal stimulus is applied at $3\pi/2$ and anodal stimulus at $\pi/2$. Extracellular electric field during the stimulus is 18V/cm. One can clearly see the onset of cathode make during the stimulus duration and the onset of anode break after the stimulus has ceased. (b) The values of the $V_m$ potential at the stimulus positions. The values of $V_m$ at the cathode are denoted with red line, and values of the $V_m$ at the anode with black line.

approach is much more realistic than monodomain, it also comes with a greater computational cost. For that reason, for some calculations we will use the equivalent monodomain model. Under the assumption of the equal anisotropies, $\sigma_i = \alpha\sigma_e$, bidomain model can be reduced to monodomain [157]. Monodomain tissue conductance ($\sigma_m$) is then related to the bidomain conductances with : $\sigma_m = \sigma_i(\sigma_i + \sigma_e)^{-1}\sigma_e$.

### Intracellular tissue inhomogeneities

The bidomain model is a continuum representation of the myocardium in which the cell conductances are homogenized in space. The heart, however is inherently heterogeneous and this has proven to be important part of the mechanisms by which external stimulus excites the tissue. Local discontinuities such as cell to cell gap junction, intracellular clefts or fiber direction changes can act as redistribution centers of intracellular and extracellular current and therefore locally hyperpolarize or depolarize the tissue. Indeed, if the cardiac fiber were strictly homogeneous, the effect of the current injection would be localized to within the $O(\lambda)$ region surrounding the electrodes, where $\lambda$ is a characteristic length scale of the model defined by:

$$\lambda^2 = \frac{\sigma_i\,\sigma_e}{\sigma_m\,\beta\,(\sigma_i + \sigma_e)}\ , \tag{2.16}$$

where $\sigma_i$ and $\sigma_e$ stand for the intra-(extra)-cellular electrical conductivities, respectively, and have units of mS cm$^{-1}$; $\sigma_m$ is the membrane conductance and has units of mS cm$^{-2}$. The conductivities are related to the previously defined diffusivities by the following equation:

$$D_i = \frac{\sigma_i}{\beta\,C_m}\,, \tag{2.17}$$

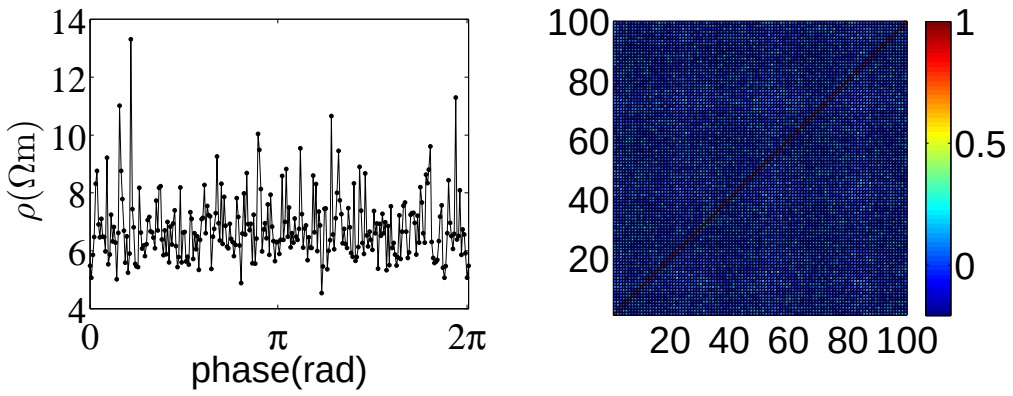


(a) (b)

Figure 2.6: Inhomogeneities in the cardiac tissue play an important role during defibrillation. Gaussian white noise is added to the intracellular conductance coefficients in the bidomain model. (a) Example of intracellular resistivity coefficients used in simulations along the ring. (b) Correlation coefficients of all the intracellular resistance coefficients used in simulations.

and a similar equation holds for defining $D_e$. By replacing parameter values of the present study in Eq. (2.16) we find $\lambda \approx 7.10^{-2}$ cm, which is indeed a typical value. The space constant is small compared with the typical spatial extent of the cardiac tissue.

Following the work of Fishler [158], we have added a gaussian white noise perturbation to the internal diffusion constants in the following way:

$$D_i(x_k) = \bar{D}_i(1 + \delta \cdot r_k) \tag{2.18}$$

where $D_i(x_k)$ is the value of the intracellular diffusion constant at site $k$ in the tissue, $\bar{D}_i$ is the average value of the intracellular diffusivity, $\delta$ is the amplitude of the noise and $r_k$ is the random number drawn from gaussian distribution with zero mean and unit variance. $\bar{D}_i$ is set to $1.5 \cdot 10^{-3}\text{cm}^2/\text{ms}$ and the amplitude of the noise $\delta$ is set to 0.15. Fig. 2.6a shows an example of the internal resistivity ($\rho_i$) obtained in this way along a one-dimensional ring of cardiac tissue.

## 2.3. Numerical methods

The full system of equations to be solved consists of the bidomain model given by Eq. (2.14), the Eq. (2.15) and the nine ODEs describing the gating dynamics (section 2.1) associated with the modified Beeler-Reuter model. To solve numerically this set of differential equations we have used finite differences as an approximation to the derivatives.

Let us first comment on the solution of the Eq. (2.15) which is the most computationally costly in the set of equations for this system. In order to solve the Eq. (2.15), it was first reduced to the form: $\mathbf{Ax} = \mathbf{b}$. $\mathbf{Ax}$ refers to the discretized version of the left-hand side of the equation and the vector $\mathbf{b}$ of the right hand side . Using finite differences, the left hand side of the Eq. (2.15) on the position $j$ on the ring is approximated with :

$$\nabla[\mathbf{D_i} + \mathbf{D_e})\nabla\phi_e] \approx \left\{(D_e^{j-1} + D_i^{j-1})\phi_e^{j-1} - (D_e^j + D_i^j + D_e^{j-1} + D_i^{j-1})\phi_e^j + (D_e^j + D_i^j)\phi_e^{j+1}\right\}/\delta x^2 \tag{2.19}$$

**A** reduces to a triangular matrix with tridiagonal values for the $i^{th}$ row : $[\phi_e^{j-1} \quad \phi_e^j \quad \phi_e^{j+1}]$. The vector **x** contains the values of the diffusion constants $[(D_e^1 + D_i^1) \quad \dots \quad (D_e^n + D_i^n)]$. The equation (2.15) is then solved for $\phi_e$ using the implementation of the iterative Krylov solver freely available within the PETSC library [159]. More precisely, the iterative method employed is the generalized minimal residual method (GMRES) [160]. The convergence of the iterative method was controlled by the residual norm relative to the norm of the right-hand side. The tolerance is set to the default value of $rtol$=$10^{-5}$ [159]. Having solved for the extracellular potential, the second bidomain equation is solved using a forward Euler explicit scheme. The time step during the defibrillation and 10 ms after the end of the shock is fixed to 0.001ms. For the rest of the stimulation, the time step is fixed to 0.01ms. Spatial discretization of the 6.7 cm long ring is set to $dx = 0.025cm$.

Besides from the change in time step after the defibrillation shock has terminated, another time saving method is applied. The parameters of the ODE equations mostly have exponential dependence. In order to avoid the repeated computation of time consuming exponential functions at every time step, look-up tables were built and used throughout the computation. In order to increase the simulation speed, some simulations were performed by using monodomain model instead of the bidomain whenever possible. This replacement is done in the following way. During the stimulus application and 10ms after the stimulus, full bidomain with time step of $dt = 0.001ms$ is used. For the next 10ms, calculations are still done with the bidomain model, but with time step equal to $dt = 0.01ms$. At this point, bidomain model is replaced with monodomain model for the rest of the simulation time. The time saved depends on the applied shock strength. If the shock strength is high, the outcome is most likely successful. In that case, simulations are stopped before the lapse time is over. If the shock leads to unsuccessful outcome, then the monodomain model replaces the bidomain model for most of the simulation time and the benefit in terms of the CPU saving is large.

## 2.4. Numerical experiment design

All the calculations presented here have been performed on a ring of cardiac tissue. The ring size ($L = 6.7$ cm) was selected in order to obtain a sustained discordant–alternans dynamics or with further modifications a chaotic dynamics. The numerical experiments designed here are used to test defibrillation shocks in the following way. We pick a very large sample of the quasiperiodic or chaotic dynamical states on the ring. Then a defibrillating shock is applied through the point electrodes for all the elements of this large sample. The defibrillation is classified as successful if all the activity has ceased in the lapse of time of 1000 ms after the end of the shock application. Otherwise, if the wave is still active after 1000 ms, the defibrillation is classified as unsuccessful. Success probability of each shock strength is calculated by averaging the results obtained with different initial conditions and different realization of Gaussian noise that are added on top of the intracellular conductivity (see section 2.2). Each added noise distribution represents a slightly different tissue to which the shock is applied. Initial conditions were obtained by saving all the variables associated with a propagating front, like the one shown in Fig.2.7a (prior to the shock application) at a randomly chosen instant in time. The random time interval between consecutive saved initial conditions is in the range of $[28, 38]$ ms. Fig. 2.7a shows one example of the above

described experiments. For time $< 0$ action potential is initiated and continues to freely circulate along the ring. Varying duration of the action potential is indicative of discordant alternans. At t=0 a monophasic shock is applied at the positions marked with white line. The anode is located at $\phi = \pi/2$ and the cathode at $\phi = 3\pi/2$. One can clearly observe a depolarized and hyperpolarized region in the vicinity of cathode and anode, respectively. In the shock shown in Fig. 2.7a the defibrillation was successful as all the pre-shock reentrant activity is eliminated. Fig.2.7b shows an action potential at one instant during the pre-shock activity. The Fig. 2.7b also shows parameters relevant for the analysis: the position of wave front $\phi_f$, wave back $\phi_b$ and the action potential duration $\Delta\phi$ expressed in term of the phase span.

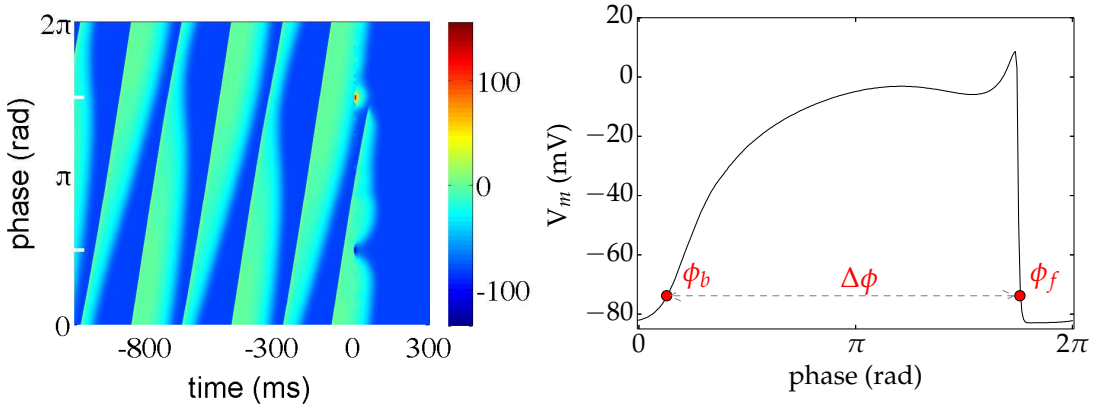


(a) (b)

Figure 2.7: (a) From [136]. Space–time plot showing the wave dynamics on the ring. The color scale represents the membrane potential $V_m$ ranging from -120 to 150 mV. The undisturbed dynamics ($t < 0$) represents discordant alternans. At $t = 0$ a monophasic shock of 8 ms duration with a corresponding electric field intensity of $E = 2$ V/cm is applied. In this particular case, the shock leads to a suppression of the wave propagation. The two electrodes are located at $\pi/2$ and $3\pi/2$ along the ring (shown by thick white segments in the figure). (b) Action potential drawn from the space-time plot on the left. $\phi_f$ and $\phi_b$ denote the position of wave front and wave back on the ring measured at 90% of repolarization. $\Delta\phi$ refers to the difference between the two (modulo $2\pi$).

### 2.4.1. Model parameters

#### 1) Dynamical state at the time of the shock

Initial condition refers to the state of the ring before the external shock is applied. By using the membrane current given by Eq.(2.1) the dynamics of the propagating wave is essentially determined by the size of the ring. If the size of the ring is large enough, the wave is in a periodic state. However, as the size of the ring is reduced, the wave will exhibit alternans and finally after a certain critical size the propagation will no longer be sustained. Examples of space-time plot with periodic, quasiperiodic and chaotic dynamic on the one-dimensional ring are shown in Fig. 2.8.

Fig. 2.9 shows return maps of action potential duration and discrete Fourier transform of two

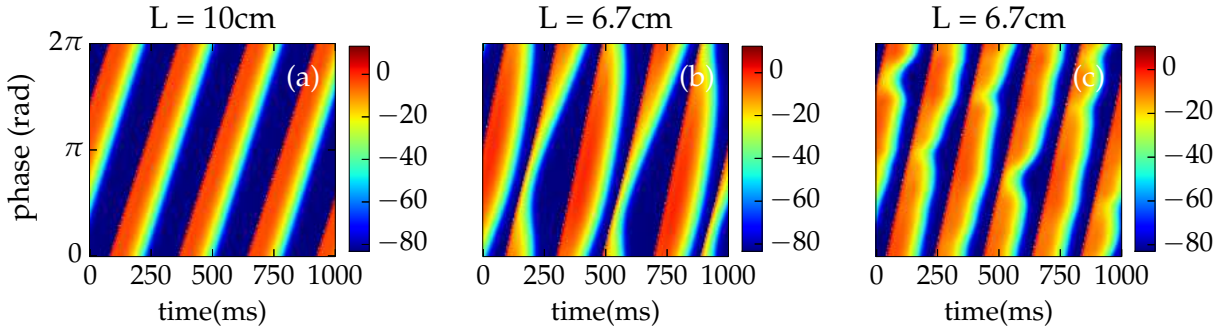


Figure 2.8: Dynamical states on a one-dimensional ring.

cases: quasiperiodic and chaotic state of the ring. Quasiperiodic state is achieved by reducing the ring size to $L = 6.7cm$ with the membrane dynamics as described in previous paragraphs. Quasiperiodic dynamics shown in Fig. 2.8 can be described with discordant alternans [161], characterized by varying duration of the action potential as it propagates. The associated frequencies can be determined by computing the Fourier spectrum. The two frequencies are approximately $f_1 = 5.07$Hz and $f_2 = 0.33$Hz. The first frequency is associated with the time it takes for a wave to make a trip around the ring, $T_1 = 197$ ms. The second frequency is associated with the time that it takes for a node (location where the action potential has a minimum duration) to make one revolution around the ring, $T_2 = 3030$ ms. Chaotic state is achieved with the same ring size, but with a perturbation added to the time-dependent potassium current ($I_{x1}$).

### Chaotic dynamical state

Recent experimental and numerical studies [162, 163] suggest that fibrillation is a form of a spatio-temporal chaos. Thus applying an external shock to the fibrillating tissue would have more resemblance to a real situation, if our numerical initial condition would also exhibit chaos. Qu et al. [138] proposed an elegant approach to study the spatio-temporal chaos in a cardiac tissue. The model used by these authors was based on the monodomain formulation for electrical propagation and the Beeler-Reuter model for the description of the cell membrane. In order to change the restitution properties, a modification is added to the time-dependent outward potassium current $\mathrm{I}_{x_1}$ of the Beeler-Reuter model. A conductance $\mathrm{g}_{x_1}$ is modified in the following way :

$$I^c_{x_1} = g_{x_1}(t')I_{x_1}x_1 \tag{2.20}$$

$$g_{x_1}(t') = \begin{cases} 1 - aF(t') & t' \in [0, \mathrm{APD}] \\ 1 - aG(t') & t' \in [0, \mathrm{DI}] \end{cases} \tag{2.21}$$

where $I^c_{x_1}$ denotes the modified version of the time-dependent potassium current. Functions $F(t')$ and $G(t')$ are given by:

$$F(t') = G(DI) + \int_0^{t'} m^3 hj\theta(x_1)dt' \tag{2.22}$$

$$G(t') = F(APD)exp(-t'/T) \tag{2.23}$$

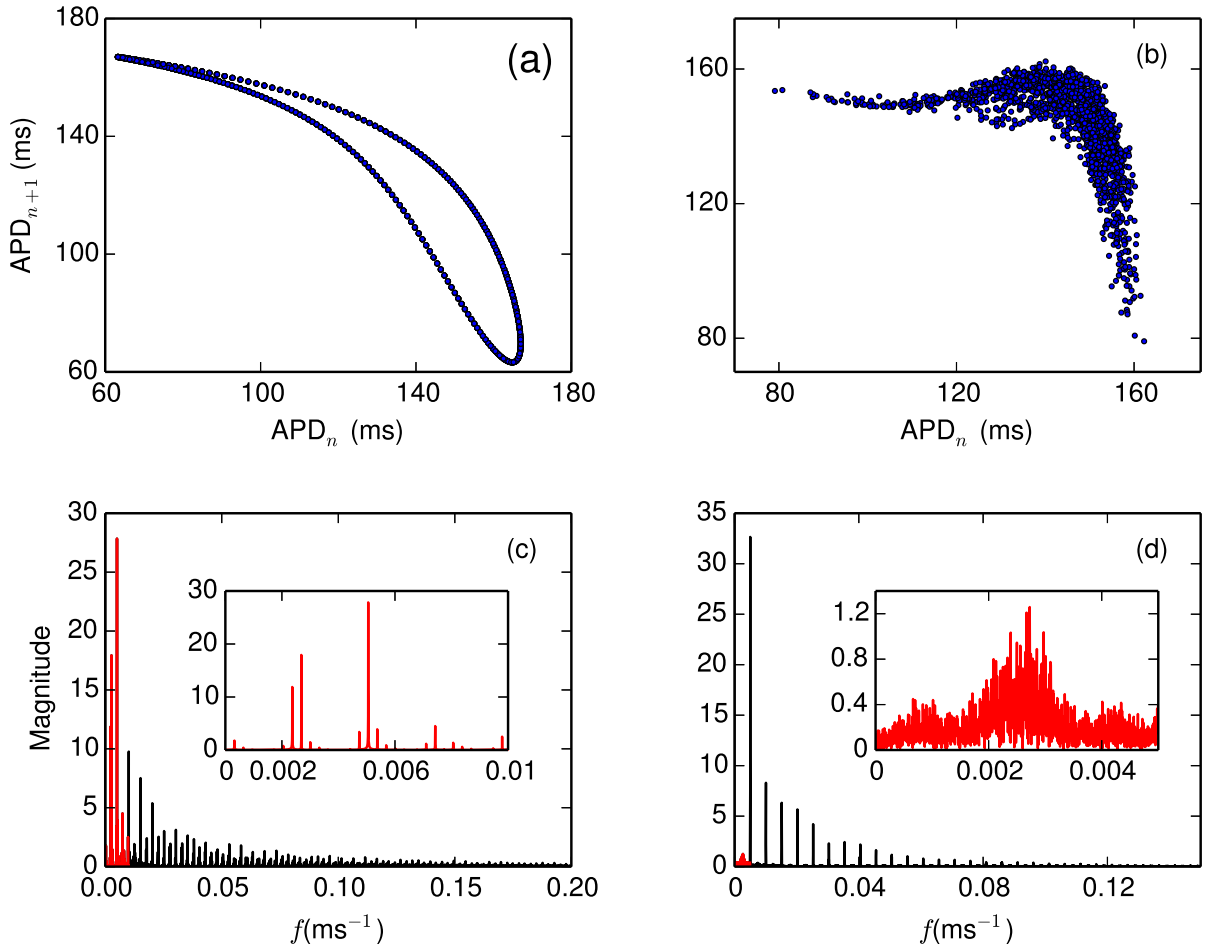


Figure 2.9: Return map of APD for (a) quasiperiodic and (b) chaotic state of the ring. Discrete Fourier transform of the transmembrane potential $V_m$ recorded at the middle of the ring ($x = \pi$) for (c) quasiperiodic and (d) chaotic state of the ring. The inset to each graph serves to enlarge the small portion of the x-axis. The enlarged area is denoted with red color in both the main graph and the inset graph.

More details can be found in [138]. By changing the constant $a$ , four regimes of dynamic were found : (1) periodic, (2) quasiperiodic with monotonic APD restitution curve, (3) quasiperiodic with non-monotonic APD restitution curve and (4) spatio-temporal chaos. Fig.2.9.b shows a return map of APD for $a = 0.9$ and ring size of $L = 6.7cm$.

### 2) Heterogeneity

As previously explained, a perfectly homogeneous heart tissue would not be capable of defibrillation. Fluctuations in conductivity act as polarization sites that can excite the tissue. The higher the noise intensity, the lower is the energy required to defibrillate the heart [164]. Throughout the thesis we will set the amplitude of heterogeneity to $\delta = 0.15$ (see eq.2.18), although in section 3.1.3 we will use other values of the $\delta$ parameter as well.

### 3) Shock protocols

The most common protocols used in commercial defibrillators are monophasic and biphasic. Now-days, most of the new defibrillators are biphasic due to their superior efficiency. An asymmetric biphasic protocol where the first phase is longer than the second phase is currently the method of choice. In Fig. 2.10 we illustrate graphically the three protocols compared throughout this thesis: monophasic (M), biphasic I (B1) and biphasic II (B2).

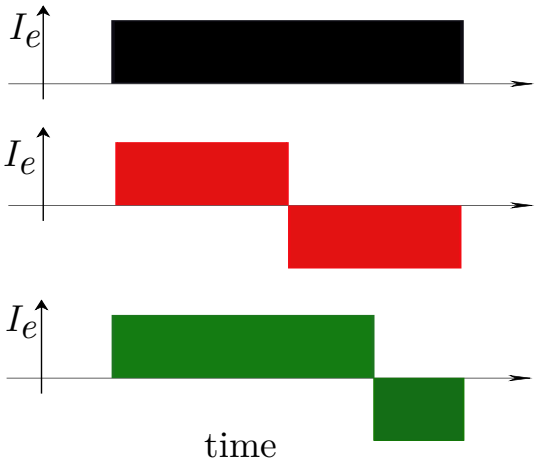


Figure 2.10: Schematic view of the three tested shock protocols. (upper) Monophasic, polarity of the actuators is fixed during the shock. (middle) Biphasic I, polarity of the actuators is reversed at the middle of the shock. (bottom) Biphasic II, polarity of the electrodes is reversed at 3/4 of the total shock duration.

### 4) Shock waveform

As shown in Fig. 2.10 defibrillation waveform is approximated with step functions for the switching on and off of the shock which is a practice common in analytical and numerical studies. Current defibrillators, both external and implanted apply a shock via a capacitive discharge. The time dependence of the applied voltage has an exponential decay : $V(t) = V_0 \cdot e^{-t/\tau_{RC}}$, where the time constant $\tau_{RC}$ is equal to product of the pathway resistance $R$ and the capacitance $C$, $\tau_{RC} = RC$. Another practice is the truncation of the exponential waveform. It was shown that cutting the trailing edge of the exponential waveform improves the efficiency [23, 87, 165]. Manufacturers truncate the waveform either by duration or tilt. Another novelty, for now present only in the scientific literature are the ascending waveforms (ramp or exponentially ascending) that show a lower defibrillation threshold compared to monophasic and biphasic waveforms [80, 83, 166]. In this thesis, we will use the simplified rectangular waveform to validate and analyze the one-dimensional model.

### 5) Shock duration

One of the basic characteristics of electrical defibrillation is the strength-duration relationship, or the effect of pulse width on defibrillation efficacy. This relationship, approximately hyperbolic,

Parameters and abbreviations

| 1-D system | | | Defibrillation | | |
|---|---|---|---|---|---|
| Intracell. diffusion constant | $\bar{D}_i$ | $1.510^{-3}cm^2/ms$ | Shock duration | T | $T \in (1, 15)ms$ |
| Extracell.diffusion constant | $\bar{D}_e$ | $1.510^{-3}cm^2/ms$ | Shock strength | E | (V/cm) |
| Noise amplitude | $\delta$ | 0.15 | Shock waveform | SW | Rectangular |
| Dynamical state | QP | Quasiperiodic | | M | Monophasic |
| | Ch. | Chaotic | Shock protocol | B1 | Biphasic I |
| | | | | B2 | Biphasic 2 |
| Ring size | $L$ | $6.7cm$ | | | |
| Membrane capacitance | $C_m$ | $1\mu F/cm^2$ | | | |

Table 2.2: This table lists the important parameters of the 1-dimensional ring study and their abbreviations as used throughout this thesis.

has served for the design of clinically applied waveforms [4, Ch. 6.1]. The construction of strength-duration curve requires a large number of experiments and therefore cannot be obtained directly for humans. The curve is usually inferred from experiments performed with animals. In chapter 3 we will analyze in detail the mechanisms behind a shock duration of 8ms. In the same chapter we will investigate the effects of shorter and longer pulse durations.

**6) Shock energy**

As expected, shock energy is another parameter influencing defibrillation. Shock strength is measured by evaluating the applied electric field resulting from the current injection (term $I_e$ in Eq. (2.15)). Its value is given by $E = (\Phi_a - \Phi_c)/\Delta L$, where $\Phi_a$ and $\Phi_c$ denote the extracellular electrical potential of the anode and the cathode and $\Delta L$ the distance between them. Note that for rectangular waveform, electric field is constant in magnitude, but switches sign after each electrode. The square of the electric field is directly proportional to the shock energy. Here we will study shocks of increasing energies. Shock strength will be increased until 100% of defibrillation is achieved. For the case of 8 ms shock duration studied in the next chapter, the shock strength will be increased from 1V/cm to 10V/cm. This will allow for the construction of percent-success [167] or dose-response curves. It is known that the curve follows a sigmoid shape that can be modeled with a logistic curve.

**7) Shock timing**

At the time of the application of the shock, we will record $\phi_i$ and $\phi_b$, defined to be location of the action potential wave front and wave back, respectively. The wave front and the wave back are defined as the points at which the membrane potential crosses a threshold value representing 10% of the maximum value of $V_m$ during depolarization.

## 2.5. Mechanisms for elimination of reentrant dynamics

After inspecting many defibrillation outcomes for different protocols and shock strengths we have come to a conclusion that these might be classified into four different mechanisms. The four identified mechanisms are shown in Fig. 2.11. The first row of Fig.2.11(a-c) illustrates three examples of the mechanism we defined as Direct block (DB). It is the least common mechanism, present only at low shock strengths and typical mainly for monophasic protocol and to a smaller extent for biphasic 2 protocol. The front, just prior to the shock is located very close to the anode and is directly blocked by the shock-hyperpolarized region in front of it. Fig. 2.11(a,c) show an examples of DB where the shock protocol is monophasic shock and shock strengths are 1V/cm and 3V/cm. Fig. 2.11(b) shows the DB mechanism with the biphasic II protocol.
Fig.2.11 (d-f) shows examples for the second identified mechanism : Annihilation (An). In this case, the reentrant dynamics is eliminated when two oppositely propagating front collide and annihilate after which there are no remaining front present in the system. Three examples shown on Fig.2.11 (d-f) illustrate annihilation for increasing shock strength. For low shock strength (E= 1V/cm), annihilation is achieved with initial front and a front emerging from the cathode. By increasing the shock strength, annihilation can be achieved with fronts emerging from virtual cathodes. The Annihillation mechanism is found to be characteristic for lower or medium shock strengths.
Delayed block, the third mechanism, is shown in Fig.2.11 (g-i) and encompasses the situation when single surviving front, that otherwise would lead to unsuccessful defibrillation, encounters a refractory region and dies out. It is characteristic of all the three tested protocols.
Direct activation (DA) is characteristic of high shocks strengths. It consists in the activation of the tissue in such a way that no posterior propagation of the wave is possible. Most of the ring is excited, the wave front cannot propagate and eventually the entire tissue is relaxed toward the rest state. The DA mechanism is the defibrillation mechanism that is usually known and referred to in the medical literature.

### Classification of defibrillation mechanisms using Artificial Neural Networks (ANNs)

Due to the large number of simulations (at least 50000 = 50 noise distributions x 1000 initial conditions for each shock strength), manual classification of the defibrillation mechanisms would result extremely time consuming. Thus we sought a method to automatize the classification process. We have chosen the artificial neural network (ANNs) tool [168], by now a widely used computational tool for machine learning and pattern recognition. ANNs are usually described as a computational tool based on neural structure of the brain, although by today "artificial neural networks are no more related to real neurons than feathers are related to modern airplanes" [168]. ANNs has two modes of operation: training and using. While in training mode, network is trained to associate input parameters with the given outputs. While in using mode, network will give the output that best corresponds to the learned input pattern. Pattern recognition, the tool we will use to classify defibrillation mechanisms, is performed using the feed-forward network which allow the signal to propagate only one way: from input to output. For each defibrillation trial, during and posterior to shock duration, ring is analyzed at every millisecond for the location and direction of all the present waveforms. At the end of the simulation, defibrillation trial is described with

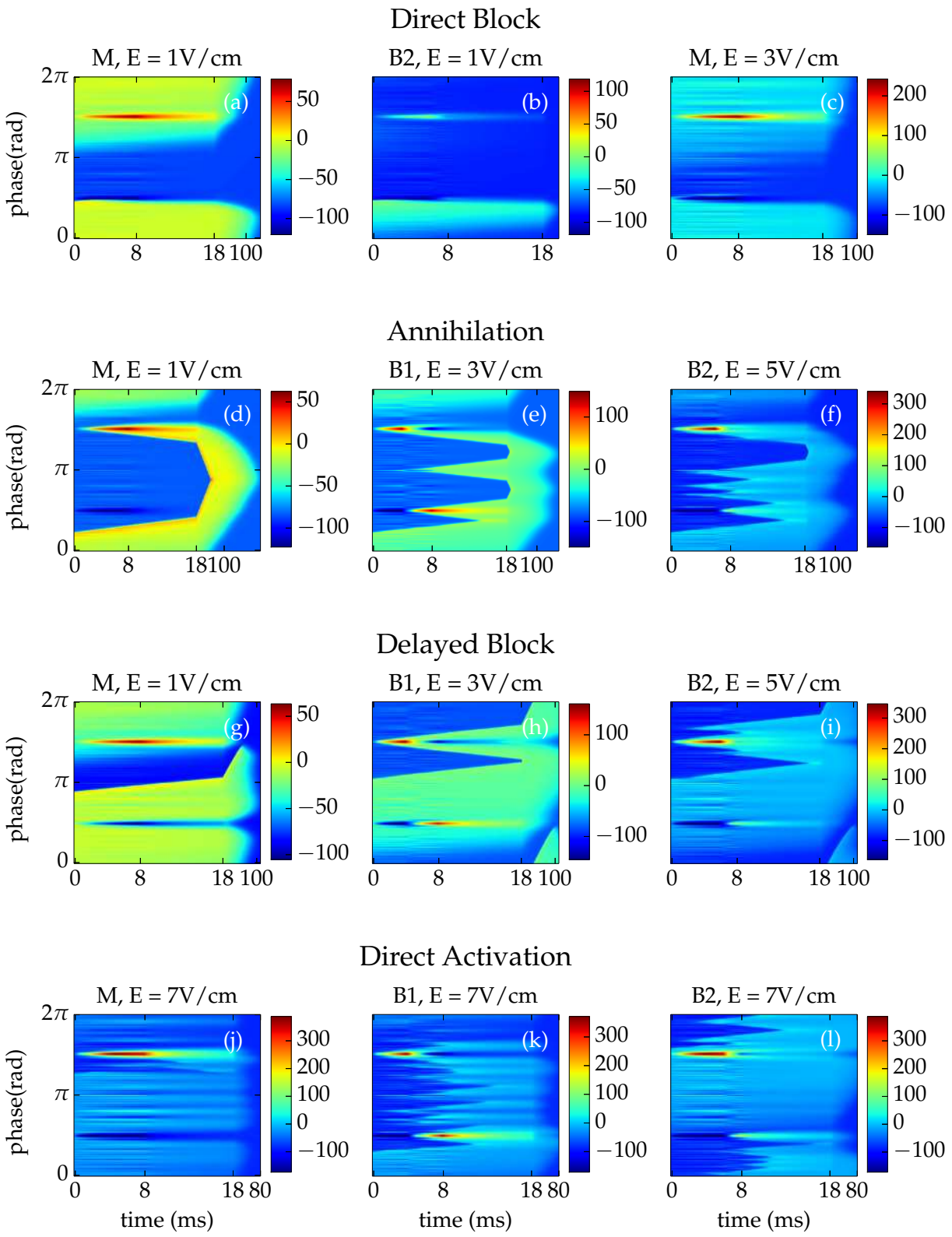


Figure 2.11: We have identified four different mechanisms that lead to successful defibrillation for a range of shock strengths giving low, medium and high success output. Each row in this figure gives an example of an identified mechanisms: (a-c) Direct block, (d-f) Annihilation, (g-i) Delayed block, (j-l) Direct activation. Examples show outcomes using one of the three protocols (M, B1, B2) and different shock strength (1V/cm, 3V/cm, 5V/cm, 7V/cm).

a number of parameters : initial front and back phase (see Fig.2.7b), wavefront width ($\phi_i - \phi_f$), percentage of maximum depolarized tissue for different threshold levels (-60mV, -30mV, 0mV) and corresponding timings, flags for two wavefronts of opposite direction and corresponding timings, etc. These parameters (total of 50) were used as an input vector for neural network training. A target vector was created by manually classifying a set of examples, different from the ones used to evaluate percent success for particular shock strength. Each target vector consisted of 400 examples for each protocol (M, B1 or B2), i.e. a total of 1200 examples for a particular shock shock strength. The set is then divided to a training set (960 trials) and a validation set (240 examples). Two neural network were then trained and validated : one with two hidden layers of 14 neurons and one with a hidden layer of 20 neurons. To further increase the accuracy, a total of five different partitions of initial set to training and validation set were created. Thus each classification was evaluated with total of ten results, two networks and five different partitions. For some cases of high shock strength, the number of ANNs is doubled to increase the accuracy. Neural network analysis is performed using MATLAB's Neural Network Toolbox [169]. Function *newpr* was used to create a pattern recognition network and function *train* to train the training data set. Resulting network is then used on a validation data set. Comparing both ANNs results for validation set and manually obtained results, a confusion matrix is calculated. The rate of false negative, false positive and true positive was used to iterate training until satisfactory result is obtained. The percentage of true positive was considered satisfactory if found greated than 90%.

# Chapter 3

# Application of the defibrillation: comparing the monophasic and biphasic shock protocols.

Having defined a one-dimensional model in the previous chapter, we will now use it to compare the three shock protocols commonly used in clinical practice : monophasic, biphasic I and biphasic II. First, a shock of duration of 8ms, which is the value typically used in commercial defibrillators, will be applied to both quasiperiodic and chaotic initial condition. Later we will test the model by varying the heterogeneity parameter $\delta$. The three models are also tested when varying the duration of the external stimulus.

## 3.1. Application of the 8ms shock

All three protocols are tested with shock strengths in the range of 1 to 10V/cm. The maximum tested shock strength, 10V/cm, already leads to the saturation of percent success to 100%, so this range of shock strengths allows for the construction of the dose-response curves and the overview of the three protocols for low, medium and high shock strengths. In addition to dose-response curve, we will compare the defibrillation mechanism of the three protocols for low, medium and high shock strength.

### 3.1.1. Quasiperiodic initial condition

#### Dose-response curves

A plot of defibrillation success versus shock strength results in a sigmoid shape curve analogous to the well known dose-response curve for a drug [91]. The percentage of success saturates for high shock strengths and approaches zero for very low shock strengths with a gradual transition in between. For this reason, defibrillation percentage of success is traditionally fitted to a logistic curve. In order to fit the logistic curve to the numerical data obtained with the one-dimensional model we will use the logistic regression, an approach often employed when one needs to predict a binary outcome given a set of continuous predictor variables. Let us denote the probability of a successful defibrillation for a given shock strength with $p$. Logistic equation can now be written

in a form better suited for regression:

$$\log\left(\frac{p}{1-p}\right) = \beta_0 + \beta_1 x \tag{3.1}$$

where x denotes the predictor, i.e. shock strength measured in the extracellular electric field. Coefficients $\beta_0$ and $\beta_1$ are evaulated using the generalized linear methods (GLM) [170]. For each value of the electric field, the collected data represents the outcomes of a total of 160,000 simulations: 2000 initial conditions times 80 realizations of the tissue heterogeneity [136]. We then compute the average probability of defibrillation for the 2000 initial conditions, so that we are left with only 80 data points for drawing the distributions. Fig. 3.1 shows both numerical results represented with box-plot and fitting results. Fitting to the logistic model (Eq. 3.1) is performed with the R software environment [171] for statistical computing using the *glm* function. The resulting coefficients are shown in Table 3.1. In addition to the logistic curve fit, we have performed an additional fit using a non-parametric approach. The reason for this second fit is twofold: (1) Box-Tidwell test [172] returned statistically significant coefficients for the added term $xlog(x)$ indicating that purely linear relationship between the predictor and the log odds might not be sufficient. (2) We will evaluate $E_{90}$ and $E_{50}$ values based on the resulting fit. $E_{50}$ and $E_{90}$ are the electric field strength values necessary to achieve 50% and 90% probability of reentrant dynamics removal. For this purpose, a non-parametric fit that follows the data closely, although lacks insights gained by modeling, could be a better choice. In addition, let us note that model fitting using least square approximation approach led to a non-normal distribution of errors. To circumvent these problems, the lack of normal distribution and the difficulty in model construction it carries, the second fit is performed with the generalized additive model (GAM) [173], an extension of the generalized linear model. The linear predictor is given by a user specified sum of smooth functions of the covariates plus a conventional parametric component of the linear predictor. The equation for the logit now takes the form:

$$\log\left(\frac{p}{1-p}\right) = \beta_0 + \beta_1 \cdot s(E) \tag{3.2}$$

in which $s(E)$ is a smooth function of the predictor which can take different forms. In order to perform the GAM fitting we will use the R package [171] *mgcv* [173–178]. The resulting fit is shown together with glm results in Fig. 3.1.

In order to compare the two fit, we report two measures of (relative) goodness of fit: Akaike information criterion (AIC) and explained deviance shown in Table 3.2. Despite the complex theoretical background in information theory, AIC criterion is frequently employed when comparing two or more models.The AIC value does not have absolute meaning, but only relative when compared to another model. The "best candidate" is then the model with the lowest AIC value. Explained deviance is one of many proposed measures of goodness of fit for the logistic regression devised to mimic the $R^2$ defined for the least squares regression methods. Explained deviance is defined as a ratio : (null deviance-residual deviance)/(null deviance). Null deviance is a deviance of a model that includes constant term only and the residual deviance is the deviance of the fitted model. Table 3.2 shows that GAM method results in lower AIC and explained deviance values when compared to the GLM output.

Both GAM and GLM results are used to evaluate $E_{50}$ and $E_{90}$. Results are shown in Table 3.1.

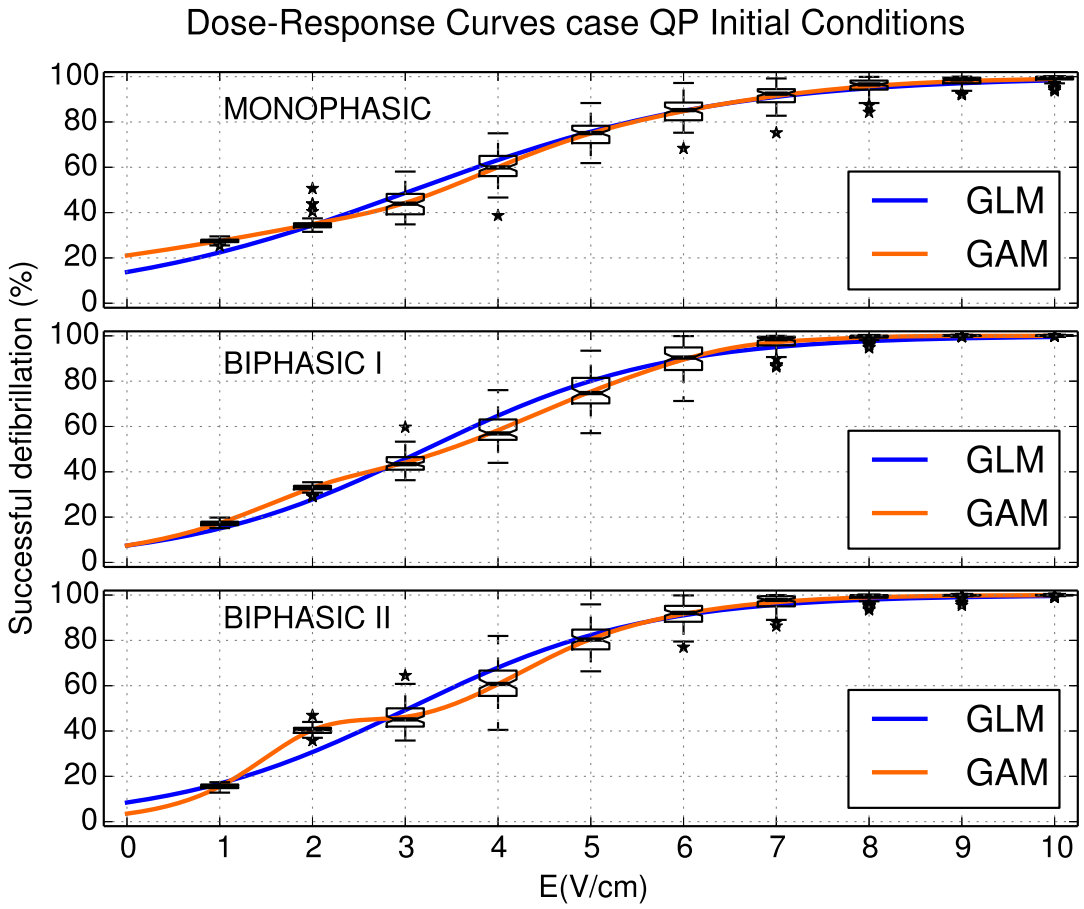


Figure 3.1: Numerical and model fitting results for a 8ms shock duration applied to quasiperiodic dynamical state of the ring with all three protocols. Numerical results are represented with boxplots. Two types of model fitting are performed. A fit to the logistic curve is performed with the GLM method and is shown with full blue line. The second fit used the GAM method and is shown with full orange line.

| | GLM | | | GAM | | |
|---|---|---|---|---|---|---|
| | Fit parameters | $E_{50}$ (V/cm) | $E_{90}$ (V/cm) | Fit parameters | $E_{50}$ (V/cm) | $E_{90}$ (V/cm) |
| M | $\beta_0 = -1.835_{(.004)}$ $\beta_1 = 0.5942_{(.001)}$ | [3.08 - 3.10] | [6.77 - 6.80] | $\beta_0 = 1.537_{(.004)}$ $\beta_1 = -$ | [3.38 - 3.41] | [6.71 - 6.77] |
| B1 | $\beta_0 = -2.521_{(.005)}$ $\beta_1 = 0.7826_{(.001)}$ | [3.21 - 3.23] | [6.02 - 6.04] | $\beta_0 = 2.71_{(.03)}$ $\beta_1 = -$ | [3.44 - 3.49] | [6.02 - 6.05] |
| B2 | $\beta_0 = -2.383_{(.005)}$ $\beta_1 = 0.7844_{(.001)}$ | [3.03 - 3.05] | [5.83 - 5.85] | $\beta_0 = 2.37_{(.01)}$ $\beta_1 = -$ | [3.37 - 3.42] | [5.77 - 5.82] |

Table 3.1: This table gives the confidence intervals (with significance level of $\alpha = 0.01$) for the electric fields needed to obtain 50% ($E_{50}$) and 90% ($E_{90}$) of successful defibrillation, respectively. Values are obtained using both GLM and GAM modeling approach. The second and the fifth column gives the fitting parameters (see Eq.(3.1)). The standard error for each of the fitting parameter is also given (small sub-indices in parentheses next to each parameter).

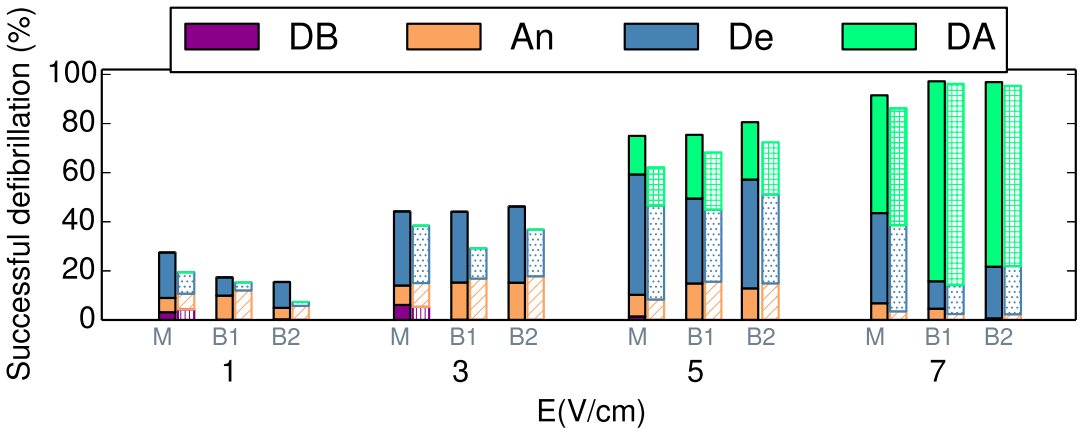


Figure 3.2: Artificial neural networks (see section 2.5) are used to classify defibrillation mechanisms for selected shock strengths. Full color denotes the results for quasiperiodic initial condition [136] and hatched patterns refer to results with chaotic initial conditions. Analyzed shock strength are 1V/cm, 3V/cm, 5V/cm and 7 V/cm. DB stands for Direct block; An stands for Annihilation; De for Delayed block; DA for Direct activation.

$E_{50}$ values are similar for all three protocols. Higher contrast between the protocols, however, is observed for $E_{90}$ values. Biphasic II protocol requires the lowest shock strength necessary to achieve 90% success rate. Biphasic I protocols then follows and monophasic results to be the least efficient. Indeed, this order of efficiency corresponds to the clinical evaluations of the three protocols. The supremacy of biphasic shocks over monophasic is so widely accepted that in some countries, monophasic defibrillators are not manufactured anymore [69]. Comparing $E_{90}$ results obtained with biphasic II and monophasic protocol, we find a decrease of approximately 26% in the energy (proportional to the square of $E_{90}$) for the biphasic II protocol relative to monophasic protocol ( with both GLM and GAM fitting methods).

Finally, let us comment on the choice of the number of initial conditions and the number of different noise distributions used to construct each box-plot and the dose-response curve. Fig. 3.3 shows resulting values for $E_{90}$ as we increase the number of initial conditions (3.3b) and noise distributions (3.3a) used to construct the curve. Results are clearly more sensitive to the number of the noise distributions than they are to the number of initial conditions. For this reason, in some of the future simulations we will use a smaller number of initial conditions. This will always be indicated. Fig. 3.3a shows results obtained with both GLM and GAM methods. Both set of results show the same trend, albeit with the slightly differing values. In case of the Fig. 3.3b results were almost overlapping, so for clarity only results obtained with the GLM method are shown.

### 3.1.2. Analysis of defibrillation mechanisms

Defibrillation mechanisms are analyzed for shock strengths : 1, 3, 5 and 7V/cm and were first published in [136]. Classification of all 160,000 examples per shock strength is performed as described in section 2.5. Fig.3.2 shows graphically ANNs results for both quasiperiodic and chaotic

| | Monophasic | | Biphasic I | | Biphasic II | |
|---|---|---|---|---|---|---|
| | GLM | GAM | GLM | GAM | GLM | GAM |
| AIC | 37662 | 32185 | 49120 | 32237 | 47547 | 32200 |
| Dev.ex(%) | 94.7 | 95.6 | 94.5 | 96.6 | 94.5 | 96.5 |

Table 3.2: This table gives the AIC and deviance explained values for two types of fit : one using GLM and second the GAM approach.

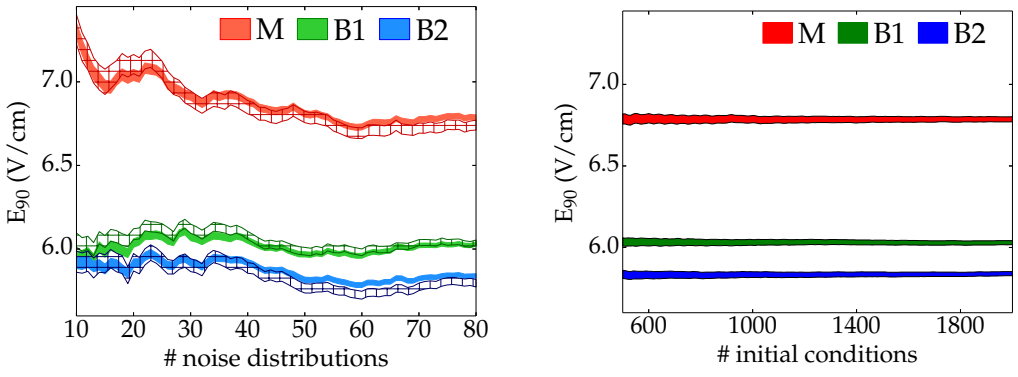


(a) (b)

Figure 3.3: Dependence of the resulting $E_{90}$ values on the a) number of noise distributions and b) number of initial conditions used to obtain the model fit. In a) hatched lines refer to results obtained with the GAM method and full lines to results obtained with the GLM method. In b) only results with GLM method are shown.

initial condition, although in this section we will focus on the quasiperiodic initial condition. These results are further analyzed with two-dimensional histograms showing the probability of a successful defibrillation as a function of the two parameters: location of the wave back on the ring $\phi_b$ and action potential duration $\Delta\phi$ (see Fig.2.7b). Results are shown in Fig. 3.4 – 3.7. The top, middle and bottom rows of each figure show results for monophasic, biphasic I and biphasic II protocol, respectively. Each column represents the percentage of success obtained with a particular defibrillation mechanism; for example the left-most column in Fig.3.4 represents the probability of successful defibrillation via the direct block mechanism.

$\phi_b$ provides information on shock timing and $\Delta\phi$ over the current state on the ring. The choice of these two parameters over a combination with $\phi_i$ (location of the wave front) is justified with results in literature and the current study. Previous research on cardiac dynamics has shown that the dynamics is more sensitive to perturbations applied to wave back compared to the perturbations applied at the wave front [179–182]. This is again confirmed in the present study. Placing $\phi_b$ on the vertical axis on the Fig. 3.4 – 3.7. reveals an interesting horizontal structure in the histograms.

**E = 1V/cm**

Applying an external electrical field of 1V/cm results in low percentage of success (for 8ms shock duration). However, a clear distinction between the protocols can be observed.

Monophasic shock is convincingly most efficient for this value of the electric field (overall success rate is 27.5%), while biphasic I (17.4%) and biphasic II (15.5%) protocols result in more similar values of percentage of success. Comparing the results of the ANNs classification shown in Fig.3.2 we can observe several features. Unique feature of the M protocol with respect to the biphasic shocks is the existence of the direct block mechanism. The overall contribution, however, of DB is small (only 3.16± 0.008). The main contribution to the success of the monophasic protocol is achieved by the delayed block mechanism.
Observing the results of the 2D histogram of the probability of success brought by individual mechanisms gives more insight (Fig.3.4). First and third row corresponding to M and B2 protocol show similar features. This indicates that for low shock strength B2 resembles to M protocol, despite the fact that the success rate is more similar to the one of the B1 protocol. Let us comment also on the Fig. 3.4a1 showing direct block mechanism. The most prominent feature is a diagonal rather than horizontal red region that is observed in other histograms. In this case, the wave front ($\phi_i$) is the more relevant quantity in describing the specific DB mechanism. Analyzing the same data in terms of ($\Delta\phi$, $\phi_i$) parameters indeed confirms that a necessary condition for the DB is positioning the wave front directly in front of the anode (data not shown). Note that although DB block is possible with B2 protocol, the total contribution is not significant (Note that the colorscale of Fig. 3.4 only ranges from 0 to 20%).

**E = 3V/cm**

Percentage of success for this shock strength is similar for all three protocols and yields values in the middle of the sigmoid curve: 44.2%,44.1%, 46.2% for M,B1 and B2, respectively. Fig.3.2 shows that all protocols result in similar values of the delayed block. Note that percentage of trials with successful outcome via annihilation is similar for B1 and B2 shock (15.16%, 15.17%), while for M shock this values is practically halved (7.92%). A closer look at 2D histograms showing distribution of annihilation shown in Fig.3.5 (a2-c2) reveals the difference between the protocols. Note that in this case B2 carries the same features as the B1 protocol. To further clarify the defibrillation outcomes with this mechanism, we have plotted specific examples of annihilation on Fig. 3.8. First row shows a set of examples whose position $(\Delta\phi, \phi_b)$ is on the upper red bar. All three protocols have resulted successful via annihilation. Wave back is located just behind the cathode. First phase is cathodal at $3\pi/2$ and all protocols give rise to cathodal break excitation that annihilates with the only front from the opposite direction. This example is identical for E=1V/cm, except for the virtual electrodes appearing between the two electrodes. Second row of images shows an example whose position $(\Delta\phi, \phi_b)$ is on the lower red bar. Monophasic shock results to be unsuccessful, while biphasic I and biphasic II still defibrillate via annihilation mechanism. The pre-shock front is moving in the counterclockwise direction. Second phase of the biphasic shock at $\pi/2$ is cathodal and results in a front that collides with the original front.
Careful observation of the Fig.3.5 (a3-c3) showing probability of delayed block, reveals that B2 protocol shares features characteristic for both M and B1 protocol. Looking at the areas with high success probability, one can see a range of values in which all three protocols defibrillate via

delayed block, areas where only B1 and B2 defibrillate and areas where only M and B2 defibrillate via delayed block mechanism. Fig. 3.9–3.12 provide an example for each of these cases. Besides E=3V/cm, same examples are also shown for E=1V/cm. Fig. 3.8 shows an example in which all three protocols for E=3V/cm defibrillate via delayed mechanism. Location of this example on the 2D histograms is $(\Delta\phi, \phi_b)$=(3.01, 5.68)rad, where indeed there is a high probability that all three protocols will defibrillate with success. Second example shown in Fig. 3.9 provides an example of similarity of M and B2 protocol. The two protocols result successful in almost identical manner, while B1 results unsuccessful. Note the difference with the same example shown for E=1V/cm. In this case, B2 also fails: the second electrode with very low shock strengh is not able to mimic the properties of M shock.

The following two examples shown in Fig. 3.11, 3.12 demonstrate similarity of the biphasic protocols: with increasing shock strength B2 is starting to resemble the B1 protocol. For both cases, monophasic shock results unsuccessful. Note the different role of biphasic electrode at $\pi/2$. In the first example (Fig.3.11), it gives onset to two oppositely propagating front. One of the fronts annihilates with the original front, while the other is blocked by the refractory tissue. In the second example (Fig.3.12), there are no break excitations, but the original front is stopped by the refractory tissue around $\pi/2$.

### E = 5V/cm

By increasing the applied electric field to 5V/cm, the outcomes yield a higher percentage of success: 75.0%, 73.4% and 80.6% for M, B1 and B2, respectively. A contribution to the overall success is provided by the direct activation mechanism for all three protocols, while delayed block still remains the prevalent mechanism of defibrillation. In Fig.3.6 we have removed the column for the DB mechanism (subscript 1 ) and added the column for the DA mechanism (subscript 4). Note that the borders of higher probability are not as sharply defined as for lower shock strength. Still, 2D histograms shown are indicative that B2 continues to blend in properties characteristic for either M or B1 shock. It is also interesting to note that the shock works much better for waves with shorter action potential duration. This result is not surprising, since for large $\Delta\phi$ there is very little tissue available to excite, as most of the system is already excited or is in a refractory state. In contrast, when $\Delta\phi$ is small, a large portion of the tissue is excitable and can be recruited to form virtual electrodes and therefore assisting defibrillation. Biphasic I protocol is the least efficient for larger $\Delta\phi$ when the phase back is between the two electrodes. Fig.3.13 shows an example. The tissue close to $3\pi/2$ is hyperpolarized and allows for the front to pass as opposed to the situation of monophasic and biphasic II protocol. Note, however the difference with the outcomes for E = 7V/cm shown in the same figure.

### E = 7V/cm

The total percentage of success for this value of external electric field is 91.5%, 97.1% and 96.9% for M, B1 and B2, respectively. Fig.3.2 shows that the dominant mechanism for B1 and B2 shock is the direct activation, while for the M protocol the delayed block still brings a significant contribution, a (37±3)% of the total events. The value of delayed block for biphasic I is (11±2)% and for biphasic II (21±2)%, placing the latter again between the two protocols. To underline the difference, let us mention that direct activation will be present in 81% and 75% of

the events for biphasic I and biphasic II, respectively. This percentage for monophasic shock is significantly less, only 48%.

These numbers indicate that the monophasic shock does not excite the tissue as well as the biphasic shocks do. Examples given on Fig.3.13 provide a convincing example. Monophasic shock will defibrillate with delayed block for both E=5V/cm and E=7V/cm. The situation for biphasic shocks is clearly different for the lower and higher shock strengths. E = 7V/cm will excite the tissue, but there will be no propagating fronts. The whole tissue will proceed to relaxation.

The second difference between the monophasic and biphasic shocks was the component of the delayed block. While this mechanism is part of the success it is also part of the failure for the monophasic shock since it will lead to failure every time tissue is not refractory. Fig.3.7 shows that least successful area for monophasic shock is centered around the anode ($\phi_b = \pi/2$) for large $\Delta\phi$. This region exhibits larger M failure for lower (Fig.3.11,3.12(a1-b3)) and higher shock strengths (Fig.3.12(d1-d3)).

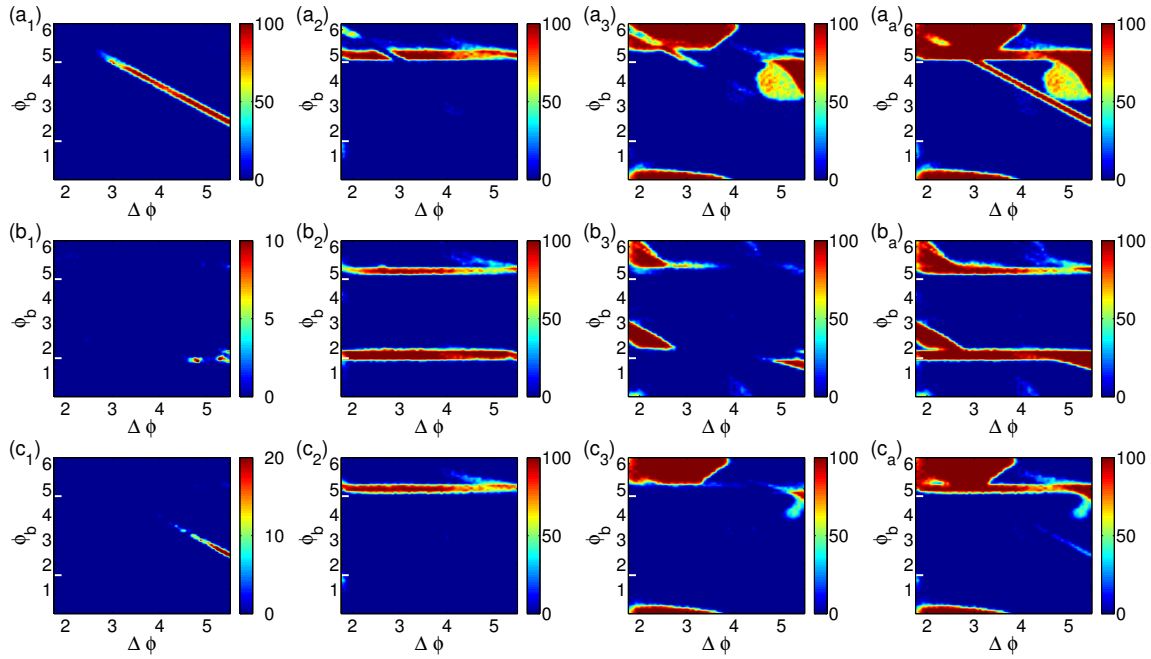


Figure 3.4: From [136] 2D histograms of the probability of successful defibrillation expressed as a percentage as a function of the wave back ($\phi_b$) and action potential duration $\Delta\phi$. White lines on the vertical axis indicate the position of the electrodes. The top, middle and bottom rows are for monophasic, biphasic I and biphasic II, respectively. Subscripts denote different defibrillation mechanisms: DB = 1, An = 2, De = 3, and the total for all mechanisms = a. Note that the fourth mechanisms (DA) is not present at low shock strength and is therefore not shown in this figure.

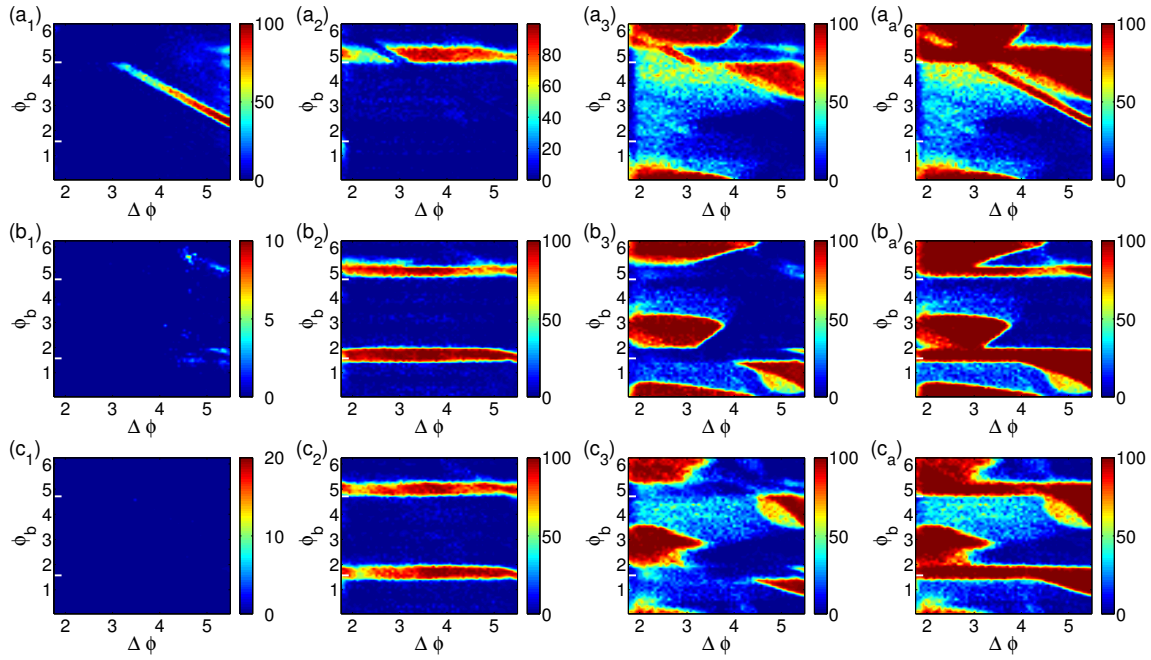


Figure 3.5: Same as Fig.3.4 for E=3 V/cm.

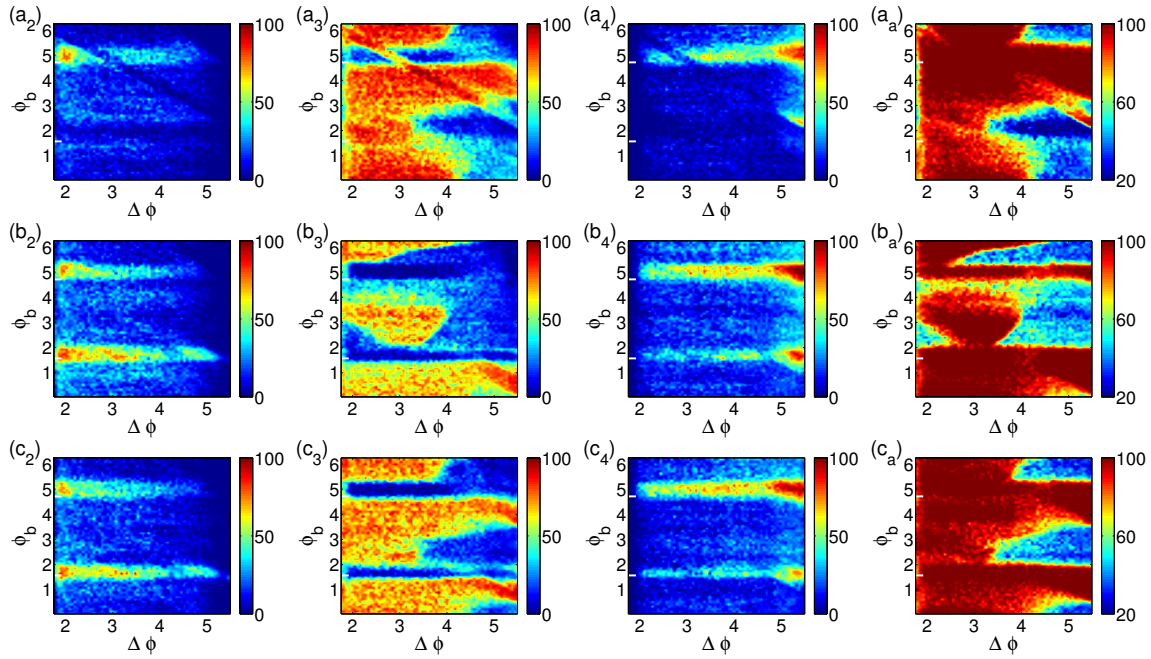


Figure 3.6: Same as Fig.3.4 for E=5V/cm. Note that DB mechanism is not shown here because it is vanishingly small. The histogram for the DA mechanism (sub-index=4) is shown instead.

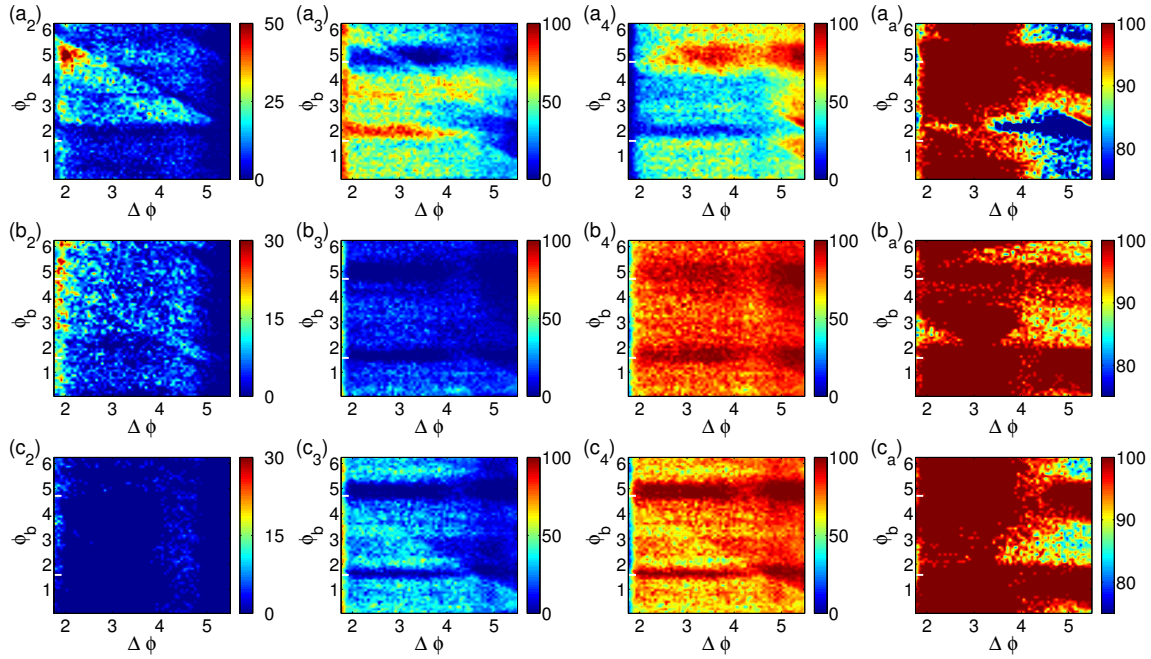


Figure 3.7: Same as Fig.3.6 for E=7 V/cm.

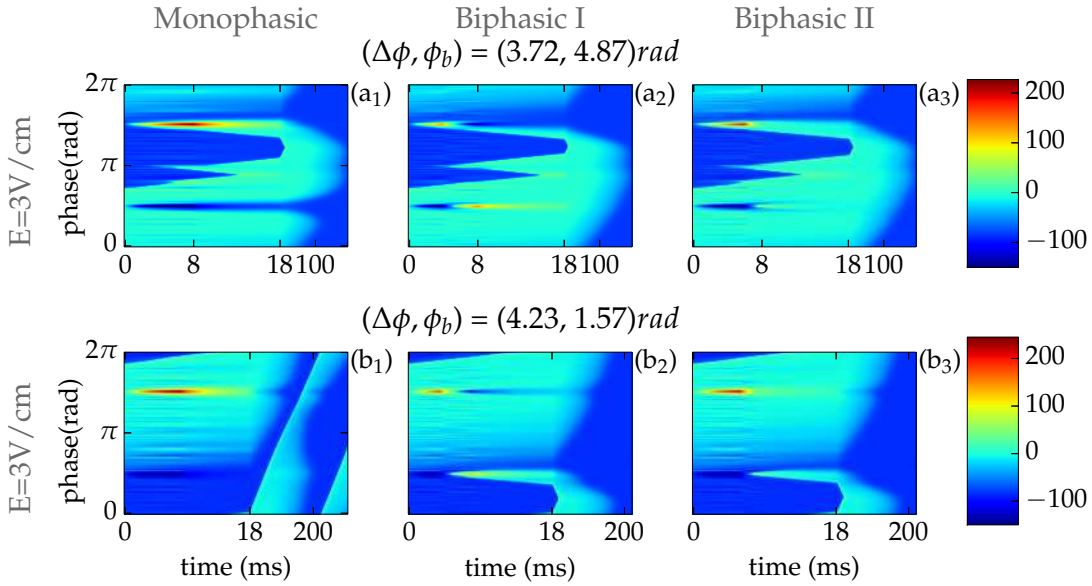


Figure 3.8: For low to medium shock shock strength, 2D histograms have shown that all three protocols can successfully defibrillate via annihilation when $\phi_b$ is close to the cathode. This is the case in (a1-a3) where original wave front collides with cathodal break excitation. (b1-b3) $\phi_b$ is localized close to the anode. Since anode turns to cathode in the second phase of the shock, biphasic protocols give onset to wave break excitation that annihilates with the original front.

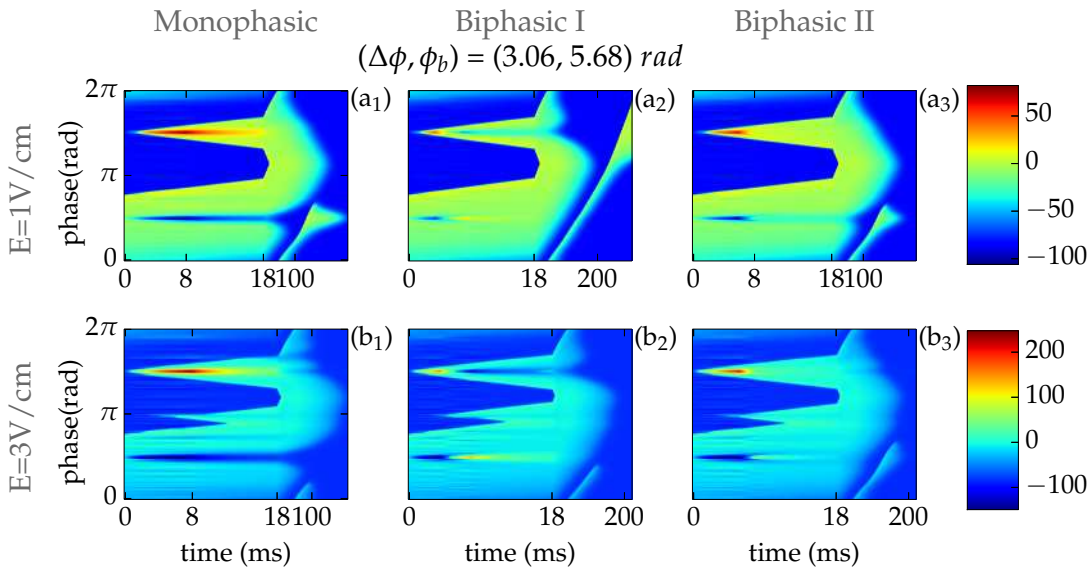


Figure 3.9: An example of defibrillation trial with $\Delta\phi, \phi_b$ localized in the region in which all three protocol have high success rate for E≥3V/cm. All three protocols defibrillate with similar scenario. Note that biphasic I results unsuccessful for E=1V/cm as it corresponds to results shown on Fig.3.4 for this value of $\Delta\phi, \phi_b$.

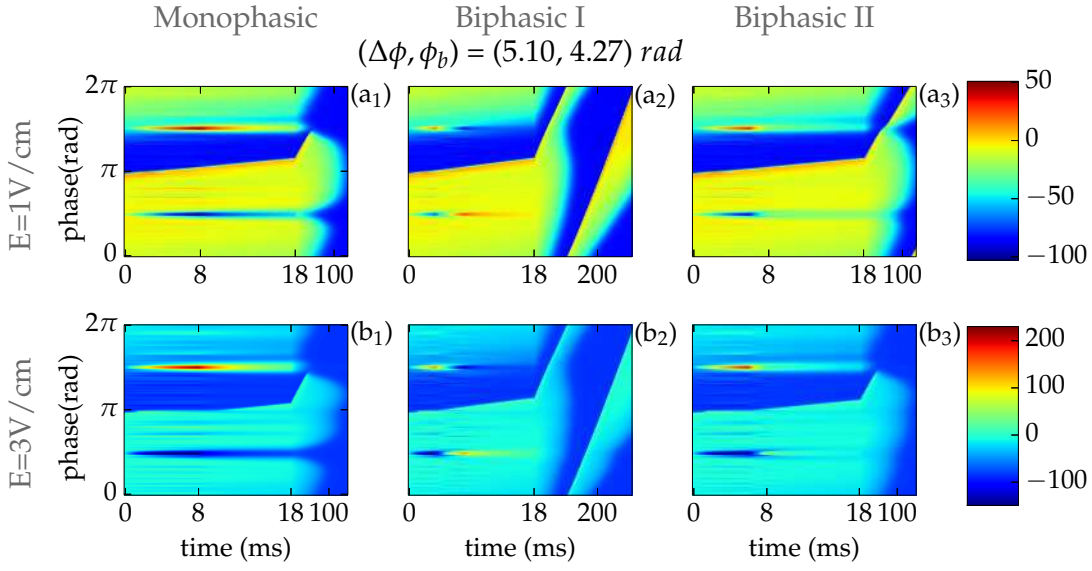


Figure 3.10: Similarity of M and B2 protocol increases as we increase the shock strength from 1V/cm to 3V/cm. Fig.3.4(a3-c3) shows clearly defined areas in the $\Delta\phi, \phi_b$ phase space in which M and B2 protocols show similar success rate.

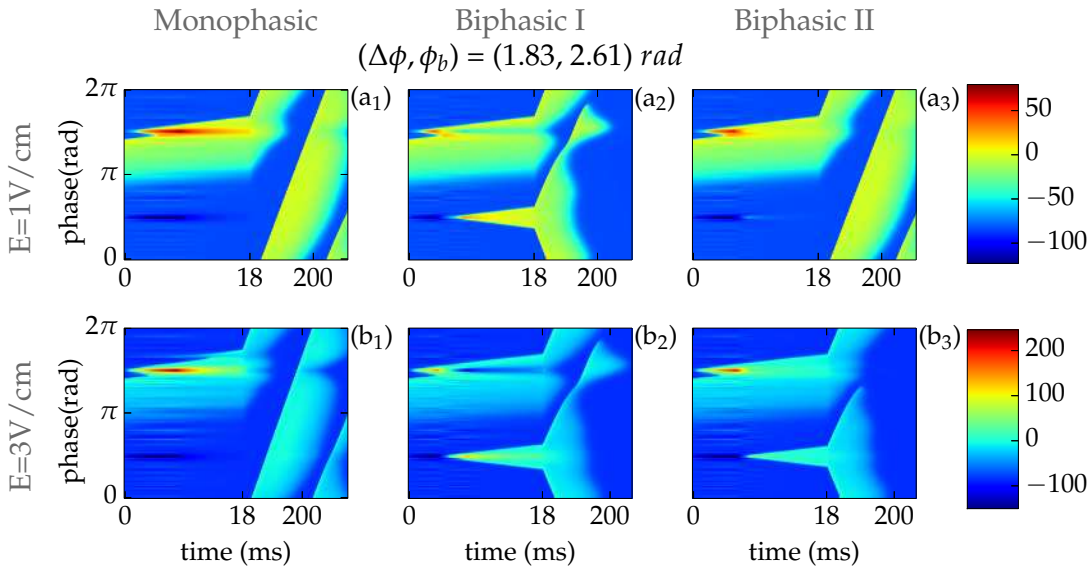


Figure 3.11: (a1-a3) Only biphasic I shock delivers a successful defibrillation. Original front is annihilated with the cathode break that gives onset to two fronts. Second front is stopped by refractory tissue. (b1-b3) Both B1 and B2 defibrillate with the same scenario as did the B1 protocol in the example with E = 1V/cm.

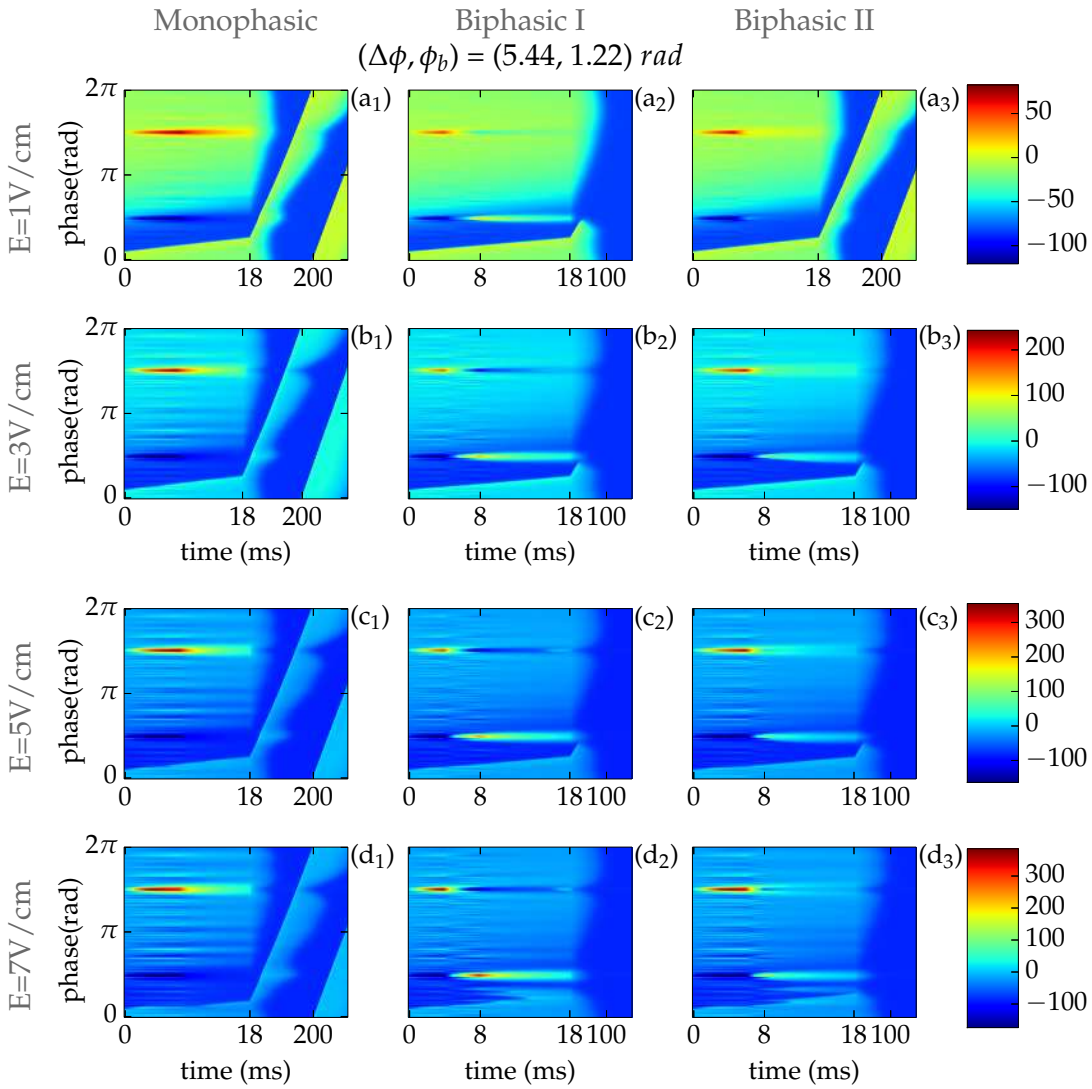


Figure 3.12: Another example in which B2 protocol shows similar defibrillatory properties of the B1 shock as the applied shock strength is increased from 1V/cm to 3V/cm. This similarity is preserved even for higher shock strengths. Monophasic shock remains unsuccessful for the entire range 1-7V/cm.

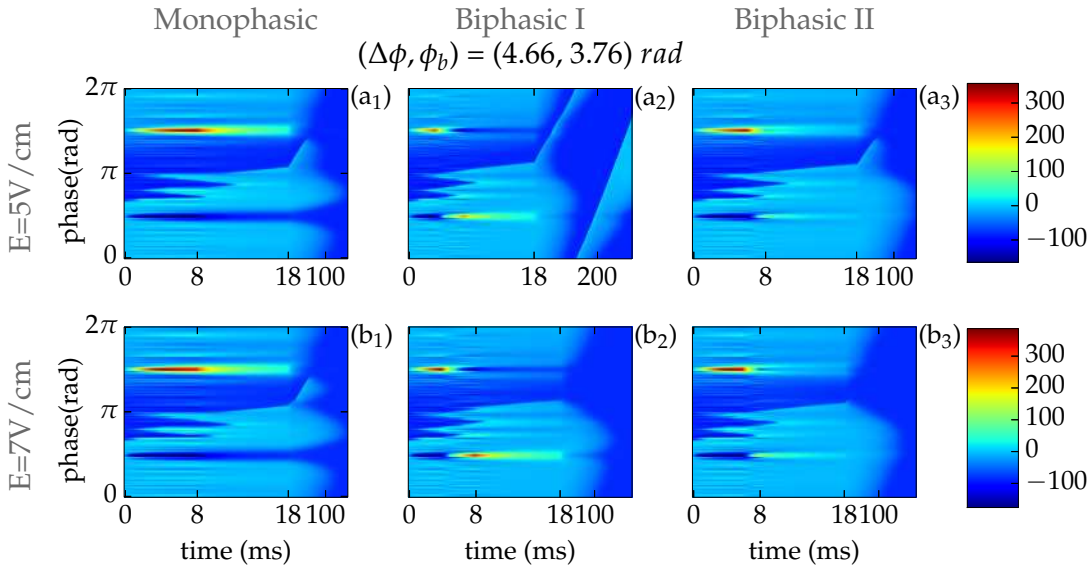


Figure 3.13: M and B2 can be similar even for E=5V/cm. The situation is different as we increase the shock strength to E=7V/cm. M is unable to excite the tissue effectively as the biphasic protocols and thus still defibrillates via the delayed block mechanism.

### 3.1.3. Comparing protocols for different conductivity fluctuations

In the previous sections and for the rest of the thesis, the amplitude of the conductivity fluctuations $\delta$ in the Eq. 2.18 was set to 0.15. This resulted in values of the critical electric fields of the three protocols to be comparable to the one found in practice. When $\delta = 0.15$ one finds that the monophasic is the least efficient, followed by symmetric biphasic which is slightly less efficient than the asymmetric biphasic (with second phase smaller than the first phase). In this section we will briefly report results with three additional values of the noise amplitude $\delta$: 0.05, 0.1 and 0.2. The corresponding defibrillation dose-response curves are shown in Fig. 3.14. All the dose-response curves are fitted with the GAM approach described in the previous section. It is important to note that the precision of the computed $E_{90}$ is smaller than for $\delta$=0.15 since we have used 30 noise distributions to compute percentage of success for each shock strength (compared to 80 in the case of $\delta = 0.15$). The resulting $E_{90}$ are shown in Fig. 3.15. Except from the smallest value of $\delta$, the relative efficiencies of the three protocols are the same. For $\delta = 0.05$, monophasic protocols is by far the most efficient of the three. Comparing the delivered energies for $\delta = 0.05$, biphasic I and biphasic II protocols would require roughly 20% and 17% more energy relative to the monophasic.

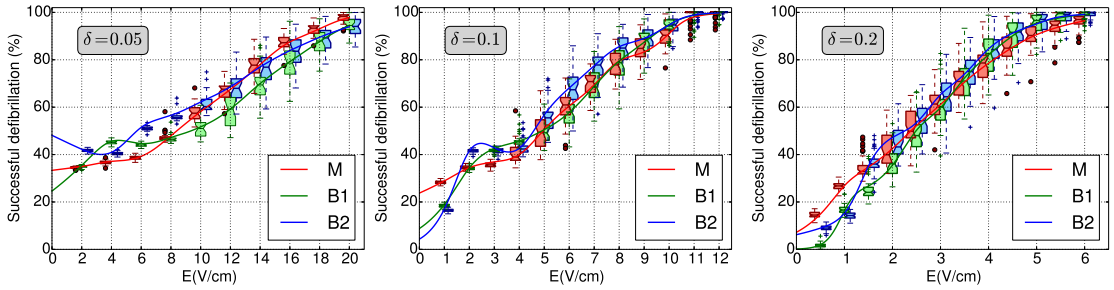


Figure 3.14: Defibrillation dose-response curves for a cardiac tissue with different values of noise amplitude $\delta$. Shock duration is 8ms. Numerical data (represented with boxplots) is fitted using the GAM approach. a) $\delta = 0.05$, b) $\delta = 0.1$, c) $\delta = 0.2$.

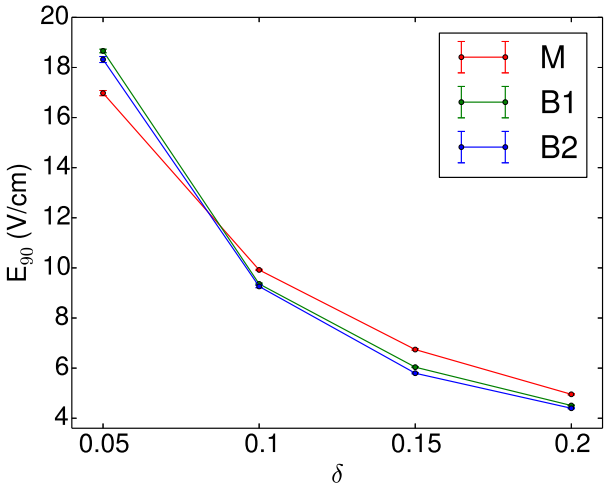


Figure 3.15: Dependence of the $E_{90}$ on the $\delta$ parameter that controls the degree of conductivity fluctuations (see Eq.2.18)

.

### 3.1.4. Defibrillation applied on chaotic initial states

Analysis similar to the one for the 8ms shock duration applied to a quasiperiodic state [136] is performed for the chaotic state with shocks of equal duration. Chaotic (Ch.) initial condition is prepared as described in section 2.4.1, following the approach of Qu et al. [138]. The parameter $a$, set to regulate transition between quasiperiodic and chaotic state is set to $a = 0.9$. Fig.2.9 (b,d) shows a return map of APD and a discrete Fourier transform of a one-dimensional wave obtained with a chosen parameter $a$.

#### Statistical comparison between the two initial dynamical states

Table 3.3 compares the median values of the defibrillation of the two dynamical states. Similar to the QP case, median values for the chaotic set of data is evaluated with 80 realizations of the noise and 2000 different initial conditions per noise. Comparison between the two sets of data is performed using Wilcoxon rank sum test for equal medians. This non-parametric test for statistical comparison was used to accommodate the fact that the data distribution around the median is not Gaussian in general ([136]). Table 3.3 shows medians for both cases for all tested shock strengths and a Z score resulting from the statistical test. Grey color is used for non-statistically significant differences at the $\alpha = 0.05$ level. Monophasic percentage of defibrillation shows no similarity for quasiperiodic and chaotic initial condition for all tested shock strengths. Quasiperiodic initial condition for monophasic protocol will always result in a more efficient defibrillation. The B1 and B2 shock have similar behaviour. For low and medium shock strengths (E$\leq$ 6V/cm), the two distributions will result different with quasiperodic initial condition leading to a more efficient defibrillation. For higher shock strengths (E $\geq$ 7V/cm), results show that there is no significant difference between the two initial dynamical states.

| E $_{(V/cm)}$ | $M_{QP}$ | $M_C$ | $Z_M$ | $B.I_{QP}$ | $B.I_C$ | $Z_{BI}$ | $B.II_{QP}$ | $B.II_C$ | $Z_{BII}$ |
|---|---|---|---|---|---|---|---|---|---|
| 1 | 27.50 | 19.53 | 11.05 | 17.33 | 15.3 | 9.71 | 15.50 | 7.25 | 11.05 |
| 2 | 34.48 | 34.13 | 2.42 | 33.10 | 20.98 | 11.05 | 40.65 | 25.50 | 11.05 |
| 3 | 43.93 | 37.83 | 6.04 | 43.38 | 27.38 | 10.58 | 45.13 | 35.40 | 8.62 |
| 4 | 59.93 | 47.08 | 9.09 | 56.93 | 44.05 | 8.55 | 60.78 | 50.95 | 6.53 |
| 5 | 75.10 | 62.03 | 8.95 | 74.75 | 67.70 | 4.52 | 80.35 | 73.15 | 5.70 |
| 6 | 85.23 | 76.00 | 6.75 | 90.43 | 88.93 | 2.01 | 92.13 | 87.90 | 3.49 |
| 7 | 92.50 | 86.75 | 5.36 | 98.53 | 97.90 | 0.84 | 97.88 | 96.55 | 1.47 |
| 8 | 96.58 | 94.45 | 3.41 | 99.90 | 99.93 | 0.45 | 99.78 | 99.85 | -0.23 |
| 9 | 98.75 | 98.08 | 2.28 | 100.00 | 100.00 | 0.49 | 100.00 | 100.00 | 0.41 |
| 10 | 99.68 | 99.28 | 2.15 | 100.00 | 100.00 | -0.05 | 100.00 | 100.00 | -0.04 |

Table 3.3: A comparison of the medians for each protocol resulting from quasiperiodic and chaotic initial condition. The statistical comparison is realized through the Wilcoxon rank sum test for equal medians. The comparison is then translated into a Z-score in order to see the significant differences more clearly.

### Dose-response curves

Numerical results for the chaotic case are shown with boxplots in Fig.3.16 along with fits performed with the GLM and GAM methods. For comparison sake, the same graph shows numerical results for the quasiperiodic case with gray boxplots. Table 3.4 reports the AIC values and explained deviance for both methods. Results again indicate that the GAM method performs a better description of the data. Table 3.5 shows the resulting corresponding coefficients of the fit and $E_{50}$, $E_{90}$ values. A comparison of the $E_{50}$ and $E_{90}$ values corresponding to the QP and Ch. initial condition confirms the results shown in Table 3.3: QP initial condition is easier to defibrillate. We find the increase of approximately 35% more energy when comparing $E_{90}$ results of Ch. ring relative to QP ring for monophasic shock. Biphasic results are less sensitive to the change of the pre-shock dynamics: the increase of approximately 14% and 15% in energy is needed for biphasic I and biphasic II relative to the QP ring. This difference is even higher when considering the $E_{50}$ values for which roughly 44% more energy is needed relative to the QP example.

These results are consistent with what is found in the literature. Clinical studies have shown that different types of arrhythmia will require different shock energies for successful antiarrhythmia shocks [183, 184]. Kerber et al. concludes that the "heart rate and electrocardiographic degree of organization of VT are important determinants of transthoracic energy" [184]. Both studies have found that the required energy for successful defibrillation will increase as one moves from organized ventricular tachycardia to polymorphic ventricular tachycardia and ventricular fibrillation. Subsequently performed simulation studies in 3D were consistent with these findings [164, 185]. Degree of organization was controlled by number of scroll waves with single scroll reentry representing the most organized dynamics. Both studies have confirmed that higher level of disorganization requires more energy to defibrillate successfully. One of the determinants speculated to be responsible for the differences is the pre-shock size of the excitable gap. Hillebrenner et al. [185] found that more organized reentry was associated with a larger size of excitable gap, while the opposite was found by Plank et al. [164], i.e. less organized reentry was characterized by larger pre-shock size of the excitable gap.

| | Monophasic | | Biphasic I | | Biphasic II | |
|---|---|---|---|---|---|---|
| | GLM | GAM | GLM | GAM | GLM | GAM |
| AIC | 59339 | 49329 | 73448 | 44438 | 57130 | 46550 |
| Dev.ex(%) | 91.9 | 93.4 | 93.3 | 96.1 | 94.7 | 95.8 |

Table 3.4: This table gives the AIC and deviance explained values for two types of fit shown in Fig.3.16: one using GLM and second the GAM approach.

### More on reentry dynamics and defibrillation outcome

What is the reason behind differing results of the two dynamical states? We have seen in the previous section how probability of defibrillation depends on the $(\Delta\phi, \phi_b)$ parameters. This dependence was pronounced for low shock strengths and reduced as we increased the shock strength. $\phi_b$

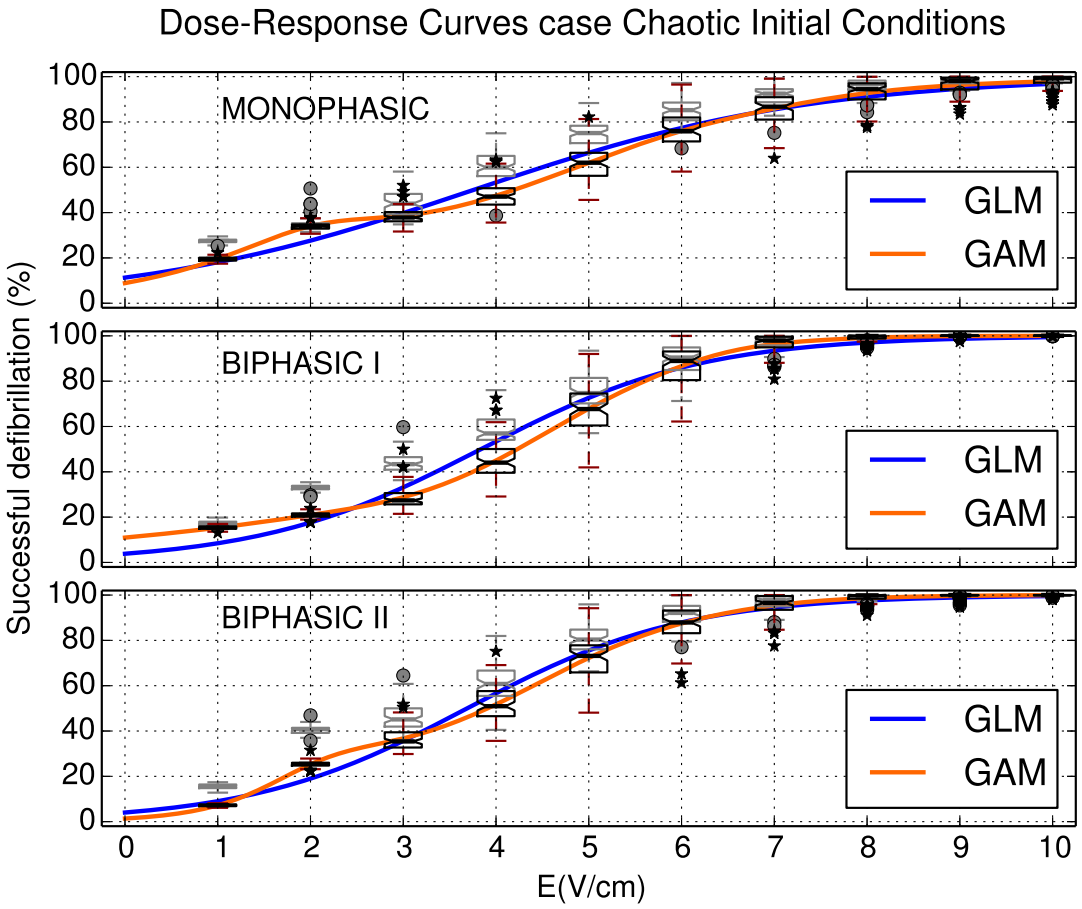


Figure 3.16: Numerical and model fitting results for a 8ms shock duration applied to the chaotic dynamical state of the ring. To visualize the difference with results corresponding to quasiperiodic ring, the latter are also represented with grey boxplots (corresponding outliers are denoted with grey dots). Black boxplots represent the data for the chaotic ring (the corresponding outliers are shown with a star symbol).

| | GLM | | | GAM | | |
|---|---|---|---|---|---|---|
| | Fit parameters | $E_{50}$ (V/cm) | $E_{90}$ (V/cm) | Fit parameters | $E_{50}$ (V/cm) | $E_{90}$ (V/cm) |
| M | $\beta_0 = -2.060_{(.004)}$ $\beta_1 = 0.5482_{(.0009)}$ | [3.75–3.77] | [7.75–7.78] | $\beta_0 = 1.051_{(.003)}$ $\beta_1 = -$ | [4.17–4.21] | [7.51–7.56] |
| B1 | $\beta_0 = -3.221_{(.006)}$ $\beta_1 = 0.840_{(.001)}$ | [3.82–3.84] | [6.44–6.47] | $\beta_0 = 2.27_{(.02)}$ $\beta_1 = -$ | [4.22–4.24] | [6.23–6.25] |
| B2 | $\beta_0 = -3.171_{(.006)}$ $\beta_1 = 0.860_{(.001)}$ | [3.68–3.70] | [6.23–6.26] | $\beta_0 = 1.91_{(.01)}$ $\beta_1 = -$ | [3.89–3.92] | [6.23–6.26] |

Table 3.5: This table gives the confidence intervals (with $\alpha = 0.01$) for the electric fields needed to get 50% ($E_{50}$) and 90% ($E_{90}$) of successful defibrillation, respectively. Values are obtained using both GLM and GAM fittings as shown in Fig.3.16. The second and the fifth column gives the fitting parameters (see Eq.(3.1)). The standard error for each of the fitting parameter is also given (small sub-indices in parentheses next to each parameter).

is a parameter that we expect to be uniformly distributed across the ring length (and indeed it is). Distribution of the action potential duration, however, differs between the two dynamical states. Fig.3.17 shows normalized histograms of $\Delta\phi$ used in the analysis of defibrillation mechanisms. Clearly, the two distributions differ significantly. Roughly 90% of the chaotic dynamical state pool of data has value $\Delta\phi > 4rad$, while for quasiperiodic ring $\Delta\phi$ is more evenly distributed roughly between 1.7–5.5$rad$. If the defibrillation mechanisms are the same, and based on the many examples we believe they are, then this difference in $\Delta\phi$ distribution will cause difference in the defibrillation percentage. Let us take another look at, for example, Fig.3.6($a_a$–$c_a$) that shows the total success probability for E = 5V/cm shock as a function $(\Delta\phi, \phi_b)$. If we split the images vertically with $\Delta\phi = 4rad$, the probability of successful defibrillation (P) differs for P($\Delta\phi < 4rad$) left side and P($\Delta\phi \geq 4rad$) right side. For monophasic shock the values are 0.89 and 0.63 for the left and for the right side, respectively. Note that the percentage of success for the chaotic dynamics is approximately 62%. Similar values for left and right probability hold for biphasic I (0.87,0.66) and biphasic II (0.93,0.70) case. This asymmetry between the P($\Delta\phi < 4rad$) and P($\Delta\phi \geq 4rad$) exists also for smaller shock strengths. For higher shock strengths it is almost nonexistent except for monophasic shock (0.97,0.87).

Fig.3.2 also provides the results of the analysis of defibrillation mechanisms performed on the data based on chaotic initial condition. Tabulated values can be found in Appendix A. Comparing these results with the QP results, one can observe that for low to medium shock strength, the main difference is caused by different values of the delayed block. This is consistent with the aforementioned analysis of the 2D histograms. Direct block does not contribute significantly, annihilation can be considered symmetric with respect to $\Delta\phi$ values, while this is not the case for the delayed block. Larger areas of high probability of successful defibrillation can be observed for $\Delta\phi < 4rad$ rather than for $\Delta\phi \geq 4rad$. To illustrate the similarities and differences, Fig. 3.18 shows 2D histograms of the total defibrillation success as a function of the previously used parameters $\phi_b$ and $\Delta\phi$ for E = 1,3,5 and 7V/cm. Comparing with the equivalent results for the QP case, we notice a great similarity for $\Delta\phi > 4rad$. For smaller values of $\Delta\phi$, we observe that the data is dispersed rather than grouped into high probability areas like it was found previously. This may be due presumably to the smaller number of data that falls into that range. Note that the range of $\Delta\phi$ values shown in Fig. 3.18 is from 2.4rad to 5.3rad. However, only 0.17% of all data falls behind $\Delta\phi$ <3rad.

**Statistical comparison between the three protocols**

In order to perform statistical comparison between the three different protocols, we have created a smaller set of data in the following way: each protocol was tested for the same initial condition $(\phi_i, \phi_b, \Delta\phi)$ and the same variation of heterogeneity. The ring is in the chaotic dynamical state. A total of 1000 initial condition is repeatedly tested with 50 different conductivity distributions for 10 values of shock strength. In the previous work, initial conditions and the conductivity distributions were uncorrelated. The data is then grouped in two ways : according to the noise distribution (50 data points per shock strength) and initial condition (1000 data points per shock strength). Table 3.6 shows the outcomes of the Wilcoxon signed rank tests performed on these two types of data groups. Again, statistical comparison is limited by the non-normal dis-

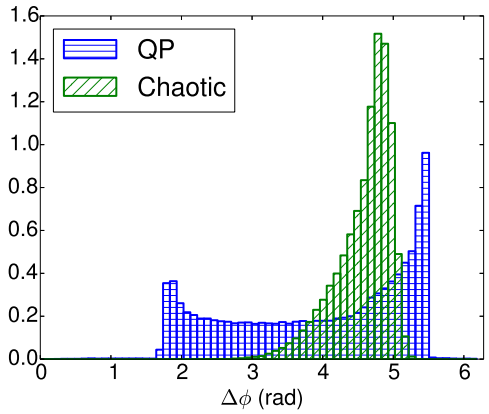


Figure 3.17: A comparison of action potential durations for chaotic and quasiperiodic dynamics that are used in the analysis of defibrillation mechanisms shown in Fig.3.2. Histograms are normalized.

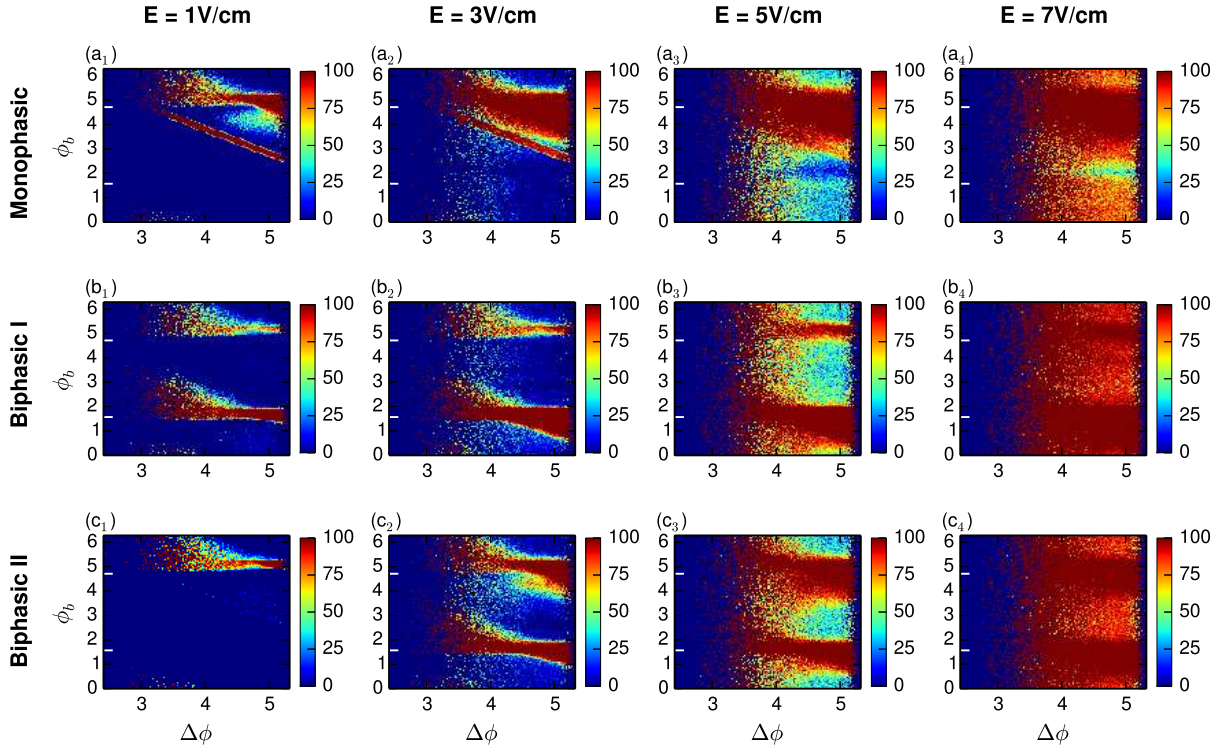


Figure 3.18: 2D histograms showing the probability of defibrillation success as a function of $\Delta\phi$ and $\phi_b$ parameters for the ring in the chaotic state.

tribution of the data. The results of the Wilcoxon signed rank test for grouping by conductivity are similar to the equivalent results based on QP dynamics [136]. For low shock strength (1-2V/cm) monophasic shock is more efficient than the biphasic shocks. For shock strengths higher than 3 or 4V/cm, biphasic shocks are more efficient. The two biphasic shock result comparable for high shock strengths (E>5V/cm). Note that for the E ranging between 2-5V/cm, biphasic II is more efficient than the biphasic I. This is consistent with the previous analysis of the defibrillation mechanisms that revealed how biphasic II combines positive properties of monophasic and biphasic I shock. The results of Wilcoxon signed rank test for grouping according to initial condition (Table 3.6b) follow the same trend for all shock strengths, but with few exceptions. In the group comparing biphasic shocks for E≥7V/cm the results are not comparable as in the previous case, but are in favor of the biphasic I shock. The differences between the groups of different initial state, even though averaged across conductivity fluctuations results significant for this case. This is possible since Wilcoxon signed rank test does not compare the values of the differences between pairs of data, but their ranks. Grouping according to the initial condition results in higher differences between B1 and B2 than it does when grouping by heterogeneity. Let us also comment on the seemingly peculiar result listed in Table 3.6b for shock strengths 1V/cm and 2Vcm. The median values are 0 and this may seem erroneous. However, as one could see in sec. 3.1.2, defibrillation outcomes are more sensitive to values of the initial condition for lower shock shock strength. Bear in mind that median values in Table 3.6b are grouped according to the initial position $\phi_i$. Due to high dependence of the outcome on the $\phi_i$, groups with certain initial value $\phi_i$ will result in zero success rate. The overall success rate is low and this results in median values equal to zero. Histograms of probability of success as a function of initial condition $\phi_i$ and shock strength for the data used in this section can be found in Appendix B.

(a) Median according to noise distribution

| E $_{(V/cm)}$ | M | $Z_{(M-BI)}$ | B.I | $Z_{(BI-BII)}$ | B.II | $Z_{(M-BII)}$ |
|---|---|---|---|---|---|---|
| 1 | 17.75 | 6.1 | 14.65 | 6.17 | 5.40 | 6.16 |
| 2 | 31.55 | 6.16 | 20.05 | -6.13 | 24.25 | 6.16 |
| 3 | 36.10 | 5.59 | 27.60 | -5.96 | 35.25 | 0.14 |
| 4 | 45.75 | 0.90 | 45.25 | -4.54 | 51.55 | -4.63 |
| 5 | 61.70 | -2.7 | 64.50 | -3.54 | 71.90 | -5.06 |
| 6 | 75.05 | -4.84 | 87.35 | -0.02 | 86.75 | -5.27 |
| 7 | 86.00 | -5.15 | 96.35 | 1.48 | 96.05 | -5.21 |
| 8 | 94.70 | -5.23 | 99.95 | 0.75 | 99.65 | -5.31 |
| 9 | 97.85 | -5.23 | 100 | 0.71 | 100 | -5.17 |
| 10 | 99.20 | -5.67 | 100 | 1.64 | 100 | -4.76 |

(b) Median according to initial condition.

| E $_{(V/cm)}$ | M | $Z_{(M-BI)}$ | B.I | $Z_{(BI-BII)}$ | B.II | $Z_{(M-BII)}$ |
|---|---|---|---|---|---|---|
| 1 | 0 | 1.14 | 0 | Inf | 0 | Inf |
| 2 | 0 | 5.45 | 0 | -2.74 | 0 | 4.42 |
| 3 | 10 | 2.02 | 8 | -3.98 | 14 | 1.88 |
| 4 | 30 | -0.26 | 30 | -1.79 | 42 | -2.12 |
| 5 | 59 | -3.02 | 63 | -4.31 | 76 | -6.99 |
| 6 | 76 | -10.14 | 88 | 1.29 | 94 | -11.97 |
| 7 | 88 | -15.88 | 98 | 6.09 | 98 | -16.06 |
| 8 | 96 | -18.91 | 100 | 4.38 | 100 | -18.54 |
| 9 | 98 | -19.32 | 100 | 7.79 | 100 | -18.55 |
| 10 | 100 | -17.62 | 100 | 7.90 | 100 | -16.06 |

Table 3.6: Comparison of the medians of the three protocols. Since simulations are performed with equal initial conditions and noise distributions for all protocols, outcomes can be grouped into two ways: according to noise distribution and according to initial condition. The statistical comparison of the resulting medians is realized through Wilcoxon signed rank test for equal medians. The comparison is then translated into a Z-score in order to see the significant differences more clearly. Gray color is used for non-statistically-significant difference at the $\alpha$=0.05 level.

## 3.2. Strength-duration curve

Until now we have analyzed the results for the shock duration equal to 8ms. The monophasic shock was proven to be less efficient than the biphasic shocks. In order to gain a broader insight into the differences between the three shock protocols we have performed the same simulations with different shock durations. The system was set in a chaotic dynamical state previous to the shock. Fig.3.19 shows dose-response curves for different shock durations ranging from the 1ms to 15ms shock duration. Fitting for each dose-response curve is performed using the GAM approach. Observing high values of the shock strength of the curve in the time-ascending order, we note that monophasic curve is clearly above the biphasic curves for 1ms shock duration. For 2ms shock duration, monophasic curve approaches biphasic curves, but still remains more efficient. For shock duration equals to 4ms, the curves almost overlap in the high shock strength range, while for longer shock durations, monophasic shock is less efficient than biphasic shock. Note that for low shock strengths monophasic is always more efficient than the biphasic shocks.
The data used to construct the dose-response curves is also used to construct the strength-duration curve, i.e. a plot of shock strength (required to achieve a certain percentage of success) vs shock duration. In this case, the data is analyzed in a slightly different way. Instead of constructing one dose-response curve for each shock duration (from 50x1000 set of points) and then evaluating a single $E_{90}$ and $E_{50}$ threshold, we have constructed 50 dose response curves and thus obtained 50 points for the $E_{90}$ and $E_{50}$. Again, each dose-response curve is fitted with the GAM approach. The total of 50 point per shock duration comes from the fact that we have used 50 different conductivity distributions for the evaluation of shock efficacy. The numerical data is shown on Fig. 3.20. The scenario described above for the Fig. 3.19 can clearly be seen on the strength-duration curve for the 90% success rate. Relative efficiencies of the three protocol are similar even for $E_{50}$ strength-duration curve. Exceptions in this case are the long shock durations for which all the values converge to one value.
The obtained data for the strength-duration curve qualitatively resembles the Lapicque strength-duration model introduced in the section 1.3.1. We have performed fitting of the Lapicque model to the obtained $E_{90}$ and $E_{50}$ thresholds using the non-linear least squares fitting. The fitting is performed with the *nls* package of the R software environment. Results of the fitting are shown in Fig.3.20 with full lines. Resulting chronaxie times and rheobase shock strength are listed in Table. 3.7. Let us note that Lapicque model can be easily linearized by multiplying the Lapicque equation with shock duration $t$: $I \cdot t = I_{rh} \cdot t + I_{rh} \cdot c$, where $I_{rh}$ denotes the rheobase current and c the chronaxie time. Performing the same multiplication with our data can indicate if, how and where the data deviates from linearity, i.e. if the Lapicque model is suitable for our data. The graphs in Appendix B show these results. We note that the biphasic protocols show strong deviations from linear behavior for the smallest shock duration : 1ms. This is the reason behind large confidence intervals for chronaxie for biphasic protocols.

### Energy-duration curves

Another characteristic of the Lapicque hyperbolic model for the strength-duration of stimulation is that it yields a U-shaped energy vs time curve (see section 1.3.1). This results follows if the applied stimulus is constant in time [96]. The optimum pulse is then obtained for shock

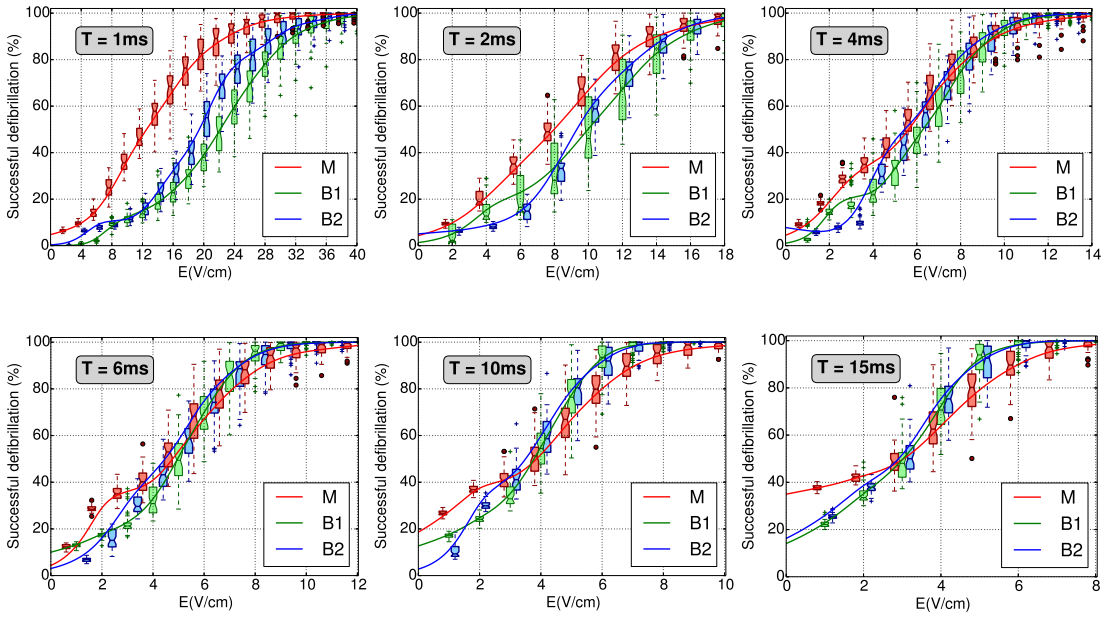


Figure 3.19: Numerical and fitting results for different shock durations. Numerical results are shown with boxplots. Fitting is perfomed using the GAM approach.

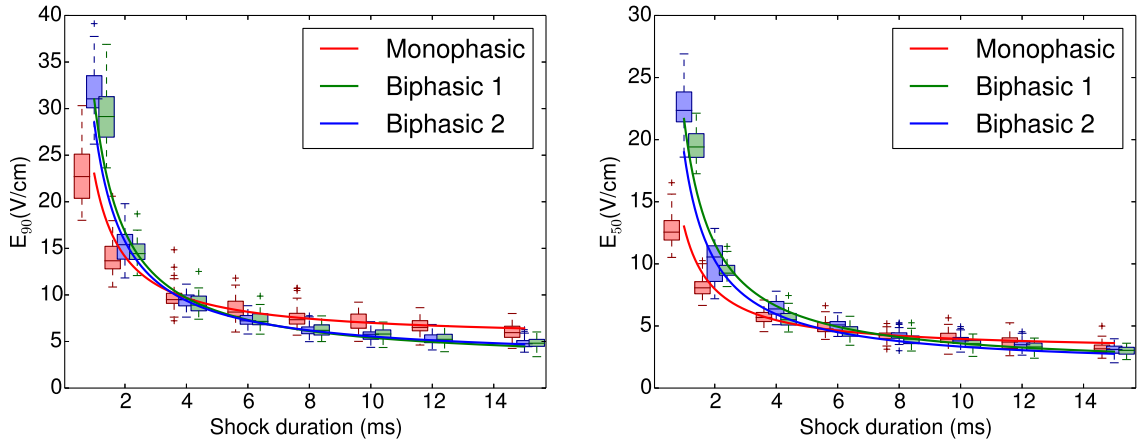


Figure 3.20: Strength-duration curves for $E_{90}$ and $E_{50}$ threshold. Full lines are fits following the Lapicque model. In order to avoid overlap of the boxplots, we have shifted the boxplots corresponding to the monophasic protocol to the left by 0.4V/cm and results corresponding to the biphasic 2 protocol are shifted to the right by 0.4V/cm.

duration equal to chronaxie. The chronaxie obtained for the M shock based on the Lapicque model is approximately 3.4ms , while values for B1 and B2 are much longer, 11ms and 8.5ms, respectively (for confidence intervals see Table 3.7).

Shock strength in present simulations is measured in extracellular electric field, although shock was applied with extracellular current (see eq. 2.15). The measured electric field was found proportional to the applied current (constant of proportionality roughly constant for all shock

| | $E_{90}$ | | $E_{50}$ | |
|---|---|---|---|---|
| | $E_{rh}$(V/cm) | c(ms) | $E_{rh}$(V/cm) | c(ms) |
| M | [5.91–5.44] | [3.20–3.65] | [2.85–3.05] | [3.23–3.60] |
| B1 | [2.38–2.78] | [10.09–14.08] | [1.43–1.75] | [11.33–14.22] |
| B2 | [2.81–3.19] | [7.89–9.21] | [1.49–1.70] | [10.09–11.75] |

Table 3.7: Strength duration curve was fitted to Lapicque model. The resulting confidence intervals (95%) for the coefficients are shown in this table.

durations). The delivered energy to the system can be calculated with $\propto \int_0^T I_e^2 \mathrm{d}x$. All results are then normalized to the energy of the monophasic shock of 8ms, the extensively analyzed case. Fig.3.21 shows values for delivered energy for the cases of shock strength necessary for 50% and 90% percentage of success. It can be observed that the monophasic shock exhibits a clear minimum between 2 and 4ms. Energy requirements increase monotonically for shock duration 4-12ms. However, the results for the 12ms and 15ms are similar. One-way anova performed on the data for 12ms and 15ms resulted in $p$ value 0.314 indicating that the means of the two sets are similar. Energy requirements for the biphasic shock differ qualitatively from the monophasic shock for the tested range of shock durations. One-way anova performed for the biphasic data showed that there is no statistically important difference in the time range 10-15ms. It would be necessary to perform simulations for longer shock durations to determine if biphasic shocks will exhibit monotonical growth in energy requirements like it is predicted by the Lapicque model.
It is not straightforward to compare these values to the experimental data. One of the reasons is that the most commonly employed experimental waveforms are exponentially decaying waveforms. Varying tilt will result in different waveform efficiency [186–189]. Shorofsky [188] studied monophasic shocks with four different tilts : 35%, 50%, 65% and 80%. The results showed that DFT is insensitive to waveform tilt in range 50% to 80%, but changes when tilt is further decreased to 35%.

Experimental evidence suggest that monophasic protocol with rectangular shaped waveform follows Lapicque hyperbolic model [167, 190, 191]. Koning [190] measured defibrillation threshold with rectangular monophasic pulses on dog hearts (in situ) and determined that the minimum defibrillation energy corresponds to shock duration of 4ms. Similar experiment on dog hearts using monophasic waveform of varying tilt was performed by Wessale [191]. Results for all tested waveforms showed similarity to Lapicque strength-duration characteristics. Results for almost rectangular waveform (tilt 5%) were consistent with chronaxie time of 3ms. Increasing the tilt of the waveform, the chronaxie values decreased below 2ms. However, not all experimental evidence supports the thesis that monophasic exponentially decaying waveforms follow Lapicque strength-duration characteristics. Clinical study by Gold et al. [192] showed clear lack of rheobase current.

Experimental results for biphasic wavefront are less clear. To the best of our knowledge, there is no experimental study using biphasic rectangular waveforms. However, there are few studies we can list in an attempt to validate our results with the experimental findings. In an experimental study (swine) by Schauerte et al. [105], biphasic waveforms with phase 1 to phase 2 ratio (60:40), but varying tilt were compared. DFT was defined as the lowest energy level with at least 80%

defibrillation success. Optimum biphasic shock corresponded for total shock duration of 5ms. Note, however that the waveform tilt used in this study is very high. According to the aforementioned study, one would expect that as the tilt is decreased, the chronaxie time would increase [188]. In a clinical study by Brugada [189] results are obtained for similar tilt and phase duration ratios. The voltage is decreased as pulse width is increased for both monophasic and biphasic pulses (monophasic data is obtained from the swine study). However, energy requirements were significantly different. For monophasic pulses, the energy doubled when duration is increased from 3 to 10ms, while for biphasic it was unchanged over the same time range. The measurement at 20ms showed statistically significant higher value of energy. To conclude, let us mention the study by Jones et al. [193] in which monophasic and symmetric biphasic waveforms were used to test excitation threshold in cultured cells. Biphasic chronaxie was found to be more than double the monophasic chronaxie (3.5ms and 1.6ms). The available data on biphasic strength-duration is scarce. Based on results found here and available experimental data we can conclude that chronaxie values will be differ significantly for monophasic and biphasic waveforms, i.e. monophasic protocols are optimum (energy-wise) for shorter shock duration than the biphasic protocols.

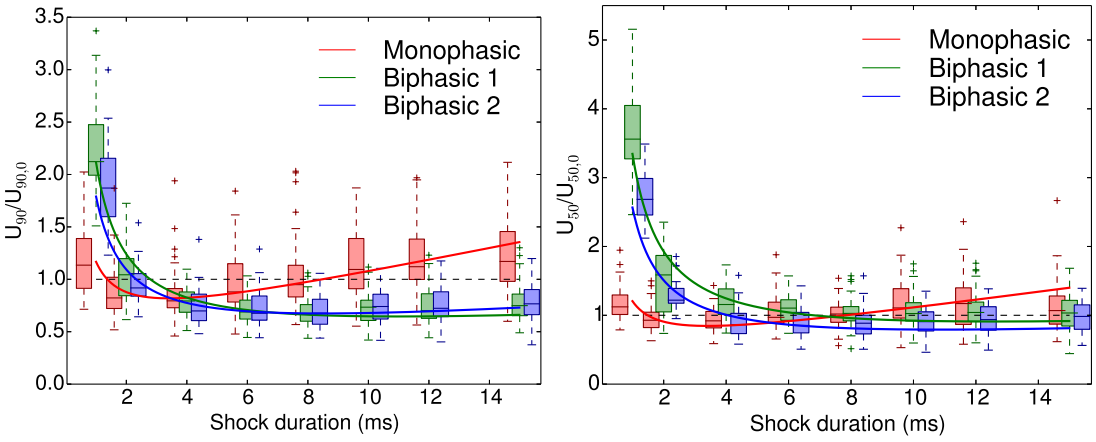


Figure 3.21: Energy delivered to the system as a function of shock duration for 90% and 50% success rate. All the results are relative to the chosen control case : monophasic shock of 8ms. Full lines are calculated based on the fit to the Lapicque model. In order to avoid overlap of the boxplots, we have shifted the boxplots corresponding to the monophasic protocol to the left by 0.4V/cm and results corresponding to the biphasic 2 protocol are shifted to the right by 0.4V/cm.

# Chapter 4

# Advantage of the four– versus the two– electrode defibrillators

Intensive research has been made in order to find optimum values for initial and final voltage of the shock, decay constant, shock duration and polarity reversal timing [25]. In the present chapter we propose a completely novel approach, in which instead of optimizing standard procedure in which the shock is applied via a two electrode system, one will look at a four electrode system. The motivation behind such a procedure comes from the analysis of results obtained with the standard two electrode system in a simple model of a one-dimensional ring of cardiac tissue [136]. $E_{50}$ threshold (shock strength corresponding to a 50% of success rate in the defibrillation shocks) is achieved mainly by front to front interaction or interaction of front and the refractory tissue, while $E_{90}$ threshold (shock strength necessary for getting a 90% success rate) is mainly obtained through a different mechanism consisting in a direct activation of the whole cardiac tissue. One suspects that the addition of two electrodes might move the $E_{90}$ threshold in the region of lower shock strengths where defibrillation is mediated mainly by wave–wave and wave–tissue interactions. The present chapter will confirm that it is indeed the case.

Fig. 4.1 depicts the scheme of the numerical experiment presented in this chapter. There are four equidistant current injection sites. For the monophasic shock, the position $X_1$ and $X_3$ are always anodal, while $X_2$ and $X_3$ are cathodal. The same positions of the shock polarities are maintained for the first phase of the biphasic shocks. In second phase, these are obviously reversed.

Apart from the change in number of the electrodes, all other relevant materials and methods are the same as the ones introduced in Chapter 2 and used in the Chapter 3, while analyzing the case of the two-electrode protocol. Using the same numerical experiment design, we will evaluate the percentage of success for a range of shock strength values yielding small to high percentage of success. This information will again be used to construct the dose-response curves and evaluate defibrillation thresholds associated with different percentages of success. Finally, the analysis of defibrillation mechanisms will provide insight into the results obtained with the four-electrode system.

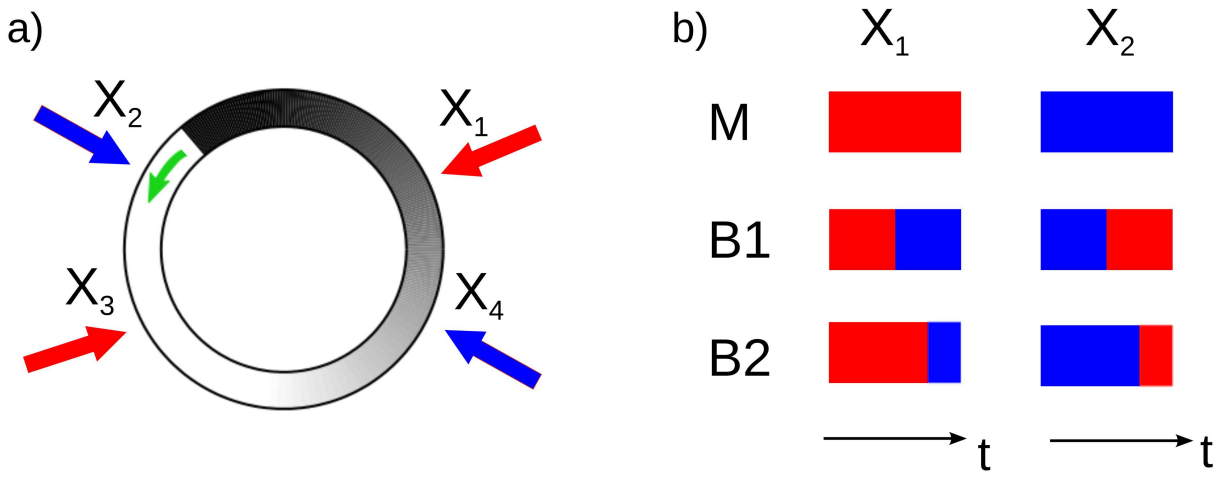


Figure 4.1: Illustration of the four-electrode system. Red arrows and red rectangles denote the anodes (injection of positive charges into the extracellular region, see Eq. 2.15). Blue arrow and blue rectangles denote cathodes. a) Positions of the electrodes on the ring (stimulus sites) for the monophasic and first phase of the biphasic shock. b) Illustration of the applied monophasic, biphasic I and biphasic II shock through the electrodes $X_1$ and $X_2$. The electrode $X_3$ receives the same charge as the electrode $X_1$. Electrode $X_4$ receives the same charge as the electrode $X_2$. The total shock duration is set to 8 ms.

### 4.0.1. Dose-response curve

Fig. 4.2 shows the numerical data and fitting results corresponding to four-electrode defibrillation for all three tested protocols. Percent success of each tested shock strength is evaluated with total of 100,000 simulations : 50 different noise distributions x 2000 initial conditions. Probability of success is then evaluated for each noise distribution and the boxplot is constructed using 50 data points for each shock strength. Monophasic and biphasic I curves are constructed with 26 values of shock strength ranging in $[0.25, 10]V/cm$. Due to sharp transition around 1.8V/cm, biphasic II curve is constructed with 32 values of the shock strength in the same range. By inspecting percentage of success results for monophasic and biphasic I protocols we can observe two plateaus : the expected saturation for high shock strengths and a small plateau around medium range values of the shock strength 2-3V/cm. Therefore, one-predictor logistic regression commonly employed in the two-electrode protocol might not be a suitable choice. This is easily confirmed by using Box-Tidwell transformation described by Hosmer and Lemeshow[172]. The transformation is designed to test for nonlinearity of the logit with respect to the predictors. The test is performed by adding a term $x\log(x)$ to the logit equation, where $x$ is the predictor with possible nonlinear relationship with the logit. If the coefficient for the added term is statistically significant, then there is evidence of nonlinearity between the logit and the predictor $x$. We added the Box-Tidwell term to the logistic regression of all three protocols and the resulting z-score proved to be significant. In order to account for the added complexity in the data, we will use the generalized additive model [173], introduced in section 3.1. In order to perform the GAM fitting we have used the corresponding R package [171] *mgcv* [173–178]. The basis $k$ of the smooth function is set to k=25 for the data coming from the M and B1 protocols, since we

have found that this value minimized the Akaiko information criteria (AIC) value. For the data coming from the B2 protocol, k was set to 21. We have found that higher values for the basis dimension lead to unrealistic fit. In order to quantify the improvement of the fit performed with the GAM (Eq. (3.2)) over the classical logistic regression (Eq. (3.1)), we can compare the Akaiko information criteria (AIC) of the two models. The classical approach for the M, B1 and B2 protocols resulted in AIC value of 169,125; 193,660 and 104,780 , respectively. In the same order, the GAM approach resulted in AIC value of 48,742; 29,537 and 30,405, respectively. Indicating that the GAM approach is justified over the classical logistic regression for the present data. In addition, Table 4.1 also provides the $R^2_{adjusted}$ for the GAM fitting. The latter values close to one indicate that the GAM fitting is indeed satisfactory.
The same table also provides the $E_{90}$ and $E_{50}$ threshold values extracted from the curve fittings with a $\alpha = 0.01$ confidence interval. For the sake of comparison, we have added the results of the $E_{90}$ and $E_{50}$ thresholds for the two-electrode system that were given earlier (see [136] or chapter 3, Table 3.5). We note that both $E_{50}$ and $E_{90}$ values are lower for four-electrode system compared to the two-electrode system. Let us first comment the values obtained for the $E_{50}$ thresholds. For the case of the two-electrode system the $E_{50}$ values are all very close to each others, while this is no longer the case for the four-electrode system. For the latter, the B1 and B2 protocols have similar values, while the M protocol has a much lower $E_{50}$ threshold value (half the biphasic values). This leads to a decrease of energy of approximately 78% when comparing the M and B1 $E_{50}$ threshold values (please remember that the energy is proportional to the square of the electric field). The situation is somewhat different when we compare the results for the $E_{90}$ threshold values, which are of higher interest for the defibrillator devices. Here as in the case of the two electrode system, the B2 protocol is the most efficient. Let us remind that difference in $E_{90}$ value between the M and B2 protocol for the two-electrode system leads to a decrease in energy of approximately 26% in favor of the B2 protocol. This result follows very closely the values found in the medical literature [22, 23]. The same comparison, in the case of the four electrode system leads to a decrease in energy of approximately 77% in favor of the B2 protocol when compared to the M protocol. Another interesting result is the $E_{90}$ value for the B1 protocol. Findings in medical practice tend to favor B1 over M protocol. However, in our study of the four electrode system, the M protocol results in lower $E_{90}$ threshold value than the B1 protocol. According to the values given in Table 4.1, the M protocol will defibrillate with 15% less energy than the B1 protocol (considering a 90% success rate).

### 4.0.2. Defibrillation mechanisms

A careful analysis of the successful defibrillation events indicate that, as in the case of the two-electrode system, there are four distinct mechanisms: (1) Direct block (DB), (2) Annihilation (An), (3) Delayed block (De) and (4) Direct activation (DA). Some examples (with the four-electrode system) are shown in Fig. 4.4. The DB mechanism is specific of the monophasic protocol. In this case, the initial front is suddenly halted by a highly hyperpolarized region created by the anodal stimulus and the wave is directly blocked. If no other fronts are created by means of virtual or real electrodes, the defibrillation is successful. An illustration of the DB mechanisms is shown in Fig. 4.4a where the shock strength is E=1V/cm and the shock protocol is monophasic. A second type of successful defibrillation can be achieved by means of

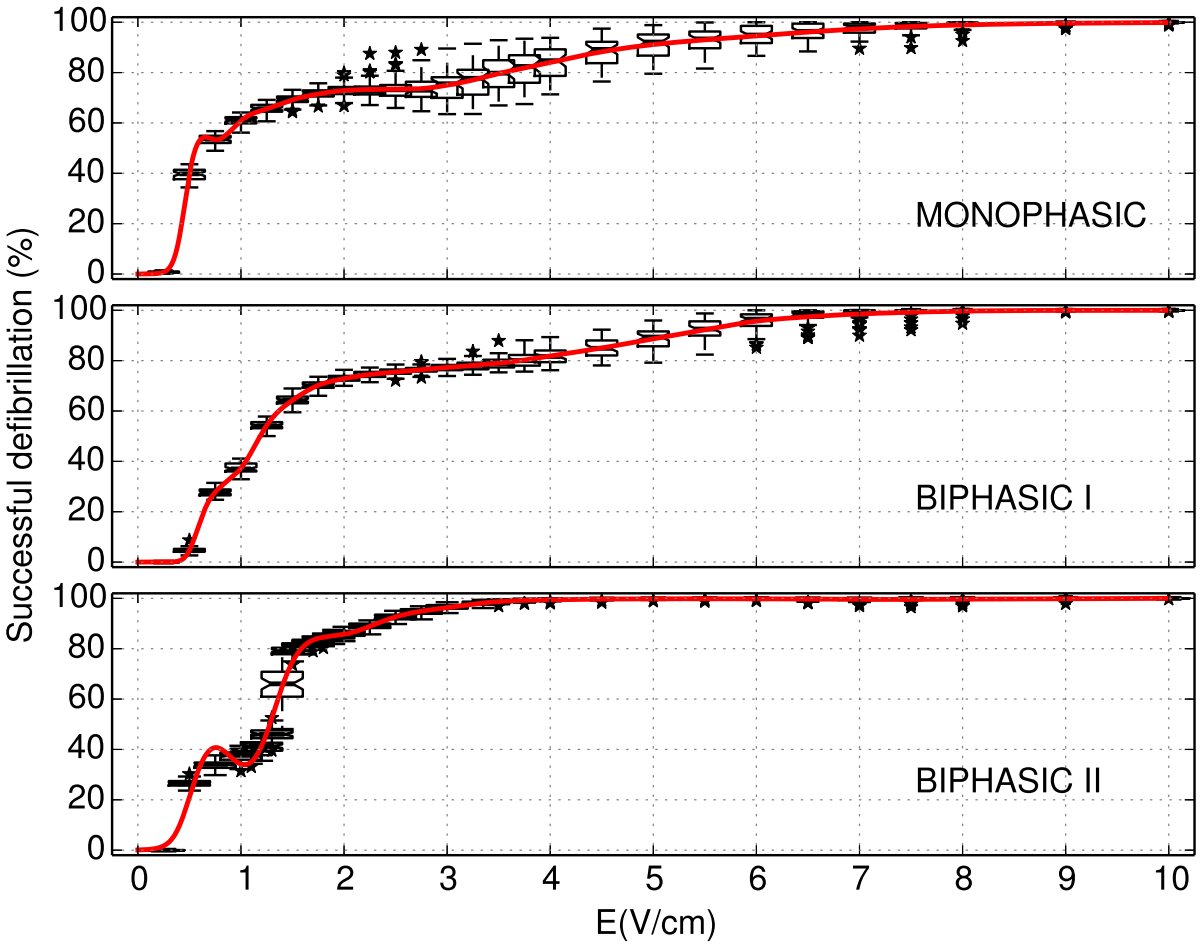


Figure 4.2: Numerical data (boxplot) and fitted dose-response curve for monophasic (top), biphasic I(middle) and biphasic II (bottom) protocol.

| | 4 electrodes | | | 2 electrodes | |
|---|---|---|---|---|---|
| | $R^2_{adj}$ | $E_{50}(V/cm)$ | $E_{90}(V/cm)$ | $E_{50}(V/cm)$ | $E_{90}(V/cm)$ |
| M | 0.968 | 0.558–0.565 | 4.73–4.81 | 3.08–3.10 | 6.77–6.80 |
| B1 | 0.993 | 1.181–1.192 | 5.16–5.22 | 3.21–3.23 | 6.02–6.04 |
| B2 | 0.988 | 1.278–1.282 | 2.31–2.33 | 3.03–3.05 | 5.83–5.85 |

Table 4.1: $E_{90}$ and $E_{50}$ values for two-electrode and four-electrode systems. $E_{90}$ and $E_{50}$ values corresponding to the four-electrode system are evaluated using the data shown in Fig. 4.2. Fitting is performed with the GAM approach. $R^2_{adjusted}$ values are also provided. For comparison, $E_{90}$ and $E_{50}$ values corresponding to the two-electrode protocol are also shown. The latter were previously published in [136].

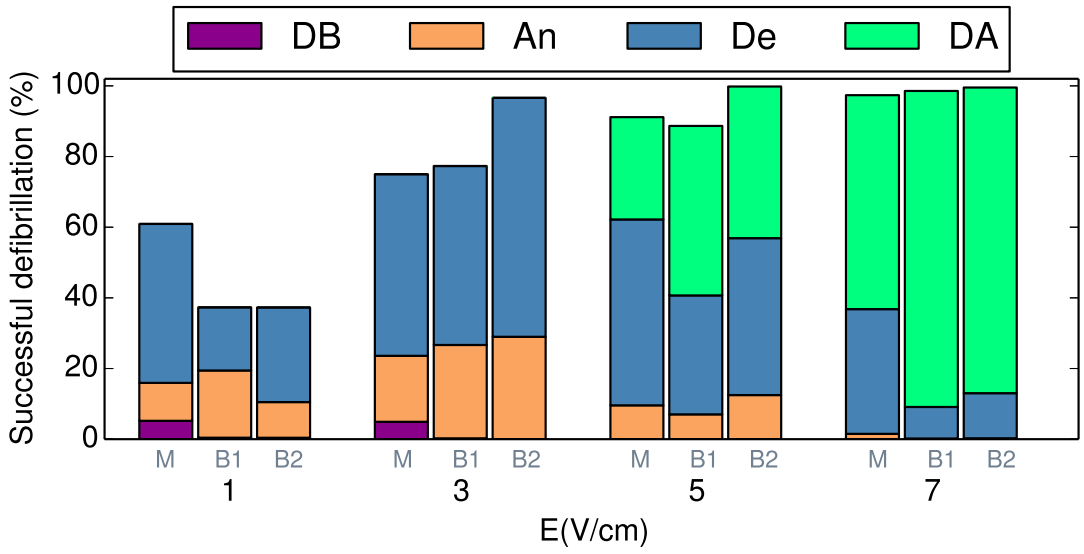


Figure 4.3: ANN is used to classify defibrillation mechanisms of the four-electrode protocol. Numerical values can be found in Table A.2. Stacked bar represent the classification of defibrillation mechanisms for M, B1 and B2 shock for shock strength values : 1V/cm, 3V/cm , 5V/cm and 7V/cm. Abbreviation stand for : DB-direct block, An-annihilation, De-delayed block and DA-direct activation.

| E (V/cm) | Protocol | Failure | Direct block | Annihilation | Delayed block | Direct activation |
|---|---|---|---|---|---|---|
| 1 | Monophasic | 39.08 | 5.20 (0.97) | 10.73 (0.28) | 44.99 (1.04) | 0 (–) |
| | Biphasic I | 62.69 | 0.42 (0.59) | 19.03 (0.90) | 17.86 (1.18) | 0 (–) |
| | Biphasic II | 62.72 | 0.41 (0.25) | 10.10 (0.33) | 26.78 (0.41) | 0 (–) |
| 3 | Monophasic | 25.01 | 4.92 (0.31) | 18.68 (0.57) | 51.39 (0.56) | 0 (–) |
| | Biphasic I | 22.69 | 0.25 (0.14) | 26.42 (1.10) | 50.65 (1.10) | 0 (–) |
| | Biphasic II | 3.39 | 0.013 (0.015) | 28.97 (1.25) | 67.62 (1.26) | 0 (–) |
| 5 | Monophasic | 8.85 | 0 (–) | 9.58 (0.49) | 52.61 (0.75) | 28.95 (0.80) |
| | Biphasic I | 11.34 | 0 (–) | 7.03 (0.74) | 33.66 (0.90) | 47.97 (0.76) |
| | Biphasic II | 0.19 | 0 (–) | 12.49 (0.67) | 44.41 (0.91) | 42.92 (1.33) |
| 7 | Monophasic | 2.64 | 0 (–) | 1.51 (0.41) | 35.30 (0.96) | 60.56 (0.68) |
| | Biphasic 1 | 1.44 | 0 (–) | 0.19 (0.067) | 8.93 (1.10) | 89.44 (1.10 |
| | Biphasic II | 0.46 | 0 (–) | 0.25 (0.12) | 12.77 (1.79) | 86.51 (1.84) |

Table 4.2: Classification of the outcomes of defibrillation obtained by the ANN analysis for shocks of four different values of shock strength. The probability (in percents) and its standard deviation (in parentheses) is given for each outcome.

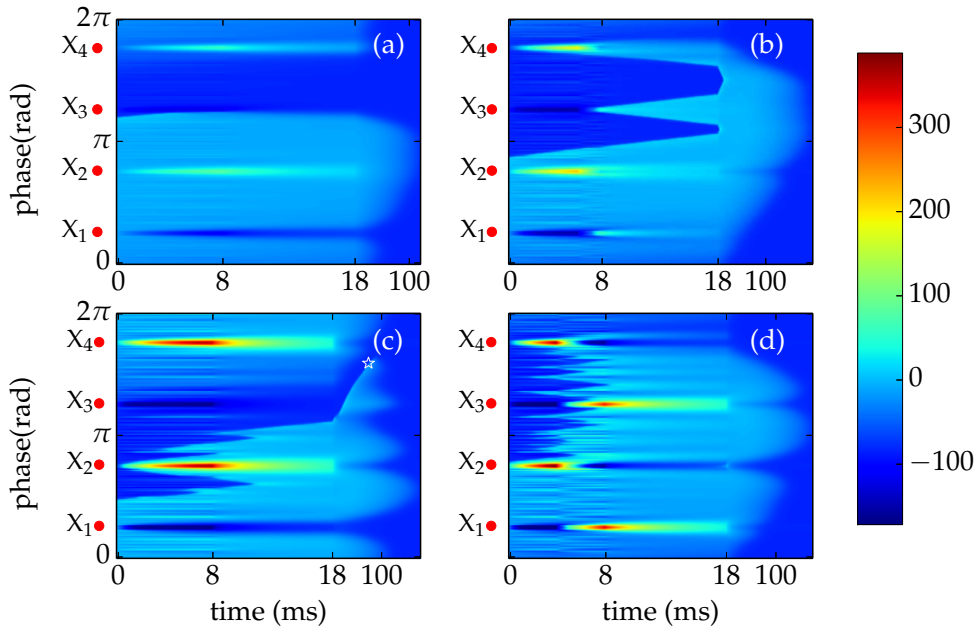


Figure 4.4: False color space-time plots of $V_m$ showing examples of defibrillation mechanisms. Defibrillation is applied with the four-electrode protocol. (a) Direct block (Monophasic, E=1V/cm) (b) Annihilation (biphasic II, E=3V/cm) (c) Delayed block (Monophasic, E=5V/cm), the white star denotes the point where the wave front was last found ($\phi_f(t')$), later used in the analysis (d) Direct activation (Biphasic 1, E=7V/cm). The shock is applied during the first 8ms of the plots. The time resolution is enlarged 10 times for t $\in$ (0,18) with respect to t $>$ 18ms. The color scale is equal for all the four plots.

the annihilation (An) mechanism, in which all the electrical activity on the ring is stopped by the collision of two oppositely propagating fronts. Figure 4.4b shows an example of the annihilation mechanism where the shock strength is E=3V/cm and the shock protocol is biphasic 2. In this case, the electrode located at position $X_3$ is anodal in the first phase (from t=0 to 6 ms) and cathodal in the second phase (from t=6 to 8 ms). For the electrode at $X_3$, the short depolarization is sufficient for eliciting two fronts. The downward front annihilates with the initial front that existed prior to the shock and the upward front annihilates with the front elicited by the electrode located at position $X_4$. A third identified mechanism of defibrillation is the so-called delayed block (De). It consists in the blockage of the surviving front passing through a region with refractory tissue. An example of this mechanism is shown in Fig. 4.4c. In this case, the shock strength is 5V/cm and the shock protocol is monophasic. In Fig. 4.4c, one observes that the shock strength is sufficient to produce virtual electrodes (VE) and one of those VE produces a new front. This front propagates until it encounters a region of refractory tissue and it is blocked. Finally, the fourth mechanism is the so–called direct activation mechanism because the shock activates a large portion of the cardiac tissue. When the tissue returns back to the rest state, none of the waves survive. An example of the direct activation mechanism is shown in Fig. 4.4d. In this case the shock strength is equal to 7V/cm and the shock protocol is the biphasic 1. The initial front is close to the $X_2$ electrode. The shock strength is large enough to produce many virtual electrodes in the region between the $X_2$ and $X_4$ electrodes.

Due to the large number of simulations, we have performed an automatic classification of the defibrillation mechanisms using artificial neural networks (ANN) [194]. The details of the classification method are described in the Sec. 2.5. Four values of shock strength, i.e., E=1, 3, 5 and 7V/cm, were analyzed in detail for each protocol. The results are shown in Fig. 4.2 and summarized in Table A.2. For low shock strengths, around E=1V/cm the monophasic shock protocol is the more efficient and the biphasic shocks have similar failure rate. Mean failure rates corresponding to the M, B1 and B2 protocols are approximately 39%, 62.7% and 62.7%, respectively. At low shock strength, one does not observe the creation of virtual electrodes, but some new fronts are created at the location of the physical electrodes, if the shock is depolarizing there. Fig. 4.2 and Table 4.2 confirm that the better efficiency of monophasic shock at E=1 V/cm is essentially due to the delayed block mechanism. Let us remind that the mean failure rates at the same shock strength (E=1 V/cm) for the two-electrode system and for the M, B1 and B2 protocols were approximately 72%, 83% and 84%, respectively [136]. Therefore, for low shock strengths, the shock outcome is substantially improved for the four-electrode system with respect to the two-electrode system.

As we increase the shock strength to 3 V/cm (see Fig. 4.2), the success rates for the M and B1 protocol reach a first plateau, while the success rate for the B2 protocol is already close to the 100% saturation. It is instructive to look at the mean values of the success rate at this shock strength (3V/cm), one gets: 76% (M), 78% (B1) and 97% (B2). Interestingly to note is that the biphasic 2 protocol already exceeds the 90% success rate which results in the aforementioned low $E_{90}$ threshold. Let us remind that for such shock strength, the corresponding mean values for the two-electrode system and the B2 protocol was only 42%. The results obtained for the M and B1 protocols, although not so efficient, are still significantly higher than in the case of the two-electrode system. The corresponding values for the two-electrode system were 43% (M) and 42%(B1). For shock strength values at E=1 and 3 V/cm, one does not observe the direct

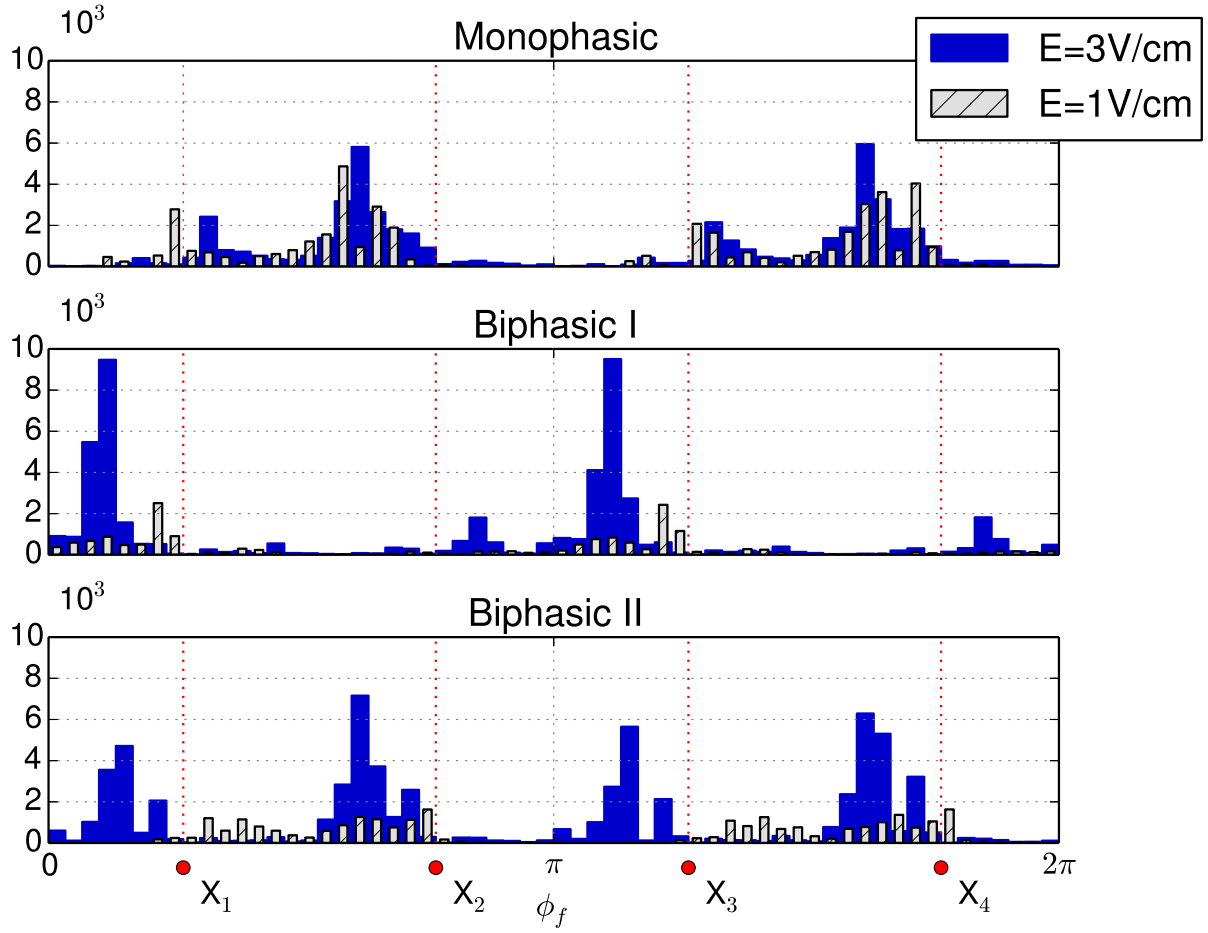


Figure 4.5: For the successful defibrillation trials via delayed block mechanism, $\phi_f$ denotes the position where the blocked front was last found. Histograms show results for Monophasic (upper), Biphasic I(middle) and Biphasic II shock (lower). Results for E=1V/cm are depicted with narrower bar width for clarity.

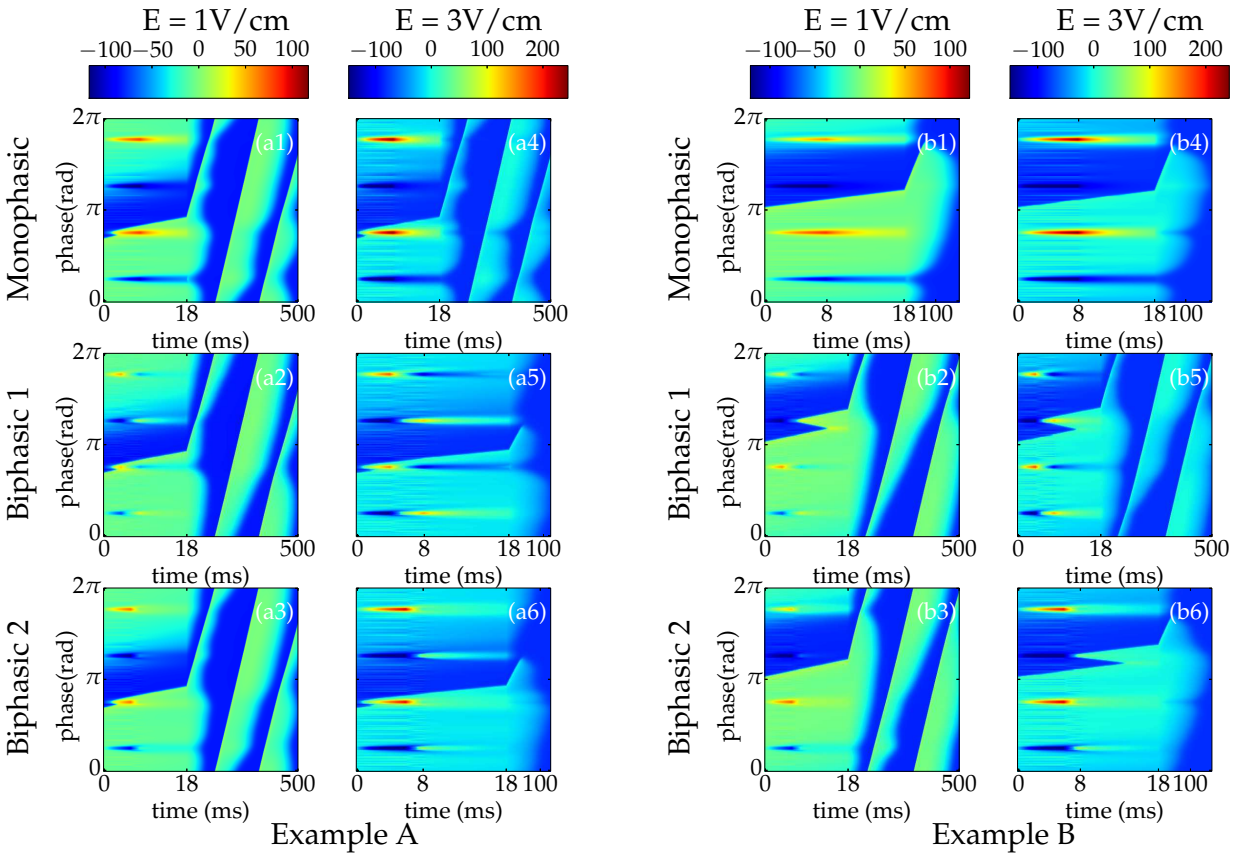


Figure 4.6: False color plots of $V_m$ for two different initial condition. Example A : $\phi_f(t=0) =$ 2.22rad and Example B: $\phi_f(t=0)$=3.27rad. External shock is applied during first 8ms. Time resolution is higher for t<18ms by one order of magnitude to highlight the effect of the shock. Space-plots are shown for two shock strengths : 1V/cm and 3V/cm (columns) and all three protocols (rows). All successful shock have defibrillated via delayed block mechanism. Note that for 3V/cm case, both B2 shock have resulted successful due to blockage of the front at two successive electrodes. In Example A biphasic II is similar to biphasic I protocol and in Example B to monophasic protocol.

activation defibrillation mechanism, just as it happened in the case of the two-electrode system. By comparing the observed defibrillation mechanisms at shock strength equals to 3V/cm in Fig. 4.3, one can see that the main difference between the B2 protocol and the other two is the very large percentage of delayed block defibrillation.

In order to further investigate this result, we have analyzed the delayed block mechanism in greater detail. We have proceeded in the following way: for every defibrillation trial that was successful via the delayed block mechanism we have kept the front location where the front was last seen. This point on the ring corresponds to $\phi_f(t = t')$ (see Fig. 2.7b), where $t'$ indicates the time where the front disappears. Fig. 4.4c shows an example of delayed block in which the corresponding $\phi_f(t')$ is indicted by a white star.

The statistics of the $\phi_f(t')$ points are shown in histograms in Fig. 4.5. In Fig. 4.5, the labels $X_1$, $X_2$, $X_3$ and $X_4$ denote the position of the electrodes matching those in Fig. 4.1. From Fig. 4.5,

one clearly sees that M protocol displays two higher peaks just behind the two cathodes located at $X_2$ and $X_4$. Let us remind that all the fronts used for the histogram are counterclockwise propagating (i.e. with increasing phase). Thus we can conclude that the delayed block mechanism occurred due to tissue depolarized by the cathode, i.e. the surviving front could not go through the refractory region created by the cathodal stimulus. Let us point out that delayed block events with the blocked front being clockwise along the ring occur in less than 1% of the total delayed block events for the M protocol. These clockwise events where omitted in the statistical analysis for simplicity. All the initial conditions are counterclockwise fronts and any resulting clockwise front is due to special defibrillation shocks. The histogram (Fig. 4.5, middle graph) corresponding to the B1 protocol shows high peaks but in this case right behind the electrodes located at $X_1$ and $X_3$. These electrodes have a second phase that is depolarizing (cathodal stimulus) and therefore generate a refractory region as in the case of the M protocol. The results for the B2 protocol are somewhat different. The histogram (Fig. 4.1, lower graph) shows four peaks just behind each of the four electrodes. In this latter case, all the electrodes have a cathodal character that generates a refractory region. Thus the high success rate of defibrillation for the B2 protocol for E=3V/cm is a result of the combined properties of the M and B1 protocols where delayed block can occur behind each of the electrodes.

In order to illustrate by examples the discussion of the previous paragraph, we have constructed space time plots corresponding to two different initial conditions (example A and example B) in Fig. 4.6. All the defibrillation protocols were tested on the two different initial conditions. Both sets show examples with shock strengths equal to 1V/cm and 3V/cm. In the cases displayed in Fig. 4.6, all the successful defibrillations were obtained via the delayed block mechanism. Let us first consider example A with a shock strength of 3V/cm. Figures 4.6.(a4-a6) show an unsuccessful M and successful B1 and B2 shocks. The latter two resulted successful due to the front blockage at $X_3$. The second phase for biphasic shocks is cathodal at location $X_3$. However, M protocols are anodal at the position $X_3$ and renders the tissue more excitable and therefore hinder the front blockage. Figures 4.6.(b4-b6) show the results corresponding to the example B. In this case, the M and B2 protocols result successful and the B1 protocol is unsuccessful. The front is blocked at location $X_4$ for both the M and B2 shocks, where the tissue is refractory. Monophasic shocks at $X_4$ are purely cathodal, but the second phases of B1 and B2 shocks at $X_4$ are anodal. However, the duration of the second phase for B2 protocol is only 2ms and therefore it is not long enough to render the tissue excitable. This is not the case for the B1 protocol, for which the second phase lasts for 4ms and it is long enough to hyperpolarize the tissue at $X_4$ and allows the front to propagate through $X_4$.

The same analysis is performed at lower shock strength for E=1V/cm. For the M protocol, the histogram in Fig. 4.1 (upper graph) shows a similar pattern as for the case of E= 3V/cm but with an overall lower frequency. The relatively high success rate for the M protocol at E= 1V/cm compared with the biphasic protocols can be explained by the fact that only the cathodal regions at $X_2$ and $X_4$ are strong enough to generate a refractory region for the M protocol for E= 1V/cm (see Fig. 4.6b1). In the examples taken in Fig. 4.6, none of the biphasic shocks (at E=1 V/cm) were strong enough to generate delayed block events.

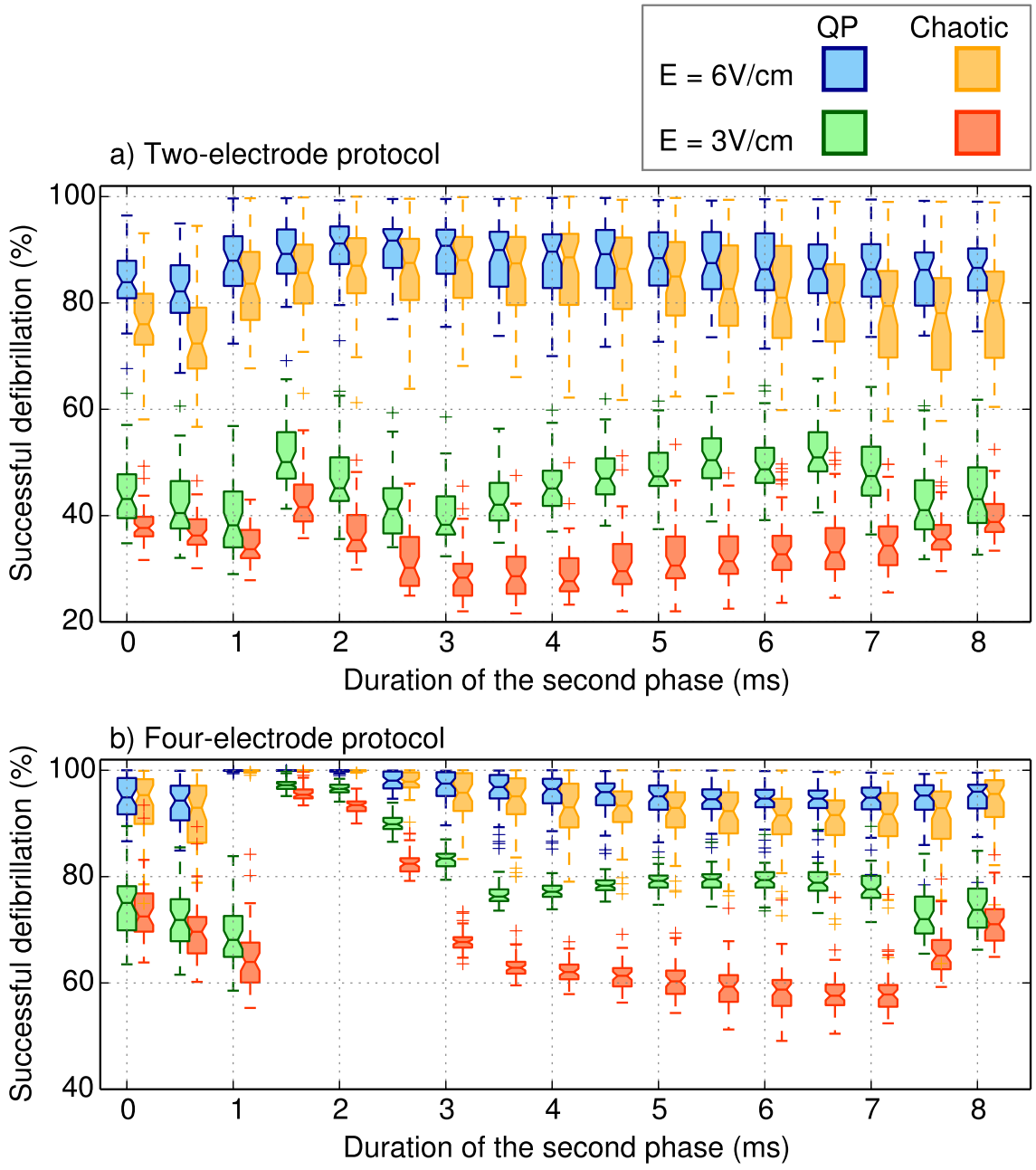


Figure 4.7: The total shock duration is fixed at 8ms, while the second phase is increased from 0ms (monophasic) to 8ms (again monophasic, but with reversed electrode positions). Shock strength is kept fixed to 3V/cm and 6V/cm. Each shock strength is tested on two dynamical states of the ring: quasiperiodic and chaotic. For clarity, the results for the two dynamical states are slightly shifted on the horizontal axis. a) Results obtained with the two-electrode protocol b) Results obtained with the four-electrode protocol.

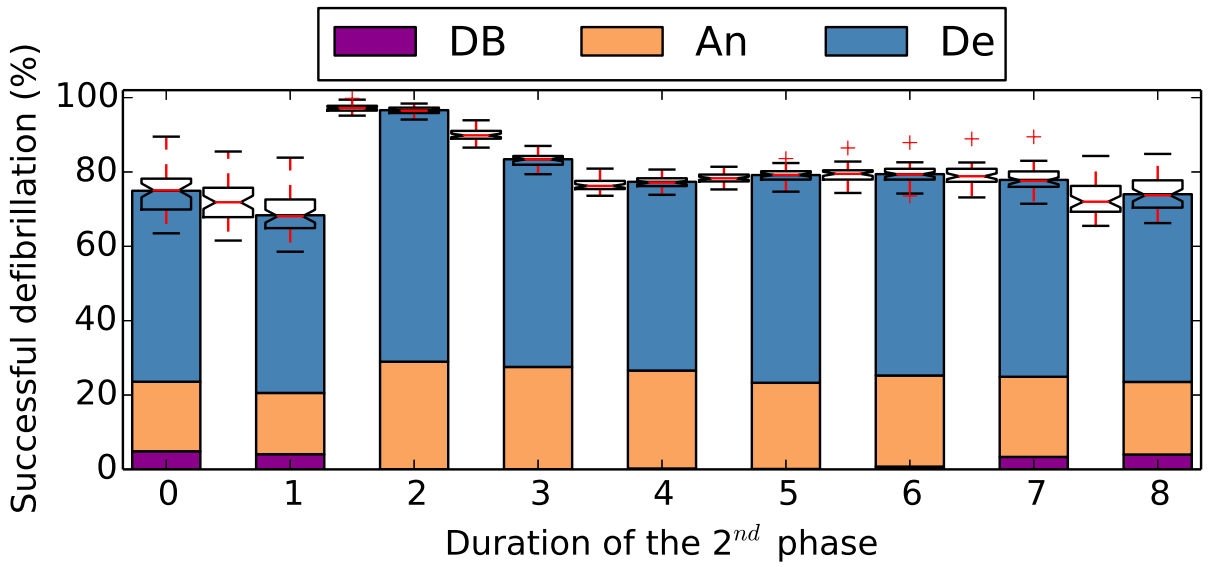


Figure 4.8: Dependence of defibrillation success on duration of the second phase of biphasic shock. Here the shock strength is fixed to 3V/cm. Initial dynamics is the QP state

### 4.0.3. The importance of the second phase

Following the discussion of the previous paragraph, one understands that the high success rate for the B2 protocol at E= 3V/cm is due to appropriate durations of the first and the second phase of the shock. These durations are such that they produce the largest amount of refractory regions along the ring and therefore lead to the maximum elimination of the propagating fronts. Following this hypothesis it would be interesting to check the influence of a modification of the duration of the second phase of the B2 protocol. Figure 4.7 displays the numerical results obtained for the success rate while varying the duration of the second phase. The total duration of the shock is 8ms, while the shock strength is kept fixed at 3V/cm and 6V/cm. Let us also note that in Fig. 4.7 when the duration of the second phase is equal to $0ms$ and $8ms$ one retrieves a monophasic shock. The former case (i.e. 0 ms) corresponds to the monophasic shock as schematized in Fig. 4.1, while the latter case (i.e. 8 ms) corresponds to a reversed placement of the anode and cathode with respect to the former case. The results of success rate for both monophasic shocks are comparable within the error bar of each other which is a further check of the consistency of our simulations.

The results presented in this chapter up to now were obtained with the ring in the quasiperiodic state. For the sake of comparison, in Fig. 4.7 we have displayed the results for both dynamical stats of the ring, i.e. quasiperiodic and chaotic. Fig. 4.7a displays the results for the two-electrode system and Fig. 4.7b for the four-electrode system. One can observe that the percentage of successful defibrillation for chaotic dynamical state is consistently lower than the corresponding results for the quasiperiodic state. The difference in percentage of success between the two dynamical states is smaller for the higher shock strength (E = 6V/cm), than it is for the lower shock strength (E = 3V/cm). These results are in the agreement with the analysis presented in the previous chapter (see Sec. 3.1.4). The two dynamical states display different

distribution of the wavefront width $\Delta\phi$. The higher the shock strength, the smaller is the dependence of the defibrillation success parameters of the reentrant wave $\Delta\phi$ and $\phi_b$. Therefore, the difference between the two dynamical states will be more prominent at smaller shock strengths.

The important message carried by Fig. 4.7 is that the percentage of defibrillation exhibits a marked maximum for a second phase duration in the range of 1.5 ms to 2 ms. This result holds for both two- and four-electrode systems and the two dynamical states. To further clarify the differences between different biphasic shocks for the four-electrode system, we have analyzed the defibrillation mechanisms for shock strength equal to 3V/cm. The results are shown in Fig. 4.8. Here the dynamics prior to the shock was the QP state. If we examine the defibrillation mechanisms corresponding to the shocks with a second phase duration equal to 2 ms with the other shocks, one can see that again the main difference lies in the higher fraction of the delayed block events than for other durations. Indeed, when comparing the mechanisms for second phase duration equal to 2 ms and 3 ms for which the fraction of the annihilation is equal within the error bar, the difference is caused solely by the larger proportion of delayed block mechanism in the case of second phase duration equals to 2 ms.

# Conclusions and Outlook

## Conclusions

In this thesis we have used a relatively simple one-dimensional model to study defibrillation mechanisms induced by three commonly applied clinical waveforms: monophasic, symmetric biphasic and asymmetric biphasic protocol. The idea behind a single numerical experiment is summarized as follows. The reentrant wave is present on the ring prior to the shock. Upon the application of the shock, the outcome is classified as successful if all electrical activity has ceased after a certain lapse time and unsuccessful if a circulating wave was still present. The aim of this simplified model is to define, validate and use a fast and reliable computational tool to study defibrillation mechanisms and new defibrillation waveforms. The one-dimensional model was defined in chapter 2, validated with well known clinical protocols in chapter 3 and finally used to study new defibrillation approaches in chapter 4. Let us stress that the idea of the one-dimensional model is built upon a work by Glass and Josephson who studied resetting and annihilation of the reentrant waves on a one-dimensional ring [27].

In the model used in this thesis, we underlie the importance of several key features. First, electrical signal propagation is modeled through the bidomain model. Second, of particular importance is the use of added heterogeneities to the internal conductivity coefficients. This was done following the work of Fishler [158] and Plank [164]. Third, two identified defibrillation related phenomena, electroporation and anode break excitation were also incorporated to the Beeler-Reuter cell membrane model [137], following the work of DeBruin and Krassowska [141] and Ranjan [151]. Despite the simplicity of the model (relative to the complicated three-dimensional structure of the heart), in chapter 2 we list a total of 7 parameters of the model that influence the defibrillation shock outcome.

In chapter 3 we study in detail three defibrillation protocols with a shock duration of 8ms. A detailed statistical analysis of close to 5 million simulations has allowed to rank the efficiency of the three tested protocols. For high shock strengths yielding a 90% success rate we have found that the biphasic II protocol is the most efficient, while monophasic protocol is the least efficient of the three. Comparing the monophasic and biphasic II protocol, we have found that biphasic II at high shock strength will defibrillate with 26% less energy than the monophasic protocol. This result is in the close agreement with the available experimental data in which a saving of 25% in energy is found when comparing monophasic and biphasic protocols [22, 23].

Careful analysis has also revealed that the successful defibrillation events can be classified into one of the four identified mechanisms: direct block, annihilation, delayed block and direct activation. Due to a large number of simulations performed, we have employed artificial neural networks

into an algorithm for automatic classification of the defibrillation events. The results revealed that the mechanisms which prevail will depend on the energy level, the current dynamical state of the system and the shock protocol. Direct activation mechanisms is characteristic of the high shock strengths and is nonexistent for shock strengths E$\leq$ 3V/cm. For the low-medium shock strength the positive defibrillation outcomes are the result of the remaining three mechanisms. The analysis of the defibrillation mechanisms has also revealed that the two parameters of the reentrant wave $(\Delta\phi, \phi_b)$ are important predictors of the defibrillation outcome. The $\phi_b$ parameter provides the information on the shock timing and the $\Delta\phi$ information on the reentrant dynamics present on the ring. This dependence of the defibrillation mechanisms on the $(\Delta\phi, \phi_b)$ parameters is more pronounced for lower shock strengths and less important for higher shock strengths.
In chapter 3 one-dimensional model is used to construct the strength-duration curves for the three tested protocols. For short shock durations (T $<$ 4ms), monophasic protocol resulted to be more successful than the biphasic protocols. For longer shock durations, biphasic protocols were more efficient. Chronaxie values were evaluated based on the Lapicque model. The chronaxie value for the monophasic protocol was approximately 3.2ms, while values for biphasic protocols were much longer, i.e. approximately 11ms for biphasic 1 and 8.5ms for the biphasic 2 protocol. According to the Lapicque model for the strength-duration curves, the optimum shock duration is equal to chronaxie (for rectangular pulses). It is often assumed that the chronaxie value is in the range of 2-5ms [195], while study presented here and some experimental studies [189, 196] suggest that in some cases chronaxie values for the biphasic protocols might be much longer. This difference in chronaxie values might have an importance for the design of the defibrillator devices since delivered energy is often the only parameter used for the waveform optimization.
In chapter 4 we propose and analyze a novel defibrillation setup in which defibrillation is applied with a four electrode system rather than a standard two-electrode system. The four-electrode system is analyzed and compared to the two-electrode system using the same one-dimensional ring model. Again three shock protocols were compared, monophasic and two biphasics. All three studied protocols applied with a four-electrode system resulted consistently more efficient than their corresponding two-electrode system counterpart. From the three studied protocols, the biphasic II protocol is the most efficient. Comparing the success rate at high shock energies, we have found that the M, B1 and B2 protocols in the four-electrode system will save 51%, 42% and 88% of energy when compared to the two-electrode system. Defibrillation events were again classified into four mechanism, direct block, annihilation, delayed block and direct activation. We have found that for high energy shocks for which the direct activation is the prevailing mechanism, the two systems (two- and four-electrode devices) do not differ much in rate of success and underlaying defibrillation mechanisms. The prevailing mechanism behind the $E_{90}$ threshold for the two electrode system is the direct activation mechanism, for which the shock strength must be high enough to excite sufficient virtual electrodes in the cardiac tissue. On the contrary, the $E_{90}$ threshold for the biphasic 2 protocol in the case of the four electrodes system is as low as E= 2V/cm. For such low shock strength, the defibrillation is achieved only by front to front interaction or interaction of front with refractory tissue. Furthermore, one has determined that the mechanism behind the supremacy of the biphasic 2 protocol is the delayed block mechanism but that a subtle tuning of the timing of the second phase of the B2 protocol is needed to obtain a very high performance defibrillation rates. One has observed that monophasic shocks block the propagating fronts by the depolarized tissue at the position of the cathodes and

the biphasic 1 at the position where the second phase is cathodal. Biphasic 2 shock can render the tissue unexcitable at the position of all four electrodes, thus having both properties of the M and B1 protocols. We have found that for the B2 protocol with phase 1 (6 ms) and phase 2 (2 ms) durations we get that, if the first phase is cathodal, the second phase is too short to render the tissue excitable. If the first phase is anodal, the second phase is long enough to render the tissue refractory. Percentage of success is also found for varying duration of the second phase (total shock duration is 8ms). It was found that higher efficiency of the biphasic protocol with the duration of the second phase 1.5ms-2ms is maintained for both: (1) two-electrode and four-electrode protocol and (2) quasiperiodic and chaotic dynamics prior to the shock. The simple message that this study of the four-electrode defibrillator conveys is that one can presumably obtain defibrillation at much lower energy if one uses a four electrode device.

## Outlook

There are two main directions in which the present study can be broadened: (1) increase the realism of the simulations by increasing the dimensionality of the model and (2) continue to use the developed 1D model to study defibrillation phenomena that are otherwise costly to analyze with more realistic models.

The idea behind a one-dimensional model presented and used in this thesis is to develop fast and reliable approach to study defibrillation phenomena. All the calculations are performed using the rectangular shock waveform. While this is a common waveform used in numerical and theoretical calculations, this is not the shock waveform found in the clinical practice. Commercially available defibrillators generate a waveform via a capacitor discharge, thus introducing additional parameters into the waveform optimization problem. In addition to the exponentially decaying waveforms generated by the capacitor discharge, one can also consider exponentially ascending waveform. Result obtained using a 0D model [80] indicates that this form of stimulus application is superior to both rectangular and exponentially decaying waveforms. The formalism presented in this thesis, in which one can classify defibrillation outcomes into four different classes could be used to compare the three waveforms: (exp) decaying, rectangular and ascending. A more mathematically rigorous approach could also be taken to explore the infinite functional space of possible waveforms. It seems interesting, although not straightforward, to apply the tools of optimal control theory to explore the optimum waveform of most efficient defibrillators.

While simplified 1D model are easier to analyze than their comparable two or three dimensional models, there are number of limitations associated with the low dimensionality of the model. For example, 1D model cannot sustain vortices and rotors which are very important in the study of arrhythmias. Experimentally, it is known that stronger shocks do not always relate to higher percentage of defibrillation [19, 165]. This characteristic of the defibrillation, related to the presence of the phase singularities [19], was not observed in the present one-dimensional model. Four-electrode defibrillator presented in chapter 4 revealed potentially important energy savings with respect to the current two-electrode system. These important energy savings obtained for the four electrode system open the door of some further study on a more realistic geometry and maybe some testing on more realistic condition. The realization of the implantable four-electrode or similar multi-electrode setup has already been patented in the 1980s [197, 198]. Note that

the first ICD device was also implanted in 1980 [4, Ch. 1.2]. Since then, to the extent of our knowledge, there has been only few attempts to test the different multi-electrode configurations [199, 200]. The simple message that this study of the four-electrode system conveys is that one can presumably obtain defibrillation at much lower energy if one uses a four electrode device. This could hopefully have some implications in the medical realm.

# Appendix A

# Supporting tables

In the tables shown in this Appendix we tabulate the results of the ANN analysis for the shock duration of 8ms. The results are displayed graphically in Fig. 3.2.

**Quasiperiodic dynamics**

| E (V/cm) | Protocol | Failure | Direct block | Annihilation | Delayed block | Direct activation |
|---|---|---|---|---|---|---|
| 1 | Monophasic | 72.51 | 3.16 (0.08) | 5.81 (0.15) | 18.51 (0.16) | 0 (−) |
| | Biphasic I | 82.64 | 0.099 (0.071) | 9.83 (0.11) | 7.42 (0.12) | 0(−) |
| | Biphasic II | 84.52 | 0.26 (0.018) | 4.67 (0.083) | 10.55 (0.08) | 0 (−) |
| 3 | Monophasic | 55.77 | 6.13 (0.25) | 7.92 (0.34) | 30.17 (0.27) | 0 (−) |
| | Biphasic I | 55.92 | 0.106 (0.08) | 15.16 (0.37) | 28.82 (0.38) | 0 (−) |
| | Biphasic II | 53.78 | 0.006 (0.01) | 15.17 (0.67) | 31.04 (0.67) | 0 (−) |
| 5 | Monophasic | 25.03 | 1.45 (1.91) | 8.80 (0.98) | 49.04 (2.17) | 15.68 (2.32) |
| | Biphasic I | 24.60 | 0.084 (0.106) | 14.80 (1.24) | 34.58 (1.51) | 25.93 (1.84) |
| | Biphasic II | 19.44 | 0.003 (0.008) | 12.88 (1.18) | 44.31 (1.66) | 23.36 (1.92) |
| 7 | Monophasic | 8.50 | 0 (−) | 6.82 (1.10) | 36.72 (2.64) | 47.96 (2.78) |
| | Biphasic I | 2.795 | 0 (−) | 4.60 (0.96) | 11.17 (2.08) | 81.44 (2.37) |
| | Biphasic II | 3.129 | 0 (−) | 0.67 (0.21) | 21.02 (1.92) | 75.18 (1.89) |

Table A.1: From [136]. Classification of the outcomes of defibrillation obtained by the ANN analysis for shocks of four different levels of energy. The probability (in percents) and its standard deviation (in parentheses) is given for each outcome. The reentrant dynamics present on the ring prior to the shock application is a quasiperiodic dynamics.

**Chaotic dynamics**

| E (V/cm) | Protocol | Failure | Direct block | Annihilation | Delayed block | Direct activation |
|---|---|---|---|---|---|---|
| 1 | Monophasic | 80.55 | 4.30 (0.15) | 6.37 (0.10) | 6.37 (0.10) | 0 (–) |
| | Biphasic 1 | 84.72 | 0.02 (0.02) | 11.99 (0.01) | 3.27 (0.02) | 0 (–) |
| | Biphasic 2 | 92.67 | 0.02 (0.01) | 5.71 (0.06) | 1.59 (0.05) | 0 (–) |
| 3 | Monophasic | 61.62 | 5.33 (0.22) | 9.70 (0.26) | 23.35 (0.17) | 0 (–) |
| | Biphasic 1 | 70.82 | 0.03 (0.02) | 16.80 (0.09) | 12.36 (0.08) | 0 (–) |
| | Biphasic 2 | 63.18 | 0.02 (0.02) | 17.76 (0.08) | 19.05 (0.07) | 0 (–) |
| 5 | Monophasic | 37.88 | 0.0005 (0.002) | 7.30 (0.41) | 38.29 (0.30) | 15.54 (0.34) |
| | Biphasic 1 | 31.75 | 0.0002 (0.0004) | 15.56 (0.36) | 29.35 (0.56) | 23.35 (0.75) |
| | Biphasic 2 | 27.63 | 0 (–) | 14.89 (0.25) | 36.20 (0.55) | 21.28 (0.56) |
| 7 | Monophasic | 13.81 | 0 (–) | 3.49 (0.30) | 35.14 (1.00) | 47.57 (1.16) |
| | Biphasic 1 | 3.82 | 0 (–) | 2.43 (0.40) | 11.79 (0.70) | 81.97 (0.82 |
| | Biphasic 2 | 4.65 | 0 (–) | 2.30 (0.57) | 19.63 (0.62) | 73.42 (0.97) |

Table A.2: Classification of the outcomes of defibrillation obtained by the ANN analysis for shocks of four different levels of energy. The probability (in percents) and its standard deviation (in parentheses) is given for each outcome. The reentrant dynamics present on the ring prior to the shock application is a chaotic dynamics.

# Appendix B

# Supporting graphics

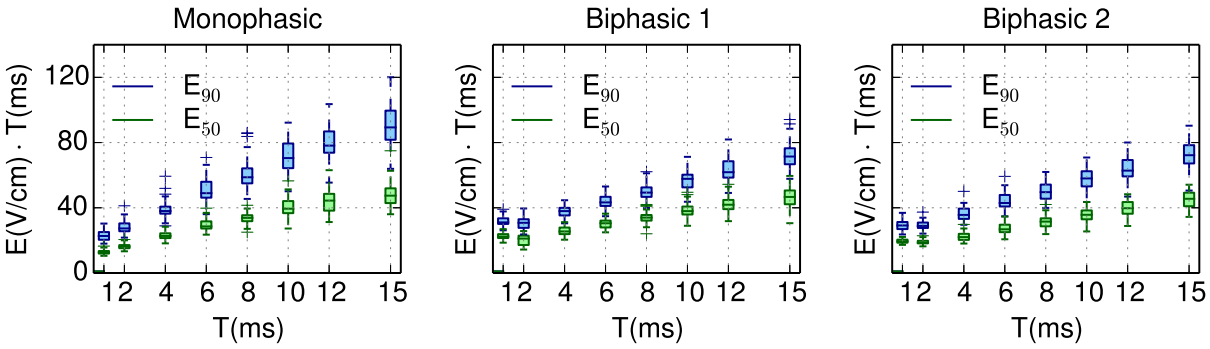


Figure B.1: Lapicque model (see Eq. 1.16): The strength-duration curve follows a hyperbolic dependence. Lapicque model can be made linear by multiplying Eq. 1.16 with the shock duration T. The graphs show $E_{90}$ and $E_{50}$ thresholds obtained with our 1D model multiplied with the shock duration T. Thus, if the Lapicque model is a suitable representation of the strength vs shock duration, one should expect an approximately linear dependence.

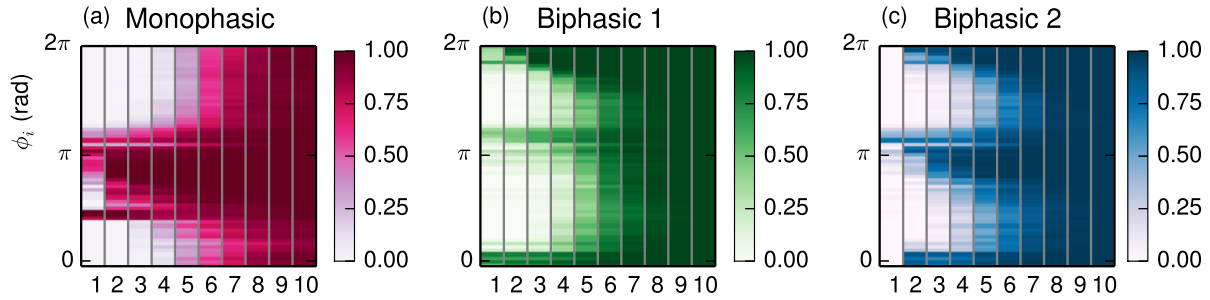


Figure B.2: False color histograms showing the probability of success as a function of the initial position of the reentrant wave $\phi_i$ and the shock energy. A total of 10 shock energy is shown in the range of E=1-10V/cm. Here the dynamics prior to the shock is in the chaotic state.

# Bibliography


[1] M. Turakhia, Z. H. Tseng. *Sudden cardiac death: epidemiology, mechanisms, and therapy.* Current problems in cardiology **32 (9)**, (2007), pp. 501–46.

[2] A. Winfree. *When Time Breaks Down: The Three- Dimensional Dynamics of Electrochemical Waves and Cardiac Arrhythmias.* Princeton University Press (1987).

[3] J. P. Nolan, J. Soar, D. A. Zideman, D. Biarent, L. L. Bossaert, C. Deakin, R. W. Koster, J. Wyllie, B. Böttiger. *European resuscitation council guidelines for resuscitation 2010 section 1. executive summary.* Resuscitation **81 (10)**, (2010), pp. 1219 – 1276.

[4] I. R. Efimov, M. W. Kroll, P. J. Tchou, eds. *Cardiac Bioelectric Therapy : Mechanisms and Pratical Implications.* Springer (2009).

[5] G. Boriani, M. Biffi, P. Silvestri, C. Martignani, C. Valzania, I. Diemberger, C. Moulder, G. Mouchawar, M. Kroll, A. Branzi. *Mechanisms of pain associated with internal defibrillation shocks: results of a randomized study of shock waveform.* Heart Rhythm **2 (7)**, (2005), pp. 708–13.

[6] T. Tokano, D. Bach, J. Chang, J. Davis, J. J. Souza, A. Zivin, B. P. Knight, R. Goyal, K. C. Man, F. Morady, S. A. Strickberger. *Effect of ventricular shock strength on cardiac hemodynamics.* J. Card. Electrophys. **9 (8)**, (1998), pp. 791–7.

[7] A. T. Sambelashvili, V. P. Nikolski, I. R. Efimov. *Virtual electrode theory explains pacing threshold increase caused by cardiac tissue damage.* American journal of physiology. Heart and circulatory physiology **286 (6)**, (2004), pp. H2183–94.

[8] V. Sharma, R. C. Susil, L. Tung. *Paradoxical loss of excitation with high intensity pulses during electric field stimulation of single cardiac cells.* Biophysical journal **88 (4)**, (2005), pp. 3038–49.

[9] A. Zivin, J. Souza, F. Pelosi, M. Flemming, B. P. Knight, R. Goyal, F. Morady, S. A. Strickberger. *Relationship between shock energy and postdefibrillation ventricular arrhythmias in patients with implantable defibrillators.* Journal of cardiovascular electrophysiology **10 (3)**, (1999), pp. 370–7.

[10] Cardiac Arrhythmia Suppression Trial (CAST) Investigators. *Preliminary report: Effect of encainide and flecainide on mortality in a randomized trial of arrhythmia suppression after myocardial infarction.* New England Journal of Medicine **321 (6)**, (1989), pp. 406–412.

[11] Cardiac Arrhythmia Suppression Trial (CAST) II Investigators. *Effect of the antiarrhythmic agent moricizine on survival after myocardial infarction.* New England Journal of Medicine **327 (4)**, (1992), pp. 227–233.

[12] A. L. Waldo, A. J. Camm, H. DeRuyter, P. L. Friedman, D. J. MacNeil, J. F. Pauls, B. Pitt, C. M. Pratt, P. J. Schwartz, E. P. Veltri. *Effect of d-sotalol on mortality in patients with left ventricular dysfunction after recent and remote myocardial infarction.* Lancet **348 (9019)**, (1996), pp. 7–12.

[13] C. Beck, W. Pritchard, H. Feil. *Ventricular fibrillation of long duration abolished by electric shock.* Journal of the American Medical Association **135 (15)**, (1947), pp. 985–986.

[14] W. Kouwenhoven, W. Milnor, G. Knickerbocker, W. Chesnut. *Closed chest defibrillation of the heart.* Surgery **42 (3)**, (1957), pp. 550–61.

[15] D. Rosenbaum, J. Jalife, eds. *Optical Mapping of Cardiac Excitation and Arrhythmias.* Futura Publishing Co., Inc., New York (2001).

[16] S. M. Dillon. *Optical recordings in the rabbit heart show that defibrillation strength shocks prolong the duration of depolarization and the refractory period.* Circulation Research **69 (3)**, (1991), pp. 842–856.

[17] S. B. Knisley, B. C. Hill, R. E. Ideker. *Virtual electrode effects in myocardial fibers.* Biophysical journal **66 (3 Pt 1)**, (1994), pp. 719–28.

[18] J. P. Wikswo, S. F. Lin, R. a. Abbas. *Virtual electrodes in cardiac tissue: a common mechanism for anodal and cathodal stimulation.* Biophysical journal **69 (6)**, (1995), pp. 2195–210.

[19] I. R. Efimov, Y. Cheng, D. R. Van Wagoner, T. Mazgalev, P. J. Tchou. *Virtual Electrode Induced Phase Singularity : A Basic Mechanism of Defibrillation Failure.* Circulation Research **82 (8)**, (1998), pp. 918–25.

[20] I. Banville, R. A. Gray, R. E. Ideker, W. M. Smith. *Shock-Induced Figure-of-Eight Reentry in the Isolated Rabbit Heart.* Circulation Research **85 (8)**, (1999), pp. 742–752.

[21] G. Plank, M. Liebmann, R. Weber dos Santos, E. J. Vigmond, G. Haase. *Algebraic multigrid preconditioner for the cardiac bidomain model.* IEEE transactions on bio-medical engineering **54 (4)**, (2007), pp. 585–96.

[22] P. S. Chen, N. Shibata, E. G. Dixon, R. O. Martin, R. E. Ideker. *Comparison of the defibrillation threshold and the upper limit of ventricular vulnerability.* Circulation **73 (5)**, (1986), pp. 1022–1028.

[23] E. G. Dixon, A. S. Tang, P. D. Wolf, J. T. Meador, M. J. Fine, R. V. Calfee, R. E. Ideker. *Improved defibrillation thresholds with large contoured epicardial electrodes and biphasic waveforms.* Circulation **76 (5)**, (1987), pp. 1176–1184.

[24] A. S. Tang, S. Yabe, J. Wharton, M. Dolker, W. M. Smith, R. E. Ideker. *Ventricular defibrillation using biphasic waveforms: The importance of phasic duration.* Journal of the American College of Cardiology **13 (1)**, (1989), pp. 207–214.

[25] M. Block, G. Breithardt. *Optimizing defibrillation through improved waveforms.* Pacing and clinical electrophysiology **18 (3 Pt 2)**, (1995), pp. 526–38.

[26] N. Trayanova, J. Constantino, T. Ashihara, G. Plank. *Modeling defibrillation of the heart: approaches and insights.* IEEE reviews in biomedical engineering **4**, (2011), pp. 89–102.

[27] L. Glass, M. Josephson. *Resetting and Annihilation of Reentrant Abnormally Rapid Heartbeat.* Physical Review Letters **75 (10)**, (1995), pp. 2059–2062.

[28] R. Klabunde. *Cardiovascular Physiology Concepts.* Lippincott Williams & Wilkins (2005).

[29] Z. F. Issa, J. M. Miller, D. P. Zipes. *Chapter 2 - cardiac ion channels.* In *Clinical Arrhythmology and Electrophysiology: A Companion to Braunwald's Heart Disease (Second Edition)*, pp. 512 – 561. W.B. Saunders, Philadelphia, second edition edn. (2012).

[30] A. S. Amin, H. L. Tan, A. A. M. Wilde. *Cardiac ion channels in health and disease.* Heart rhythm : the official journal of the Heart Rhythm Society **7 (1)**, (2010), pp. 117–26.

[31] D. Noble. *A modification of the Hodgkin–Huxley equations applicable to Purkinje fibre action and pace-maker potentials.* The Journal of physiology **160**, (1962), pp. 317–52.

[32] A. L. Hodgkin, A. F. Huxley. *A quantitative description of membrane current and its application to conduction and excitation in nerve.* The Journal of physiology **117 (4)**, (1952), pp. 500–44.

[33] F. H. Fenton, E. M. Cherry. *Models of cardiac cell* **3 (8)**, (2008), p. 1868.

[34] C. L. B. M. Pullan, A.J. *Mathematical modelling the electrical activity of the heart : from cell to body surface and back again.* World Scientific Publishing Co. Pte. Ltd (2005).

[35] O. H. Schmitt. *Biological information processing using the concept of interpenetrating domains.* In K. Leibovic, ed., *Information Processing in The Nervous System*, pp. 325–331. Springer Berlin Heidelberg (1969).

[36] L. Tung. *A bi-domain model for describing ischemic myocardial dc potentials.* Ph.D. thesis, Massachusetts Institute of Technology (1978).

[37] F. H. Fenton, E. M. Cherry, L. Glass. *Cardiac arrhythmia* **3 (7)**, (2008), p. 1665.

[38] A. G. Mayer. *Rhythmical pulsation in Scyphomedusae.* Carnegie Institution of Washington„ Washington,.

[39] G. R. Mines. *On dynamic equilibrium in the heart.* The Journal of physiology **46 (4-5)**, (1913), pp. 349–83.

[40] M. A. Alleesie, F. I. M. Bonke, F. J. G. Schopman. *Circus Movement in Rabbit Atrial Muscle as a Mechanism of Tachycardia.* Circulation Research **33 (1)**, (1973), pp. 54–62.

[41] J. M. Davidenko, P. F. Kent, D. R. Chialvo, D. C. Michaels, J. Jalife. *Sustained vortex-like waves in normal isolated ventricular muscle.* Proceedings of the National Academy of Sciences of the United States of America **87 (22)**, (1990), pp. 8785–9.

[42] J. M. Davidenko, A. V. Pertsov, R. Salomonsz, W. Baxter, J. Jalife. *Stationary and drifting spiral waves of excitation in isolated cardiac muscle.* Nature **355 (6358)**, (1992), pp. 349–51.

[43] A. M. Pertsov, J. M. Davidenko, R. Salomonsz, W. T. Baxter, J. Jalife. *Spiral waves of excitation underlie reentrant activity in isolated cardiac muscle.* Circulation research **72 (3)**, (1993), pp. 631–50.

[44] M. A. Allessie, F. I. Bonke, F. J. Schopman. *Circus movement in rabbit atrial muscle as a mechanism of tachycardia. III. The "leading circle" concept: a new model of circus movement in cardiac tissue without the involvement of an anatomical obstacle.* Circulation Research **41 (1)**, (1977), pp. 9–18.

[45] G. Moe. *On the multiple wavelet hypothesis of atrial fibrillation.* Arch Int Pharmacodyn Ther **1409**, (1962), pp. 183–188.

[46] G. K. Moe, W. C. Rheinboldt, J. Abildskov. *A computer model of atrial fibrillation.* American Heart Journal **67 (2)**, (1964), pp. 200–220.

[47] M. Guevara, G. Ward, A. Shrier, L. Glass. *Electrical alternans and period doubling bifurcations.* IEEE Comp. Cardiol **562**, (1984), pp. 167–170.

[48] J. B. Nolasco, R. W. Dahlen. *A graphic method for the study of alternation in cardiac action potentials.* Journal of applied physiology **25 (2)**, (1968), pp. 191–6.

[49] F. Fenton, A. Karma. *Vortex dynamics in three-dimensional continuous myocardium with fiber rotation: Filament instability and fibrillation.* Chaos: An Interdisciplinary Journal of Nonlinear Science **8 (1)**, (1998), pp. 20–47.

[50] F. Fenton, S. Evans, H. Hastings. *Memory in an Excitable Medium: A Mechanism for Spiral Wave Breakup in the Low-Excitability Limit.* Physical Review Letters **83 (19)**, (1999), pp. 3964–3967.

[51] J. M. Cao, Z. Qu, Y. H. Kim, T. J. Wu, A. Garfinkel, J. N. Weiss, H. S. Karagueuzian, P. S. Chen. *Spatiotemporal heterogeneity in the induction of ventricular fibrillation by rapid pacing: importance of cardiac restitution properties.* Circulation research **84 (11)**, (1999), pp. 1318–31.

[52] A. Garfinkel, Y. H. Kim, O. Voroshilovsky, Z. Qu, J. R. Kil, M. H. Lee, H. S. Karagueuzian, J. N. Weiss, P. S. Chen. *Preventing ventricular fibrillation by flattening cardiac restitution.* Proceedings of the National Academy of Sciences of the United States of America **97 (11)**, (2000), pp. 6061–6.

[53] E. M. Cherry, F. H. Fenton. *Suppression of alternans and conduction blocks despite steep APD restitution: electrotonic, memory, and conduction velocity restitution effects.* American journal of physiology. Heart and circulatory physiology **286 (6)**, (2004), pp. H2332–41.

[54] Z. Qu, A. Garfinkel, P.-S. Chen, J. N. Weiss. *Mechanisms of Discordant Alternans and Induction of Reentry in Simulated Cardiac Tissue.* Circulation **102 (14)**, (2000), pp. 1664–70.

[55] K. H. W. J. ten Tusscher, A. V. Panfilov. *Alternans and spiral breakup in a human ventricular tissue model.* American journal of physiology. Heart and circulatory physiology **291 (3)**, (2006), pp. H1088–100.

[56] B. R. Choi, T. Liu, G. Salama. *The Distribution of Refractory Periods Influences the Dynamics of Ventricular Fibrillation.* Circulation Research **88 (5)**, (2001), pp. e49–e58.

[57] B. R. Choi. *Life Span of Ventricular Fibrillation Frequencies.* Circulation Research **91 (4)**, (2002), pp. 339–345.

[58] M. Valderrabano. *Frequency Analysis of Ventricular Fibrillation in Swine Ventricles.* Circulation Research **90 (2)**, (2001), pp. 213–222.

[59] J. M. Rogers, J. Huang, W. M. Smith, R. E. Ideker. *Incidence, Evolution, and Spatial Distribution of Functional Reentry During Ventricular Fibrillation in Pigs.* Circulation Research **84 (8)**, (1999), pp. 945–954.

[60] T. Lewis. *The Mechanism and Graphic Registration of the Heart Beat ... 3rd Edition [of "The Mechanism of the Heart Beat." With a Bibliography].* Shaw & Sons (1925).

[61] N. L. Gurevich. *The main principles of cardiac defibrillation [in russian].* Medicine, Moscow .

[62] J. Jalife. *Ventricular fibrillation: mechanisms of initiation and maintenance.* Annual review of physiology **62**, (2000), pp. 25–50.

[63] J. Chen, R. Mandapati, O. Berenfeld, A. C. Skanes, J. Jalife. *High-Frequency Periodic Sources Underlie Ventricular Fibrillation in the Isolated Rabbit Heart.* Circulation Research **86 (1)**, (2000), pp. 86–93.

[64] A. V. Zaitsev, O. Berenfeld, S. F. Mironov, J. Jalife, A. M. Pertsov. *Distribution of Excitation Frequencies on the Epicardial and Endocardial Surfaces of Fibrillating Ventricular Wall of the Sheep Heart.* Circulation Research **86 (4)**, (2000), pp. 408–417.

[65] F. H. Samie, O. Berenfeld, J. Anumonwo, S. F. Mironov, S. Udassi, J. Beaumont, S. Taffet, A. M. Pertsov, J. Jalife. *Rectification of the Background Potassium Current: A Determinant of Rotor Dynamics in Ventricular Fibrillation.* Circulation Research **89 (12)**, (2001), pp. 1216–1223.

[66] M. Haïssaguerre, M. Shoda, P. Jaïs, A. Nogami, D. C. Shah, J. Kautzner, T. Arentz, D. Kalushe, D. Lamaison, M. Griffith, F. Cruz, A. de Paola, F. Gaïta, M. Hocini, S. Garrigue, L. Macle, R. Weerasooriya, J. Clémenty. *Mapping and ablation of idiopathic ventricular fibrillation.* Circulation **106 (8)**, (2002), pp. 962–7.

[67] T.-J. Wu, S.-F. Lin, J. N. Weiss, C.-T. Ting, P.-S. Chen. *Two types of ventricular fibrillation in isolated rabbit hearts: importance of excitability and action potential duration restitution.* Circulation **106 (14)**, (2002), pp. 1859–66.

[68] K. Chatterjee. *Cardiology: An Illustrated Textbook.* Jaypee Brothers, Medical Publishers (2011).

[69] C. D. Deakin, J. P. Nolan, K. Sunde, R. W. Koster. *European Resuscitation Council Guidelines for Resuscitation 2010 Section 3. Electrical therapies: automated external defibrillators, defibrillation, cardioversion and pacing.* Resuscitation **81 (10)**, (2010), pp. 1293–304.

[70] L. Liem. *Implantable Cardioverter-Defibrillator: A Practical Manual*. Springer (2001).

[71] J. Prevost, F. Batelli. *La mort par les courants électriques-courants alternatifs a haute tension*. Journale de Physiologie et de Pathologie Generale **ii**, (1899), pp. 427–442.

[72] N. Paradis, H. Halperin, K. Kern, V. Wenzel, D. Chamberlain, eds. *Cardiac Arrest : The Science and Practice of Resuscitation Medicine*. Cambridge University Press (2007).

[73] D. R. Hooker, W. B. Kouwenhoven, O. R. Langworthy. *The effect of alternating electrical currentson the heart*. American Journal of Physiology **103 (2)**, (1933), pp. 444–454.

[74] W. B. Kouwenhoven, R. D. Hooker. *Resuscitation by countershock*. Electrical Engineering **52 (7)**, (1933), pp. 475–477.

[75] B. Lown, R. Amarasingham, J. Neuamn. *New method for terminating cardiac arrhythmias. Use of synchronized capacitor discharge.* JAMA : the journal of the American Medical Association **182**, (1962), pp. 548–55.

[76] J. C. Schuder, H. Stoeckle, J. H. Gold, J. A. West, P. Y. Keskar. *Experimental ventricular defibrillation with an automatic and completely implanted system.* Transactions - American Society for Artificial Internal Organs **16**, (1970), pp. 207–12.

[77] M. Mirowski. *Standby Automatic Defibrillator*. Archives of Internal Medicine **126 (1)**, (1970), p. 158.

[78] M. Mirowski, P. R. Reid, M. M. Mower, L. Watkins, V. L. Gott, J. F. Schauble, A. Langer, M. S. Heilman, S. A. Kolenik, R. E. Fischell, M. L. Weisfeldt. *Termination of malignant ventricular arrhythmias with an implanted automatic defibrillator in human beings.* The New England journal of medicine **303 (6)**, (1980), pp. 322–4.

[79] W. Irnich. *Optimal Truncation of Defibrillation Pulses*. Pacing and Clinical Electrophysiology **18 (4)**, (1995), pp. 673–688.

[80] M. G. Fishler. *Theoretical predictions of the optimal monophasic and biphasic defibrillation waveshapes*. IEEE Transactions on Biomedical Engineering **47 (1)**, (2000), pp. 59–67.

[81] J. C. Schuder, G. A. Rahmoeller, H. Stoeckle. *Transthoracic Ventricular Defibrillation with Triangular and Trapezoidal Waveforms*. Circulation Research **19 (4)**, (1966), pp. 689–694.

[82] E. Raugalas, Z. Blazek, M. Vrána. *Efficacy of monophasic electrical impulses with steep leading and trailing edges in cardiac defibrillation.* Cor et vasa **19 (4-5)**, (1977), pp. 376–84.

[83] S. R. Shorofsky, E. Rashba, W. Havel, P. Belk, P. Degroot, C. Swerdlow, M. R. Gold. *Improved defibrillation efficacy with an ascending ramp waveform in humans.* Heart Rhythm **2 (4)**, (2005), pp. 388–394.

[84] J. Huang, G. P. Walcott, R. B. Ruse, S. J. Bohanan, C. R. Killingsworth, R. E. Ideker. *An Ascending Ramp Biphasic Waveform Has a Lower Defibrillation Threshold and Releases Less Troponin I Than a Truncated Exponential Biphasic Waveform.* Circulation **126 (11)**, (2012), pp. 1328–33.

[85] G. H. Bardy, T. D. Ivey, M. D. Allen, G. Johnson, R. Mehra, H. Greene. *A prospective randomized evaluation of biphasic versus monophasic waveform pulses on defibrillation efficacy in humans.* Journal of the American College of Cardiology **14 (3)**, (1989), pp. 728–733.

[86] K. M. Kavanagh, A. S. Tang, D. L. Rollins, W. M. Smith, R. E. Ideker. *Comparison of the internal defibrillation thresholds for monophasic and double and single capacitor biphasic waveforms.* Journal of the American College of Cardiology **14 (5)**, (1989), pp. 1343–1349.

[87] S. A. Feeser, A. S. Tang, K. M. Kavanagh, D. L. Rollins, W. M. Smith, P. D. Wolf, R. E. Ideker. *Strength-duration and probability of success curves for defibrillation with biphasic waveforms.* Circulation **82 (6)**, (1990), pp. 2128–2141.

[88] R. A. Cooper, C. A. Alferness, W. M. Smith, R. E. Ideker. *Internal cardioversion of atrial fibrillation in sheep.* Circulation **87 (5)**, (1993), pp. 1673–1686.

[89] T. Schneider, P. R. Martens, H. Paschen, M. Kuisma, B. Wolcke, B. E. Gliner, J. K. Russell, W. D. Weaver, L. Bossaert, D. Chamberlain. *Multicenter, Randomized, Controlled Trial of 150-J Biphasic Shocks Compared With 200- to 360-J Monophasic Shocks in the Resuscitation of Out-of-Hospital Cardiac Arrest Victims.* Circulation **102 (15)**, (2000), pp. 1780–1787.

[90] D. Hayes, S. Asirvatham. *Dictionary of Cardiac Pacing, Defibrillation, Resynchronization, and Arrhythmias.* Second edition edn. (2007).

[91] J. C. Schuder, H. Stoeckle, A. M. Dolan. *Transthoracic Ventricular Defibrillation with Square-wave Stimuli: One-Half Cycle, One Cycle, and Multicycle Waveforms.* Circulation Research **15 (3)**, (1964), pp. 258–264.

[92] D. L. Jones, W. D. Irish, G. J. Klein. *Defibrillation efficacy. Comparison of defibrillation threshold versus dose-response curve determination.* Circulation research **69 (1)**, (1991), pp. 45–51.

[93] M. F. Rattes, D. L. Jones, A. D. Sharma, G. J. Klein. *Defibrillation threshold: a simple and quantitative estimate of the ability to defibrillate.* Pacing and clinical electrophysiology **10 (1 Pt 1)**, (1987), pp. 70–7.

[94] J. C. Schuder. *Ventricular Defibrillation in the Dog With a Bielectrode Intravascular Catheter.* Archives of Internal Medicine **132 (2)**, (1973), p. 286.

[95] G. P. Walcott, R. G. Walker, A. W. Cates, W. Krassowska, W. M. Smith, R. E. Ideker. *Choosing the optimal monophasic and biphasic waveforms for ventricular defibrillation.* Journal of cardiovascular electrophysiology **6 (9)**, (1995), pp. 737–50.

[96] L. A. Geddes, J. D. Bourland. *The Strength-Duration Curve.* IEEE Transactions on Biomedical Engineering **BME-32 (6)**, (1985), pp. 458–459.

[97] H. A. Blair. *On the intensity-time relations for stimulation by electric currents. II.* The Journal of general physiology **15 (6)**, (1932), pp. 731–55.

[98] H. A. Blair. *On the intensity-time relations for stimulation by electric currents. I.* The Journal of general physiology **15 (6)**, (1932), pp. 709–29.

[99] J. H. Gold, J. C. Schuder, H. Stoeckle, T. A. Granberg, S. Z. Hamdani, J. M. Rychlewski. *Transthoracic ventricular defibrillation in the 100 kg calf with unidirectional rectangular pulses.* Circulation **56 (5)**, (1977), pp. 745–750.

[100] C. D. Swerdlow, J. E. Brewer, R. M. Kass, M. W. Kroll. *Application of Models of Defibrillation to Human Defibrillation Data : Implications for Optimizing Implantable Defibrillator Capacitance.* Circulation **96 (9)**, (1997), pp. 2813–2822.

[101] M. W. Kroll. *A minimal model of the single capacitor biphasic defibrillation waveform.* Pacing and clinical electrophysiology **17 (11 Pt 1)**, (1994), pp. 1782–1792.

[102] M. W. Kroll. *A minimal model of the monophasic defibrillation pulse.* Pacing and clinical electrophysiology **16 (4 Pt 1)**, (1993), pp. 769–77.

[103] B. G. Cleland. *A conceptual basis for defibrillation waveforms.* Pacing and clinical electrophysiology **19 (8)**, (1996), pp. 1186–95.

[104] J. B. White, G. P. Walcott, J. L. Wayland, W. M. Smith, R. E. Ideker. *Predicting the relative efficacy of shock waveforms for transthoracic defibrillation in dogs.* Annals of emergency medicine **34 (3)**, (1999), pp. 309–20.

[105] P. Schauerte, F. A. Schöndube, M. Grossmann, H. Dörge, F. Stein, B. Dohmen, A. Moumen, K. Erena, B. J. Messmer, P. Hanrath, C. Stellbrink. *Influence of phase duration of biphasic waveforms on defibrillation energy requirements with a 70-microF capacitance.* Circulation **97 (20)**, (1998), pp. 2073–8.

[106] C. D. Swerdlow, W. Fan, J. E. Brewer. *Charge-Burping Theory Correctly Predicts Optimal Ratios of Phase Duration for Biphasic Defibrillation Waveforms.* Circulation **94 (9)**, (1996), pp. 2278–2284.

[107] G. Mouchawar, M. Kroll, J. E. Val-Mejias, D. Schwartzman, J. McKenzie, D. Fitzgerald, S. Prater, M. Katcher, E. Fain, Z. Syed. *ICD waveform optimization: a randomized, prospective, pair-sampled multicenter study.* Pacing and clinical electrophysiology **23 (11 Pt 2)**, (2000), pp. 1992–5.

[108] G. A. Mouchawar, L. A. Geddes, J. D. Bourland, J. A. Pearce. *Ability of the Lapicque and Blair strength-duration curves to fit experimentally obtained data from the dog heart.* Biomedical Engineering, IEEE Transactions on **36 (9)**, (1989), pp. 971–4.

[109] S. Weidmann. *Electrical constants of trabecular muscle from mammalian heart.* The Journal of physiology **210 (4)**, (1970), pp. 1041–54.

[110] A. G. Kléber, C. B. Riegger. *Electrical constants of arterially perfused rabbit papillary muscle.* The Journal of physiology **385**, (1987), pp. 307–24.

[111] R. Plonsey, R. C. Barr. *Effect of microscopic and macroscopic discontinuities on the response of cardiac tissue to defibrillating (stimulating) currents.* Medical & Biological Engineering & Computing **24 (2)**, (1986), pp. 130–136.

[112] V. G. Fast, S. Rohr, A. M. Gillis, A. G. Kleber. *Activation of Cardiac Tissue by Extracellular Electrical Shocks : Formation of 'Secondary Sources' at Intercellular Clefts in Monolayers of Cultured Myocytes.* Circulation Research **82 (3)**, (1998), pp. 375–385.

[113] X. Zhou, S. B. Knisley, W. M. Smith, D. Rollins, A. E. Pollard, R. E. Ideker. *Spatial Changes in the Transmembrane Potential During Extracellular Electric Stimulation.* Circulation Research **83 (10)**, (1998), pp. 1003–1014.

[114] S. B. Knisley, T. F. Blitchington, B. C. Hill, A. O. Grant, W. M. Smith, T. C. Pilkington, R. E. Ideker. *Optical measurements of transmembrane potential changes during electric field stimulation of ventricular cells.* Circulation Research **72 (2)**, (1993), pp. 255–270.

[115] L. Clerc. *Directional differences of impulse spread in trabecular muscle from mammalian heart.* The Journal of physiology **255 (2)**, (1976), pp. 335–46.

[116] N. G. Sepulveda, B. J. Roth, J. P. Wikswo. *Current injection into a two-dimensional anisotropic bidomain.* Biophysical journal **55 (5)**, (1989), pp. 987–99.

[117] M. Neunlist, L. Tung. *Spatial distribution of cardiac transmembrane potentials around an extracellular electrode: dependence on fiber orientation.* Biophysical journal **68 (6)**, (1995), pp. 2310–22.

[118] S. B. Knisley. *Transmembrane Voltage Changes During Unipolar Stimulation of Rabbit Ventricle.* Circulation Research **77 (6)**, (1995), pp. 1229–1239.

[119] W. E. Garrey. *The nature of fibrillary contraction of the heart: its relation to tissue mass and form.* American Journal of Physiology **33**, (1914), p. 397.

[120] D. P. Zipes, J. Fischer, R. M. King, Nicoll A deB, W. W. Jolly. *Termination of ventricular fibrillation in dogs by depolarizing a critical amount of myocardium.* The American journal of cardiology **36 (1)**, (1975), pp. 37–44.

[121] F. X. Witkowski, P. A. Penkoske, R. Plonsey. *Mechanism of cardiac defibrillation in open-chest dogs with unipolar DC-coupled simultaneous activation and shock potential recordings.* Circulation **82 (1)**, (1990), pp. 244–60.

[122] A. Fabiato, P. Coumel, R. e. a. Gourgon. *Le seuil de réponse synchrone des fibres myocardiques. application e comparaison expérimentale de l'efficacité des différentes formes de chocs électriques de défibrillation.* Arch Mal Coeur **60**, (1967), pp. 527–544.

[123] P. S. Chen, N. Shibata, E. G. Dixon, P. D. Wolf, N. D. Danieley, M. B. Sweeney, W. M. Smith, R. E. Ideker. *Activation during ventricular defibrillation in open-chest dogs. Evidence of complete cessation and regeneration of ventricular fibrillation after unsuccessful shocks.* The Journal of clinical investigation **77 (3)**, (1986), pp. 810–23.

[124] N. Shibata, P. S. Chen, E. G. Dixon, P. D. Wolf, N. D. Danieley, W. M. Smith, R. E. Ideker. *Influence of shock strength and timing on induction of ventricular arrhythmias in dogs.* Am J Physiol Heart Circ Physiol **255 (4)**, (1988), pp. H891–901.

[125] P. S. Chen, P. D. Wolf, S. D. Melnick, N. D. Danieley, W. M. Smith, R. E. Ideker. *Comparison of activation during ventricular fibrillation and following unsuccessful defibrillation shocks in open-chest dogs.* Circulation Research **66 (6)**, (1990), pp. 1544–1560.

[126] P. S. Chen, G. K. Feld, J. M. Kriett, M. M. Mower, R. Y. Tarazi, R. P. Fleck, C. D. Swerdlow, E. S. Gang, R. M. Kass. *Relation between upper limit of vulnerability and defibrillation threshold in humans.* Circulation **88 (1)**, (1993), pp. 186–192.

[127] S. M. Dillon, K. F. Kwaku. *Progressive depolarization: a unified hypothesis for defibrillation and fibrillation induction by shocks.* Journal of cardiovascular electrophysiology **9 (5)**, (1998), pp. 529–52.

[128] B. J. Roth. *A mathematical model of make and break electrical stimulation of cardiac tissue by a unipolar anode or cathode.* IEEE Transactions on Biomedical Engineering **42 (12)**, (1995), pp. 1174–1184.

[129] K. Skouibine, N. Trayanova, P. Moore. *Success and failure of the defibrillation shock: insights from a simulation study.* Journal of cardiovascular electrophysiology **11 (7)**, (2000), pp. 785–96.

[130] Y. Cheng, K. A. Mowrey, D. R. Van Wagoner, P. J. Tchou, I. R. Efimov. *Virtual Electrode-Induced Reexcitation : A Mechanism of Defibrillation.* Circulation Research **85 (11)**, (1999), pp. 1056–66.

[131] A. Pumir, V. I. Krinsky. *How does an electric field defibrillate cardiac muscle?* Physica D: Nonlinear Phenomena **91 (1-2)**, (1996), pp. 205–19.

[132] T. Krogh-Madsen, D. Christini. *Pacing-induced spatiotemporal dynamics can be exploited to improve reentry termination efficacy.* Physical Review E **80 (2)**, (2009), p. 021924.

[133] S. Sinha, D. Christini. *Termination of reentry in an inhomogeneous ring of model cardiac cells.* Physical Review E **66 (6)**, (2002), p. 061903.

[134] P. Comtois, A. Vinet. *Resetting and annihilation of reentrant activity in a model of a one-dimensional loop of ventricular tissue.* Chaos: An Interdisciplinary Journal of Nonlinear Science **12 (3)**, (2002), pp. 903–922.

[135] N. F. Otani. *Termination of reentrant cardiac action potential propagation using far-field electrical pacing.* Biomedical Engineering, IEEE Transactions on **58 (7)**, (2011), pp. 2013–22.

[136] J. Bragard, A. Simic, J. Elorza, R. Grigoriev, E. Cherry, R. Gilmour, N. Otani, F. H. Fenton. *Shock-induced termination of reentrant cardiac arrhythmias: Comparing monophasic and biphasic shock protocols.* Chaos: An Interdisciplinary Journal of Nonlinear Science **23 (4)**, (2013), pp. –.

[137] G. W. Beeler, H. Reuter. *Reconstruction of the action potential of ventricular myocardial fibres.* The Journal of physiology **268 (1)**, (1977), pp. 177–210.

[138] Z. Qu, J. Weiss, A. Garfinkel. *Spatiotemporal Chaos in a Simulated Ring of Cardiac Cells.* Physical Review Letters **78 (7)**, (1997), pp. 1387–1390.

[139] I. R. Efimov, V. I. Krinsky, J. Jalife. *Dynamics of rotating vortices in the Beeler-Reuter model of cardiac tissue.* Chaos Solitons Fractals **5 (3-4)**, (1995), pp. 513–526.

[140] M. Courtemanche, A. T. Winfree. *R-entrant Rotating Waves in a Beeler-Reuter based model of Two-dimensional Cardiac Electrical Activity.* International Journal Of Bifurcation And Chaos **1 (2)**, (1991), pp. 431–444.

[141] K. a. DeBruin, W. Krassowska. *Electroporation and shock-induced transmembrane potential in a cardiac fiber during defibrillation strength shocks.* Annals of biomedical engineering **26 (4)**, (1998), pp. 584–96.

[142] S. B. Knisley, A. O. Grant. *Asymmetrical electrically induced injury of rabbit ventricular myocytes.* Journal of Molecular and Cellular Cardiology **27 (5)**, (1995), pp. 1111–1122.

[143] O. Tovar, L. Tung. *Electroporation and recovery of cardiac cell membrane with rectangular voltage pulses.* The American journal of physiology **263 (4 Pt 2)**, (1992), pp. H1128–36.

[144] O. Tovar, L. Tung. *Electroporation of Cardiac Cell Membranes with Monophasic or Biphasic Rectangular Pulses.* Pacing and Clinical Electrophysiology **14 (11)**, (1991), pp. 1887–1892.

[145] I. Kodama, N. Shibata, I. Sakuma, K. Mitsui, M. Iida, R. Suzuki, Y. Fukui, S. Hosoda, J. Toyama. *Aftereffects of high-intensity DC stimulation on the electromechanical performance of ventricular muscle.* The American journal of physiology **267 (1 Pt 2)**, (1994), pp. H248–H258.

[146] A. Al-Khadra, V. Nikolski, I. R. Efimov. *The Role of Electroporation in Defibrillation.* Circulation Research **87 (9)**, (2000), pp. 797–804.

[147] K. Ohuchi, Y. Fukui, I. Sakuma, N. Shibata, H. Honjo, I. Kodama. *A dynamic action potential model analysis of shock-induced aftereffects in ventricular muscle by reversible breakdown of cell membrane.* Biomedical Engineering, IEEE Transactions on **49 (1)**, (2002), pp. 18–30.

[148] X. Zhou, W. M. Smith, D. L. Rollins, R. E. Ideker. *Transmembrane potential changes caused by shocks in guinea pig papillary muscle.* American Journal of Physiology **271 (6 Pt 2)**, (1996), pp. H2536–H2546.

[149] P. F. Cranefield, B. F. Hoffman, A. A. Siebens. *Anodal Excitation of Cardiac Muscle.* Am J Physiol – Legacy Content **190 (2)**, (1957), pp. 383–390.

[150] E. Dekker. *Direct Current Make and Break Thresholds for Pacemaker Electrodes on the Canine Ventricle.* Circulation Research **27 (5)**, (1970), pp. 811–823.

[151] R. Ranjan, N. Chiamvimonvat, N. V. Thakor, G. F. Tomaselli, E. Marban. *Mechanism of anode break stimulation in the heart.* Biophysical journal **74 (4)**, (1998), pp. 1850–63.

[152] G. Biermans, J. Vereecke, E. Carmeliet. *Effect of external K on the block of the inward rectifier during hyperpolarization in guinea-pig ventricular myocytes by external Na.* Biomedica biochimica acta **48 (5-6)**, (1989), pp. S358–63.

[153] E. Cerbai, M. Barbieri, A. Mugelli. *Occurrence and Properties of the Hyperpolarization-Activated Current If in Ventricular Myocytes From Normotensive and Hypertensive Rats During Aging.* Circulation **94 (7)**, (1996), pp. 1674–1681.

[154] H. Yu, F. Chang, I. S. Cohen. *Pacemaker current i(f) in adult canine cardiac ventricular myocytes.* The Journal of physiology **485 ( Pt 2)**, (1995), pp. 469–83.

[155] C. H. Luo, Y. Rudy. *A model of the ventricular cardiac action potential. Depolarization, repolarization, and their interaction.* Circulation research **68 (6)**, (1991), pp. 1501–26.

[156] B. J. Roth, J. Chen. *Mechanism of anode break excitation in the heart: the relative influence of membrane and electrotonic factors .* Journal of Biological Systems **7**, (1999), pp. 541–552.

[157] J. P. Keener, J. Sneyd. *Mathematical Physiology.* Springer-Verlag (1998).

[158] M. G. Fishler, E. A. Sobie, L. Tung, N. V. Thakor. *Cardiac responses to premature monophasic and biphasic field stimuli. results from cell and tissue modeling studies.* J Electrocardiol **28 Suppl**, (1995), pp. 174–9.

[159] S. Balay, J. Brown, K. Buschelman, W. D. Gropp, D. Kaushik, M. G. Knepley, L. C. McInnes, B. F. Smith, H. Zhang. *PETSc Web page* (2012). Http://www.mcs.anl.gov/petsc.

[160] Y. Saad, M. H. Schultz. *Gmres - a Generalized Minimal Residual Algorithm for Solving Nonsymmetric Linear-Systems.* Siam Journal on Scientific and Statistical Computing **7 (3)**, (1986), pp. 856–869.

[161] M. A. Watanabe, F. H. Fenton, S. J. Evans, H. M. Hastings, A. Karma. *Mechanisms for Discordant Alternans.* Journal of Cardiovascular Electrophysiology **12 (2)**, (2001), pp. 196–206.

[162] A. Garfinkel, P. S. Chen, D. O. Walter, H. S. Karagueuzian, B. Kogan, S. J. Evans, M. Karpoukhin, C. Hwang, T. Uchida, M. Gotoh, O. Nwasokwa, P. Sager, J. N. Weiss. *Quasiperiodicity and chaos in cardiac fibrillation.* The Journal of clinical investigation **99 (2)**, (1997), pp. 305–14.

[163] J. N. Weiss, A. Garfinkel, H. S. Karagueuzian, Z. Qu, P.-S. Chen. *Chaos and the Transition to Ventricular Fibrillation : A New Approach to Antiarrhythmic Drug Evaluation.* Circulation **99 (21)**, (1999), pp. 2819–2826.

[164] G. Plank, L. J. Leon, S. Kimber, E. J. Vigmond. *Defibrillation depends on conductivity fluctuations and the degree of disorganization in reentry patterns.* Journal of cardiovascular electrophysiology **16 (2)**, (2005), pp. 205–16.

[165] J. Schuder, H. Stoeckle, J. A. West, P. Y. Keskar. *Transthoracic Ventricular Defibrillation in the Dog with Truncated and Untruncated Exponential Stimuli.* IEEE Transactions on Biomedical Engineering **18 (6)**, (1971), pp. 410–415.

[166] F. Qu, L. Li, V. P. Nikolski, V. Sharma, I. R. Efimov. *Mechanisms of superiority of ascending ramp waveforms: new insights into mechanisms of shock-induced vulnerability and defibrillation.* American journal of physiology. Heart and circulatory physiology **289 (2)**, (2005), pp. H569–77.

[167] L. A. Geddes, W. A. Tacker, C. F. Babbs, B. J. D. *Ventricular defibrillating threshold : strength-duration and percent-success curves.* Med. Biol. Eng. Comput **35**, (1997), pp. 301–305.

[168] K. Priddy, P. Keller. *Artificial Neural Networks: An Introduction.* Tutorial Text Series. Society of Photo Optical (2005).

[169] MATLAB. *version 7.12.0 (R2011a).* The MathWorks Inc., Natick, Massachusetts (2011).

[170] A. Dobson. *An Introduction to Generalized Linear Models.* Texts in Statistical Science. Chapman & Hall/CRC, second edn. (2001).

[171] R Development Core Team. *R: A Language and Environment for Statistical Computing.* R Foundation for Statistical Computing, Vienna, Austria (2008). ISBN 3-900051-07-0.

[172] D. Hosmer, S. Lemeshow. *Applied Logistic regression.* New York: Wiley (1989).

[173] S. Wood. *Generalized Additive Models: An Introduction with R.* Chapman and Hall/CRC (2006).

[174] S. Wood. *mgcv: Mixed GAM Computation Vehicle with GCV/AIC/REML smoothness estimation* (2013).

[175] S. N. Wood. *Modelling and smoothing parameter estimation with multiple quadratic penalties.* Journal of the Royal Statistical Society (B) **62 (2)**, (2000), pp. 413–428.

[176] S. N. Wood. *Thin-plate regression splines.* Journal of the Royal Statistical Society (B) **65 (1)**, (2003), pp. 95–114.

[177] S. N. Wood. *Stable and efficient multiple smoothing parameter estimation for generalized additive models.* Journal of the American Statistical Association **99 (467)**, (2004), pp. 673–686.

[178] S. N. Wood. *Fast stable restricted maximum likelihood and marginal likelihood estimation of semiparametric generalized linear models.* Journal of the Royal Statistical Society (B) **73 (1)**, (2011), pp. 3–36.

[179] M. Li, N. Otani. *Controlling alternans in cardiac cells.* Ann. of Biomed. Eng. **32 (6)**, (2004), pp. 784–92.

[180] D. Allexandre, N. Otani. *Preventing alternans-induced spiral wave breakup in cardiac tissue: An ion-channel-based approach.* Phys. Rev. E **70**.

[181] A. Garzon, R. O. Grigoriev, F. H. Fenton. *Model-based control of cardiac alternans on a ring.* Phys. Rev. E **80**.

[182] A. Garzon, R. O. Grigoriev, F. H. Fenton. *Model-based control of cardiac alternans in Purkinje fibers.* Phys. Rev. E **84**.

[183] R. A. Winkle, E. B. Stinson, S. M. Bach, D. S. Echt, P. Oyer, K. Armstrong. *Measurement of cardioversion/defibrillation thresholds in man by a truncated exponential waveform and an apical patch-superior vena caval spring electrode configuration.* Circulation **69 (4)**, (1984), pp. 766–71.

[184] R. E. Kerber, M. G. Kienzle, B. Olshansky, A. L. Waldo, D. Wilber, M. D. Carlson, A. M. Aschoff, S. Birger, L. Fugatt, S. Walsh. *Ventricular tachycardia rate and morphology determine energy and current requirements for transthoracic cardioversion.* Circulation **85 (1)**, (1992), pp. 158–63.

[185] M. G. Hillebrenner, J. C. Eason, N. A. Trayanova. *Mechanistic inquiry into decrease in probability of defibrillation success with increase in complexity of preshock reentrant activity.* American journal of physiology. Heart and circulatory physiology **286 (3)**, (2004), pp. H909–17.

[186] J. F. Swartz, R. D. Fletcher, P. E. Karasik. *Optimization of biphasic waveforms for human nonthoracotomy defibrillation.* Circulation **88 (6)**, (1993), pp. 2646–2654.

[187] A. Natale, J. Sra, D. Krum, A. Dhala, S. Deshpande, M. Jazayeri, K. Newby, A. Wase, K. Axtell, W. L. VanHout, M. Akhtar. *Relative efficacy of different tilts with biphasic defibrillation in humans.* Pacing and clinical electrophysiology **19 (2)**, (1996), pp. 197–206.

[188] S. R. Shorofsky, A. H. Foster, M. R. Gold. *Effect of waveform tilt on defibrillation thresholds in humans.* Journal of cardiovascular electrophysiology **8 (5)**, (1997), pp. 496–501.

[189] J. Brugada, B. Herse, B. Sandsted, U. Michel, B. D. Schubert, S. J. Hahn. *Clinical evaluation of defibrillation efficacy with a new single-capacitor biphasic waveform in patients undergoing implantation of an implantable cardioverter defibrillator.* Europace **3 (4)**, (2001), pp. 278–84.

[190] G. Koning, H. Schneider, A. J. Hoelen, R. S. Reneman. *Amplitude-duration relation for direct ventricular defibrillation with rectangular current pulses.* Medical & Biological Engineering **13 (3)**, (1975), pp. 388–395.

[191] J. L. Wessale, J. D. Bourland, W. A. Tacker, L. A. Geddes. *Bipolar catheter defibrillation in dogs using trapezoidal waveforms of various tilts.* Journal of Electrocardiology **13 (4)**, (1980), pp. 359–365.

[192] M. R. Gold, S. R. Shorofsky. *Strength-Duration Relationship for Human Transvenous Defibrillation.* Circulation **96 (10)**, (1997), pp. 3517–3520.

[193] J. L. Jones, R. E. Jones, G. Balasky. *Improved cardiac cell excitation with symmetrical biphasic defibrillator waveforms.* The American journal of physiology **253 (6 Pt 2)**, (1987), pp. H1418–24.

[194] C. Bishop. *Neural Networks for Pattern Recognition.* Oxford University Press (1995).

[195] Y. Yamanouchi, S. X. Garrigue, K. A. Mowrey, B. L. Wilkoff, P. J. Tchou. *Optimal biphasic waveforms for internal defibrillation using a 60 muF capacitor.* Experimental and clinical cardiology **7 (4)**, (2002), pp. 188–92.

[196] D. Lang, D. Swanson, S. Bach, J. Shapland. *Strength-duration relationship for biphasic defibrillation in dogs.* In *Images of the Twenty-First Century. Proceedings of the Annual International Engineering in Medicine and Biology Society*, pp. 80–81. IEEE.

[197] W. A. J. Tacker, C. F. Babbs, B. J. Dan, L. A. Geddes. *Aparatus for controlling cardiac ventricular tachyarrhythmias.* European Patent No EP 0095726(A1) (1983).

[198] K. F. A. A. Smits. *Cardioversion and defibrillation lead method.* United States Patent No US 4641656 (1987).

[199] J. Rhude, J. Sweeney, J. Reighard, T. Brandon. *Circumferential switching between multiple electrode pairs within a biphasic shock lowers implantable defibrillator thresholds.* In *Proceedings of the First Joint BMES/EMBS Conference. 1999 IEEE Engineering in Medicine and Biology 21st Annual Conference and the 1999 Annual Fall Meeting of the Biomedical Engineering Society (Cat. No.99CH37015)*, vol. 1, p. 317. IEEE (1999).

[200] D. McGee, D. K. Swanson, J. G. Whayne. *Systems and methods for multi-site cardiac defibrillation using multiple electrode structures.* United States Patent No US 5855592 (1999).

# Summary

In the study presented in this thesis we have used one-dimensional model to study mechanisms associated with the application of the external stimulus to the cardiac tissue. Arrhythmic dynamics is approximated with the reentrant wave on a ring of cardiac tissue. Successful defibrillation is modeled with the complete removal of the reentrant dynamics. The propagation of the electrical signal is modeled with the bidomain model, while cellular membrane current is modeled with the modified Beeler-Reuter model. Three well known and clinically used defibrillation protocols have been compared for different parameters of the system: monophasic, symmetric biphasic and asymmetric biphasic. Extensive numerical simulations performed for the shock duration of 8ms confirmed common medical wisdom that biphasic shocks are superior to monophasic shocks. More precisely, to yield a 90% success rate, a asymmetric biphasic protocol will require 26% less energy than the monophasic protocol. The order of efficiency of the three protocols is maintained for shock duration T $\geq$4 ms, while for smaller durations of the shock, monophasic protocols results to be the most successful of the three. Energy required to produce 50% and 90% success rate will also depend on the dynamics of the reentrant wave present on the ring prior to the shock. We have compared defibrillation protocols applied to reentrant quasiperiodic and chaotic dynamics. The results reveal that it is easier to defibrillate quasiperiodic that the chaotic dynamics. Careful examination of the defibrillation trials revealed, that for the shock duration of 8ms, all successful defibrillation trials can be classified into one of the four defibrillation protocols. These are: direct block, annihilation, delayed block and direct activation. Which defibrillation mechanism prevails depends on the energy level, the current dynamic state of the system and the shock protocol.
Having tested and analyzed the validity of the one-dimensional model with the well known defibrillation protocols, the model was also used to examine the efficiency of a non-standard approach to defibrillation: application of the shock with the four electrode system instead of the common approach with two electrodes. Results revealed that a drastic reduction in defibrillation threshold is achieved with the four electrode technique with respect to the standard two electrode technique. The highest saving in required energy is achieved with the asymmetric biphasic protocol. When compared to the two-electrode monophasic protocol, it was found that the required energy reduced approximately 88%. Mechanism of successful defibrillation are analyzed and revealed that the advantage of biphasic shocks for the case of four electrodes protocol lies behind the interplay of the duration of the cathodal and anodal phase. While this study rely heavily on numerical results in a very simplified geometry, one would be tempted to hypothesize that some of the important findings will continue to hold in a more detailed and realistic study of defibrillation. The realization of the implantable four-electrode or similar multi-electrode setup has already been patented [197, 198]. Both patents are relatively old and date to the same decade of the first implanted defibrillator (1980). Given the advancement of the technological aspect of the implanted defibrillators over the past 30 years and the optimistic results obtained with four electrode setup, one simple message of this study is that the idea of the four-electrode setup is worth pursuing with a more detailed three dimensional study and possibly with animal experiments.

# Resumen

En el estudio que se presenta en esta tesis hemos utilizado un modelo unidimensional para estudiar mecanismos asociados con la aplicación de estimulos externos a tejido cardiaco. La dinámica de la arritmia es aproximada con la onda reentrante en un anillo de tejido cardiaco. La defibrilación exitosa es modelada con la completa eliminación de la dinámica reentrante. La propagación de la señal eléctrica es modelada con un modelo de dominio dual, mientras que la corriente a tráves de la membrana celular es modelada con el modelo modificado de Beeler-Reuter. Tres protocolos bien conocidos y utilizados clínicamente han sido comparados para diferentes parámetros del sistema: monofásico, simétrico bifásico y asimétrico bifásico. Extensas simulaciones numéricas realizadas para el choque de duración de 8 ms confirman la sabiduría medica común que descargas bifásicas son mas efectivas que descargas monofásicas. Mas precisamente, para lograr la tasa de éxito de 90 % , un protocolo asimétrico bifásico necesitara 26 % menos energía que un protocolo monofásico. El orden de eficiencia de los tres protocolos se mantiene para los choques de duración $T \geq 4$ ms, mientras que para los choques con menor duraciónes, protocolos monofásicos resultan ser los más exitosos de los tres. La energía requerida para producir 50 % y 90 % tasa de éxito también depende de la dinámica de la onda reentrante que se encuentra en el anillo previamente a la descarga. Hemos comparado protocolos de desfribilación aplicados a dinámica reentrante cuasi-periódica y caótica. Los resultados revelan que es más sencillo desfibrilar una dinámica cuasi-periódica que una caótica. Examinación detallada de los ensayos de defribilación revelan que, para una descarga de duración de 8 ms, todos los ensayos de defribilación exitosos pueden ser clasificados en uno de los cuatro protocolos de la desfirilación. Estos son: bloqueo directo, aniquilación, bloqueo retardado, y activación directa. Que mecanismo de defibrilación prevalece depende del nivel de energía, el estado dinámico actual del sistema y el protocolo de descarga.

Habiendo testeado y analizado la validez del modelo unidimensional con uno de los protocolos de defibrilación bien conocidos, el modelo fue utilizado también para examinar la eficacia de la desfribilación con un choque no estándar: la aplicación del choque con un sistema de cuatro electrodos en lugar del choque común de dos electrodos. Resultados revelan que una drástica reducción en el umbral de desfibrilación es obtenido con la técnica de cuatro electrodos con respecto a la tecnica estándar de dos electrodos. El mayor ahorro en energía requerida es logrado con el protocolo asimétrico bifásico. Cuando comparado al protocolo de dos electrodos monofásico, se ha encontrado que la energía requerida se ha reducido aproximadamente un 88 %. Mecanismos de desfibrilación exitosa son analizados y revelan que la ventaja de las descargas bifásicas para el protocolo de cuatro electrodos reside en la interacción de la duración de la fase catódica y anodica. Mientras que este estudio se basa fuertemente en simulaciones numéricas en una geometría muy simplificada, uno sentiría la tentación de hipotetizar que algunos de los hallazgos importantes continuaran valiendo en un estudio más detallado y realista de la desfibrilación. La realización de un defibrilador implantable de cuatro electrodos o similar multielectrodo ha sido patentado [197, 198]. Ambos patentes son relativamente antiguas y se remontan a la misma época de los primeros desfibriladores implantados (1980). Dado los avances de los aspectos tecnológicos de los desfibriladores implantables en los últimos 30 años y los resultados optimisticos obtenidos con los dispositivos de cuatro electrodos, un simple mensaje de este estudio es que la idea del defibrilador con cuatro electrodes es importante de proseguir con un estudio tridimensional mas detallado y posiblemente con experimentos en animales.